

# White matter tract transcranial ultrasound stimulation, a computational study

Ciara Felix<sup>a</sup>, Davide Folloni<sup>b,1</sup>, Haoyu Chen<sup>a</sup>, Jerome Sallet<sup>b,1</sup>, Antoine Jerusalem<sup>a,\*</sup>

<sup>a</sup>*Department of Engineering Science, University of Oxford, Oxford, UK*

<sup>b</sup>*Wellcome Centre for Integrative Neuroimaging (WIN), Department of Experimental Psychology, University of Oxford, Oxford, UK*

<sup>c</sup>*Currently: Department of Neuroscience and Friedman Brain Institute, Icahn School of Medicine at Mount Sinai, New York, NY, USA*

<sup>d</sup>*Currently: Inserm, Stem Cell and Brain Research Institute, Université Lyon 1, Bron, France*

---

## Abstract

Low-intensity transcranial ultrasound stimulation (TUS) is poised to become one of the most promising treatments for neurological disorders. However, while recent animal model experiments have successfully quantified the alterations of the functional correlations between a sonicated target cortical region and other cortical regions of interest (ROIs), the varying degree of alteration between these different connections remains unexplained. We hypothesise here that the incidental sonication of the tracts leaving the target region towards the different ROIs could participate in explaining these differences. To this end, we propose a tissue level phenomenological numerical model of the coupling between the ultrasound waves and the white matter electrical activity. The model is then used to reproduce *in silico* the sonication of the anterior cingulate cortex (ACC) of a macaque monkey and measure the neuromodulation power within the white matter tracts leaving the ACC for five cortical ROIs. The results show that the more induced power a white matter tract proximal to the ACC and connected to a secondary ROI receives, the more altered the connectivity fingerprint of the ACC to this region will be after sonication. These results point towards the need

---

\*Corresponding author

Email address: [antoine.jerusalem@eng.ox.ac.uk](mailto:antoine.jerusalem@eng.ox.ac.uk) (Antoine Jerusalem)

to isolate the sonication to the cortical region and minimise the spillage on the neighbouring tracts when aiming at modulating the target region without losing the functional connectivity with other ROIs. Those results further emphasise the potential role of the white matter in TUS and the need to account for white matter topology when designing TUS protocols.

*Keywords:* Ultrasound neuromodulation, Homogenised continuum flexoelectricity, Electromechanical coupling

*2010 MSC:* 00-01, 99-00

---

Neurological disorders are a leading cause of disability and fatality [1]. These disorders are expected to present an increasing challenge, and cause serious threats to public health and health service delivery with the growth in population and increase in life expectancy [2]. While pharmacological interventions  
5 are already in use, not every patient respond well to these [3]. Surgical methods [4] and deep brain stimulation (DBS) are effective but are extremely invasive and thus prone to additional complications. Transcranial direct current stimulation (tDCS) and transcranial magnetic stimulation (TMS) are non-invasive methods but suffer from low spatial resolutions and cannot stimulate deep brain  
10 structures the way invasive approaches do [5]. On the other hand, transcranial ultrasound stimulation (TUS) can propagate through the skull bone [6], focus on a small targeted volume, and interact with the brain tissues through thermal and non-thermal mechanisms [4]. High-intensity focused ultrasound has shown to be extremely effective for ablative purposes [7]. More recently, low-intensity  
15 TUS has been gaining attention by being able to induce prominent and reversible mechanical bio-effects on brain tissue without significantly heating or damaging them [8] as observed in previous research on rodents [9], rabbits [10], sheep [11], pigs [12], primates [13], and in humans [14]. Finally, TUS provides an increased spatial selectivity over TMS and tDCS and has the ability to target  
20 deep structures within the brain [15], thus providing avenues for examining the neuronal mechanisms of cognitive, sensory, and motor functions in the brain [16]. Nevertheless, the mechanisms of action of ultrasound and its ability to

modulate the brain are yet to be fully understood. In particular, the growing body of research in recent years aimed at optimising sonication parameters and effect localisation is pointing towards the need to better understand how the multiphysics properties of neurons leads—or at the very least, is connected to—the functional alterations observed at the organ scale [17].

Such need is particularly important in light of recent experimental results where the sonication of the anterior cingulate cortex (ACC) of a macaque monkey was observed to lead to alterations in the connectivity between the ACC and a number of regions of interest (ROIs) in the cortex [13]. These changes were, however, not of the same magnitude across the different ROIs, hinting that the sole characterisation of the sonicated ACC is not enough to universally predict how its connectivity with various ROIs is altered. In particular, with recent work demonstrating how white matter could also be modulated [18, 19, 20, 21, 22, 23], one explanation for this discrepancy could lie in the understanding of how the tracts leaving the sonicated region are themselves sonicated in the neighbourhood of the ACC. Doing so requires a thorough understanding and predicting model of how white matter tract electrophysiology can be altered in the presence of a given pressure field.

Flexoelectricity describes the phenomenon leading to current creation when a dielectric material is submitted to a time-varying strain gradient (while piezoelectric current arises from time-varying strain). It has been widely observed in dielectric materials such as crystalline materials [24], semiconductors [25], polymers [26], bones [27] and biomembranes [28]. With the support of a wealth of flexoelectric models developed in the context of biological membranes [29], flexoelectricity has been proposed as a key mechanism linking cellular mechanical deformation to many biological processes, such as vesicle equilibrium [30], tether formation [31], thermal fluctuation [32], ion transport [33], cochlear amplification and sharp frequency discrimination, or outer hair cell electromotility [34]. In particular, and building on the long-standing evidence of electromechanical coupling in the electrical activity of the nervous system [35], as well as on a series of recent modelling efforts aimed at capturing such coupling [36, 37, 38, 39],

a model of membrane flexoelectricity in the context of ultrasound neuromodu-  
55 lation has recently been proposed [40]. While the proposed framework is able  
to capture some of the key characteristics of ultrasound-induced electrical ac-  
tivity, the need to account for the microstructural description of the underlying  
dielectric polarisation restricts this model to cellular observations and precludes  
any simulation of large scale assemblies of multiple biological cells. Further-  
60 more, other coupling mechanisms might be at play and membrane flexoelectric-  
ity might not be the driving neuromodulation mechanism. This, and the fact  
the current experimental programmes leading the development of TUS focus on  
the organ scale, further highlight the need for a phenomenological multiphysics  
continuum framework defined without the need to account explicitly for the  
65 underlying microstructure.

To this end, this work proposes, develops and validates a theoretical frame-  
work of continuum bulk flexoelectricity able to capture electromechanical cou-  
pling at the macroscale of bundles of flexoelectric cylinders in brain white matter  
using finite element method. While calibrated here against the microscale for-  
70 mulation of Ref. [40] to ensure multiscale compatibility, this approach can be  
used directly at the macroscale for the description of strain-gradient-induced  
electromechanical coupling without the need to account for any microstructural  
considerations. The development of the theoretical framework includes the flex-  
oelectric coupling model as well as the estimation of the axonal density within  
75 each voxel from DTI data. This work also details the validation of the ap-  
proach, and its application to white matter tracts in the context of TUS in a  
macaque monkey. Finally, the model predicts that the more induced power a  
white matter tract leaving the ACC and connected to a secondary ROI receives,  
the more altered the connectivity fingerprint of the ACC to this region will be  
80 after sonication.

## 1. Materials and Methods

This section first briefly covers the animal model results on which the numerical model is applied, see Ref. [13] for more detail. The homogenised flexoelectric model is then presented (further detail in Supplementary Materials) followed by  
85 the 3D in silico head model.

### 1.1. Animal model

#### 1.1.1. Subjects

In-vivo diffusion MRI data were obtained from both hemispheres of 1 rhesus monkeys (*Macaca mulatta*, female) using a 3T MRI Siemens scanner. For a  
90 detailed description of the resting-state functional Magnetic Resonance Imaging (re-fMRI) data acquisition, preprocessing, activity coupling analysis analyses and TUS protocol see Ref. [13].

#### 1.1.2. MRI data collection and anesthesia protocol

Protocols for animal care, magnetic resonance imaging, and anesthesia were  
95 carried out under authority of personal and project licenses in accordance with the UK Animals (Scientific Procedures) Act (1986, revised 2013). Macaques were maintained with intermittent positive pressure ventilation to ensure a constant respiration rate during the diffusion-weighted scan. Respiration rate, inspired and expired CO, and inspired and expired isoflurane concentration were  
100 monitored and recorded using VitalMonitor software (Vetronic Services Ltd., Devon). In addition to these parameters, core temperature and SpO were monitored throughout the scan. For a detailed description of the anesthesia protocol used see Ref. [41]. A four-channel phased-array radio-frequency coil in conjunction with a local transmission coil was used for data acquisition (Dr. H. Kolster,  
105 Windmiller Kolster Scientific, Fresno, CA, USA). Whole-brain diffusion MRI data were collected in 2016 at the University of Oxford using a twice-refocused diffusion-weighted spin echo sequence [42]. Six non-diffusion weighted ( $b = 0$   $s/mm^2$ ) and six diffusion-weighted ( $b = 1000$   $s/mm^2$ ) datasets with 60 isotropically distributed diffusion directions each were collected. Diffusion MRI data

110 were acquired using a sequence with TE/TR: 102 ms/8.3 s; resolution: 1×1 mm; slice thickness: 1 mm; 60 isotropically distributed diffusion directions. To correct for image distortion, images were acquired using a head-foot and foot-head phase encoding (PE) direction. Images acquired with both PE direction protocols were subsequently combined using TOPUP. The datasets acquired in  
 115 a single session the animal were then averaged to create a single set of data. The structural data were collected at 0.5 mm isotropic resolution across the entire brain.

### 1.1.3. Data preprocessing

Analyses were carried out with the FSL package, version 5.0 (<http://fsl.fmrib.ox.ac.uk/fsl>).  
 120 Following preprocessing, a diffusion tensor model was fit to each voxel using DTIFIT [43]. Voxel-wise crossing-fiber model fitting of diffusion orientations was performed using FSL’s BedpostX [44]. Up to three fiber orientations per voxel were allowed during preprocessing. This analysis resulted into voxel-wise posterior distributions of fiber orientations that were  
 125 subsequently used in probabilistic tractography.

Note that, in this study, we used a well-established approach to modelling of multiple fiber orientation estimation and used this information to reconstruct the path of interest within the brain [44, 45]. Although alternative approaches are indeed possible, the one used in this study has shown more advantages,  
 130 especially within complex areas of the brain represented by crossing fibers or for fibre bundles characterised by strong curvature along their path. Moreover, its application was already successful in the reconstruction of both in vivo and post-mortem fibre bundles within both macaque monkey and human brains [46, 47, 13].

### 1.1.4. Probabilistic tractography

135 The probabilistic tractography protocol used here to reconstruct the cingulum bundle (CB) fibers interconnecting the ACC area with other frontal regions closely resembled the one reported by Folloni and colleagues [48]. The seed mask

of the CB was drawn in the white matter rostral to the macaque monkey ACC  
 140 where TUS was applied by Folloni et al. [13]. The target cortical areas (Figure  
 2) were drawn on the white matter/gray matter border at the same coordinates  
 as in Ref. [13]. In order to reconstruct the projections between the seed mask  
 and the target areas, the tractography algorithm was run using this regions as  
 targets.

## 145 1.2. Theoretical framework

### 1.2.1. Flexoelectric coupling model

At the axonal scale, flexoelectricity in the membrane can be formulated as  
 a local change in the electric polarisation of the membrane when submitted to  
 strain gradient [28]:

$$P_i = f_{ijkl} \frac{\partial \varepsilon_{jk}}{\partial x_l} \quad (1)$$

where  $\mathbf{P}$  is the (dielectric) membrane polarisation,  $\mathbf{f}$  is the membrane flexoelec-  
 tricity tensor,  $\varepsilon$  is the membrane strain tensor, and  $\mathbf{x}$  is the spatial coordinate  
 vector. The electric polarisation generates an electric field within the mem-  
 brane, e.g., the electronic distribution and the nuclear positions are altered,  
 displacing the charges in the molecules without escaping them, thus producing  
 small electric dipoles within the material [49]. The resulting induced current  $dI$   
 passing across a patch of membrane of area  $S$  can then be obtained from  $\mathbf{P}$  by  
 [40]:

$$dI = \frac{\partial \iint_S \mathbf{P} \cdot \mathbf{n} dS}{\partial t} \quad (2)$$

where  $\mathbf{n}$  is the normal vector to the membrane.

A direct consequence of flexoelectricity is that any state of deformation in-  
 volving strain gradient, e.g., bending or local bulging, will induce current across  
 150 the membrane. While previous work considered localised bulging as the main  
 deformation mechanisms [40], we assume here instead that ultrasound is more  
 likely to locally bend axons and thus focus on this deformation mode. In par-  
 ticular, bending of a cylindrical representation of the axon would locally stretch  
 the membrane on one side of the axon, and compress it on the diametrically

155 opposed side of the axon, thus leading to current flowing in on one side, and out on the other side, see Fig. 1-a. When considering a representative volume element (RVE) of white matter, the net current contribution of each axonal's current can be calculated with (2), where, e.g.,  $S \in \{S_1, S_2, S_3\}$  for each one of the three axons in Fig. 1.

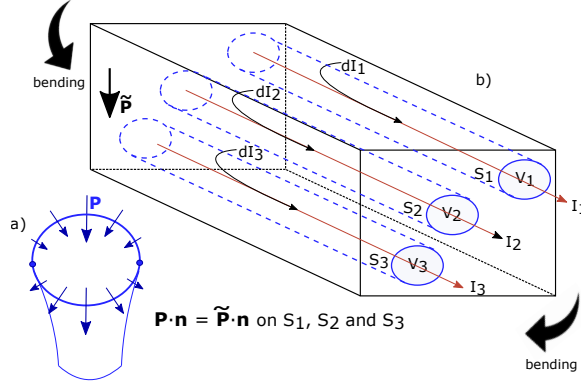


Figure 1: Continuum bulk flexoelectricity framework: a) membrane polarisation  $\mathbf{P}$  (naturally orthogonal to the membrane) arises from bending of the axons; b) in the bulk the homogenised bulk polarisation  $\tilde{\mathbf{P}}$  is defined at the tissue level (here with three axons of volume  $V_1, V_2$  and  $V_3$  and surface  $S_1, S_2$  and  $S_3$ ) and coincides with its membrane counterpart when projected orthogonally to the membrane.

Noting that  $dI = dI_1 + dI_2 + dI_3$ , the total contribution of all three axons in the RVE calculated from all the membrane areas, contribute to a net current flowing in the axonal direction at the RVE level, we propose in the following to rewrite this contribution as a bulk contribution. To do so, we postulate the existence of a fictitious volumetric flexoelectric tensor  $\tilde{\mathbf{f}}$  defined within the bulk of the fibrous tissue such that the current created through polarisation flows in the fibre direction. Note that this is not the same as  $\mathbf{f}$  in (1) as  $\mathbf{f}$  is only defined in the membrane to quantify the current flowing through it. A volumetric polarisation  $\tilde{\mathbf{P}}$  is defined as

$$\tilde{P}_i = \tilde{f}_{ijkl} \frac{\partial \varepsilon_{jk}}{\partial x_l} \quad (3)$$



where  $\boldsymbol{\varepsilon}$  is the strain tensor now defined in the bulk, and such that  $\tilde{\mathbf{P}}$  (defined in the entire volume) coincides with  $\mathbf{P}$  (defined on the axonal membranes) on the fibres' surface  $S$ :

$$\tilde{\mathbf{P}} \cdot \mathbf{n} = \mathbf{P} \cdot \mathbf{n} \text{ on } S \quad (4)$$

where, as in (2),  $\mathbf{n}$  is the normal vector to the membrane. Combining both equations and making use of the divergence theorem then leads to a new definition for the overall current created in the RVE:

$$dI = \frac{\partial \iiint_V \nabla \cdot \tilde{\mathbf{P}} dV}{\partial t} \quad (5)$$

160 where  $V$  is the volume of all fibres enclosed in  $S$  within the RVE. Note that, at the cross-sections of the fibres on the boundaries of the RVE,  $\mathbf{P}$  is assumed here to be defined and perpendicular to  $\mathbf{n}$  for the equivalence to hold.

This formulation can be used without the need to account explicitly for the underlying microstructure and can be used in any problem involving strain-gradient-induced electrical activity, whether or not flexoelectricity is the mechanism dominating at the microscopic level as long as it is phenomenologically so at the macroscale. Finally, as flexoelectricity is now defined as a bulk property related to the underlying fibre orientation, it is thus dependent on it and can be rotated following [50]

$$\tilde{f}_{rmns} = Q_{ri} Q_{mj} Q_{nk} Q_{sl} \tilde{f}_{ijkl} \quad (6)$$

where  $\tilde{f}_{rmns}$  is the rotated flexoelectric tensor coefficient,  $\tilde{f}_{ijkl}$  is the unrotated flexoelectric tensor coefficient and  $\mathbf{Q}$  is the rotation matrix.

It is worth noting that in 2D (where fibers are parallel to the 2D plane), when the bulk strain coincides with the membrane strain on  $S$ , by virtue of (1), (3) and (4), and using the fact that

$$\tilde{\mathbf{f}} = \mathbf{f} \text{ on } S, \quad (7)$$

165 one can take  $\tilde{\mathbf{f}} = \mathbf{f}$  for the whole 2D RVE. Unfortunately, this is not straightforwardly true in 3D as  $\mathbf{f}$  rotates with the curvature along the circular cross-section

of the membrane while  $\tilde{\mathbf{f}}$  remains fixed within the bulk for a constant fibre orientation. It is however assumed here as a first approximation without loss of generality.

### 170 1.2.2. Density and orientation of axonal fibres

By virtue of the volumetric integration of (5), and as explained in more detail in the finite element implementation (see Supplementary Materials), the density of fibres needs to be evaluated locally. This can be directly extracted from white matter diffusion tensor imaging (DTI) data by approximating the axonal density within each voxel  $\rho_a$  by using neurite orientation dispersion and density imaging (NODDI) following:

$$\rho_a = 1 - \sqrt{\frac{1}{2} \left( \frac{3\bar{\lambda}_h}{d} - 1 \right)} \quad (8)$$

where  $d$  is the intrinsic free diffusivity given as  $1.7 \times 10^{-3} \text{ mm}^2\text{s}^{-1}$  [51]. The heuristical corrected mean diffusivity,  $\bar{\lambda}_h$  is given as:

$$\bar{\lambda}_h = \lambda + \frac{b}{6} \left( \sum_{i,j=1}^3 \frac{1 + 2\delta_{ij}}{15} \lambda_i \lambda_j \right) \quad (9)$$

where  $b$  is the  $b$ -value (a factor that reflects the strength and timing of the gradients used to generate diffusion-weighted images),  $\delta_{ij}$  is the Kronecker delta function, and  $\lambda$  is the mean diffusivity given by [51]:

$$\lambda = \frac{\lambda_1 + \lambda_2 + \lambda_3}{3} \quad (10)$$

The orientation of fibres is obtained from the principal DTI eigenvector  $\mathbf{V1}$ , which is a measure of the principal direction of diffusion within each voxel:

$$\begin{aligned} V1_1 &= \cos \psi \\ V1_2 &= \cos \phi \\ V1_3 &= \cos \varphi \end{aligned} \quad (11)$$

where  $\psi$ ,  $\phi$  and  $\varphi$  are the angles with respect to the DTI  $x$ -,  $y$ - and  $z$ -directions, respectively [52].

### 1.3. Finite element implementation and validation

See Supplementary Materials.

## 175 2. Results

The results of this work are two-fold: i) the numerical model per se, making use of the constitutive framework proposed above and ii) its use against a specific experimental setup to study the effect of white matter tract sonication. The finite element implementation of the former for a healthy female macaque  
180 monkey is first presented followed by the latter in the context of ACC sonication.

### 2.1. In silico model

A monkey head model was created from a full-head MRI of a healthy female macaque monkey with  $0.5 \times 0.5 \times 0.5$  mm voxel resolution. The structures of the head were segmented using Amira [53] into white matter, grey matter,  
185 brainstem, cerebral spinal fluid (CSF), cerebellum, and ventricles. The skin, scalp, muscles and eyes were segmented as one material. The material properties of the monkey head model were informed from a range of sources, sometimes involving the use of human data. They are listed in Table 1 along with the references from which they were extracted.

190 Probabilistic tractography [48] was used to reconstruct the projections or the white matter tracts from the ACC, which was the ultrasound target area, to other ROIs that the ACC is interconnected with [13]. With the assumption that the macaque monkey brain is mostly symmetrical, only the tracts on the left hemisphere of the brain were reconstructed. A seed mask for the ACC was  
195 created by selecting a few voxels on the white matter next to the ACC grey matter region. For each of the ROIs, two different masks were created. The first one is the grey matter mask. This was created by selecting the voxels covering the ROI grey matter region. The second one is the white matter mask. This was created by selecting a few voxels in the white matter next to each ROI  
200 grey region. The seed mask and the white matter masks were the ones used in

Table 1: Sound speed and density of the brain regions included the macaque monkey head model.

Materials	Sound speed ( $m/s$ )	Density ( $kg/m^3$ )
White matter	1600 [54]	1030 [55, 54]
Grey matter	1550 [55, 54]	1050 [54]
Ventricles	1515 [55]	1006 [55]
CSF	1515 [55]	1006 [55]
Cerebellum	1537 [56]	1030 [55]
Brainstem	1575	1030 [55]
Skull	3700 [57]	1912 [55]
Flesh	1540 [58]	1059 [59]

the probabilistic tractography to recreate each of the tracts between the ACC and the ROIs [48]. Subsequently, the resulting tractograms were transformed from the volumetric space into structural space to match the segmented monkey head model. The transformed tractograms were then thresholded to weaken the signal and reduce the width of the tracts to ease the selection of a single line of voxels that was used as the final white matter tract in the TUS simulations. All the final tracts started at the same voxel within the seed mask just next to the ACC grey matter region. The last voxel selected was the one closest to each ROI grey matter after extending the tract within the white matter mask to reach the edge of the ROI grey matter.

The relatively low resolution of the macaque diffusion data used in this model constrains the capability of the tractographic algorithms to reconstruct tracts brain areas with a high degree of crossing fibers. Therefore, the white matter tracts for all the brain regions that the ACC is interconnected with were not all recreated. The only tracts obtained were from the ACC to Brodmann areas 8m, 9mc, 24ab, 9-46v and 47-12o. These brain regions can be seen in Fig. 2. The white matter tracts have difference lengths, where the tract for Brodmann area 24ab has 17 voxels, area 9-46v has 16 voxels, area 8m has 38 voxels, area

9m has 28 voxels, and area 47-12o has 28 voxels. The density of axons in each  
 220 voxel within each of the tracts was obtained using (8). For the orientation  
 of the axons in each voxel, the DTI eigenvector  $\mathbf{V1}$  from (11) could not be  
 used because of data corruption when transformed from the volumetric space  
 to structural space due to the low resolution. As a result, each voxel within  
 each of the tracts was instead given a certain orientation to match the direction  
 225 in which the tracts were heading to reach each of the ROIs. The flexoelectric  
 coefficients were  $\tilde{f}_{55} = 0 \text{ C/m}$ ,  $\tilde{f}_{44} = 2 \times 10^{-9} \text{ C/m}$ ,  $\tilde{f}_{33} = 0 \text{ C/m}$ ,  $\tilde{f}_{22} = 0 \text{ C/m}$   
 and  $\tilde{f}_{11} = 0 \text{ C/m}$  [40] for the transversely isotropic flexoelectric tensor.

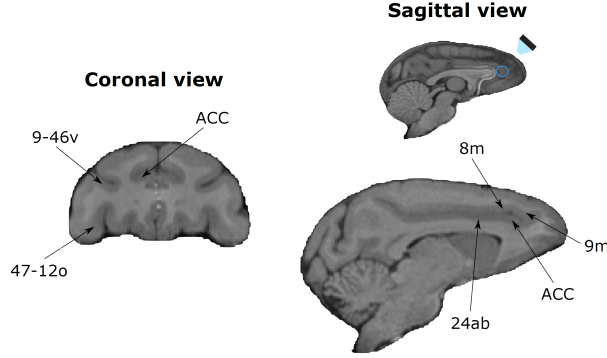


Figure 2: The different ROIs in the monkey brain, and the position of the transducer and coupling cone on the head.

## 2.2. White matter sonication

k-Wave was used to simulate ultrasound propagation by solving a series of  
 230 coupled first-order partial differential equations based on the conservation of  
 mass, momentum and energy within the material, which, when combined, lead  
 to the second-order partial differential single wave equation. The software solves  
 the coupled acoustic equations using the k-space pseudo spectral method where  
 the spatial derivative is solved using fast Fourier transform and the temporal  
 235 derivative is solved using the finite difference scheme. As the finite difference ap-  
 proximation of the temporal derivative limits the size of the time step, a  $k$ -space

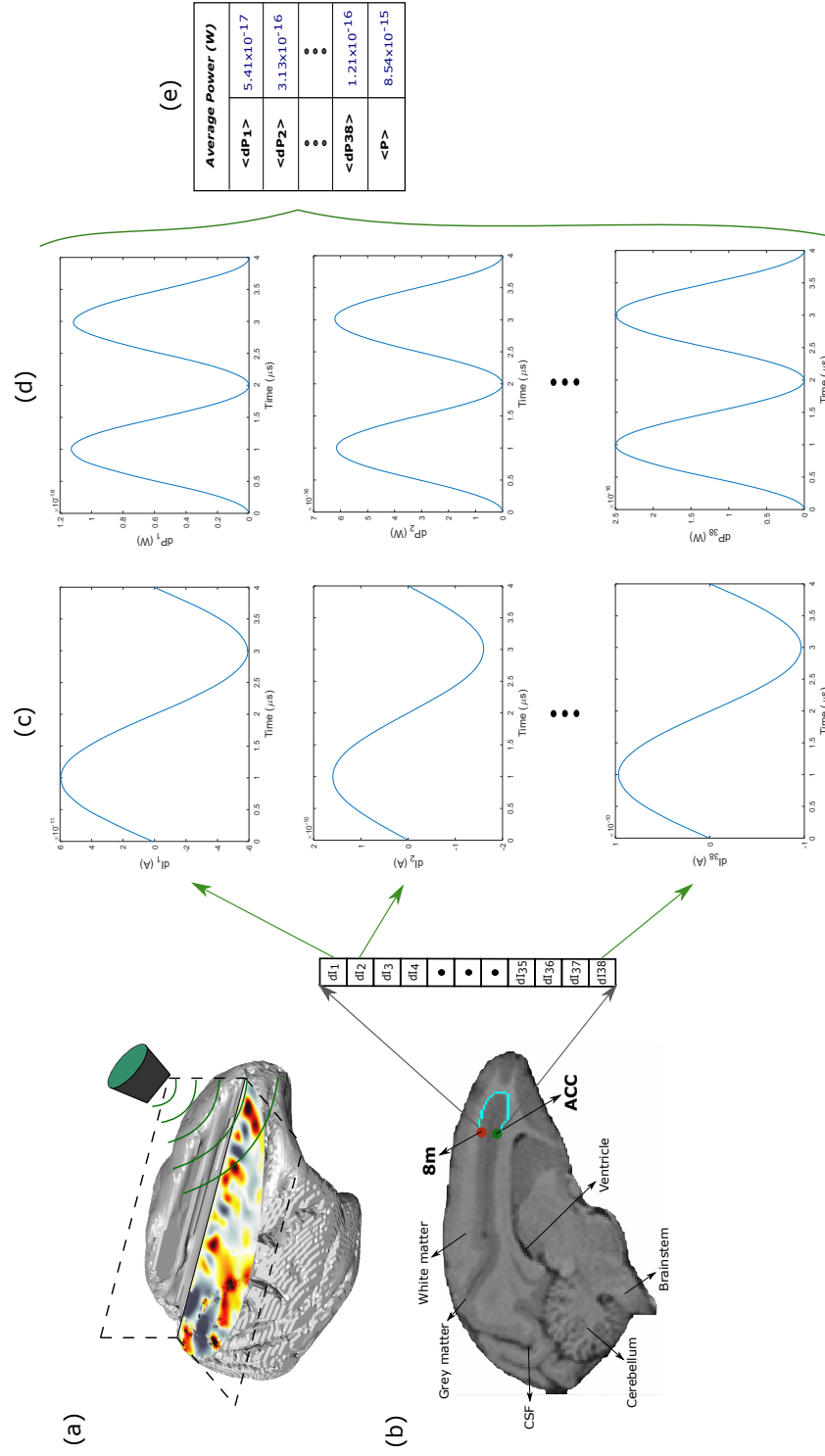


Figure 3: (a) In silico macaque head model sonicated with k-Wave; (b) white matter tract between the target region (ACC) and one of the ROIs, here 8m; (c) induced current for each element within the white matter tract after steady state is reached; (d) corresponding maximum induced power; (e) corresponding steady state average induced power and over all average induced power for the entire tract.

method (a temporal propagator expressed in the spatial frequency domain) is used to relax this limitation, thus allowing for larger time steps without compromising on accuracy. k-Wave also uses a staggered spatial and temporal scheme for additional accuracy and stability [60]. The staggered grid defines the pressure on the non-staggered nodes and the velocity on the staggered nodes where the  $x$ -velocity and the  $y$ -velocity is defined on the staggered nodes. k-Wave can also provide both the  $x$ - and  $y$ -velocities on the non-staggered nodes. The  $x$ -,  $y$ - and  $z$ -velocity values were obtained from k-Wave and integrated to obtain the displacement values on the nodes. The remaining  $x$ -,  $y$ -, and  $z$ -displacements on the staggered grid were obtained by taking the average between neighbouring non-staggered nodes.

A train of continuous sinusoidal ultrasound wave of  $250\text{ kHz}$  and  $1.17\text{ MPa}$  was applied to the target region (ACC) using a transducer with a  $64\text{ mm}$  diameter and  $63\text{ mm}$  radius of curvature, as in the experimental setup [13]. This was positioned towards the front of the head at an inclination of  $30^\circ$  to the ACC. Water with material properties of  $1480\text{ m/s}$  and  $1000\text{ kg/m}^3$  [55] and a thickness of  $47\text{ mm}$  was placed between the transducer and the monkey head to allow for full acoustic coupling between the transducer and the head or scalp. Fig. 2 shows the position of the coupling cone with water and the transducer on the head model, noting that this figure does not include the flesh and skull in the illustration. The simulation for each white matter tract was run for  $8\text{ ms}$  reaching the steady state at around  $7\text{ ms}$ , which took  $\sim 38$  days using a single compute node with 14 cores for processing, see illustration of the simulation in Fig. 3-a.

The induced current in each voxel  $dI$  was calculated using (5) after steady state was reached in all tracts linking ACC to 8m, 9mc, 24ab, 9-46v and 47-12o, see Figures 3-b and 3-c for the 8m ROI. The power  $dP$  “absorbed” by one voxel (and transformed into cell excitation energy) can then be defined as:

$$dP = dI^2 R \quad (12)$$

where  $R$  is the electrical resistance of the brain white matter within the voxel:

$$R = \frac{\rho_R L}{A} \quad (13)$$

$\rho_R = 3.91 \Omega m$  is the resistivity of white matter [61],  $L$  is the length of the axon and  $A$  is the cross-sectional area of the axon within the voxel, see Fig. 3-d for the 8m ROI.

The total maximum current  $I$  and total maximum power  $P$  were obtained by summing  $dI$  and  $dP$  for all the voxels within the white matter tract and taking the peak value  $dI_{peak}$  for one cycle. The average current  $\langle dI \rangle$  for each voxel is given by:

$$\langle dI \rangle = \sqrt{\frac{dI_{peak}^2}{2}} \quad (14)$$

and the total average current  $\langle I \rangle$  is taken by summing all the voxels within the white matter tract. Noting that  $\langle dI^2 \rangle = \frac{dI_{peak}^2}{2}$  where  $dI_{peak}$  is the peak value of the sinusoidal induced current, the average power  $\langle dP \rangle$  per cycle for each voxel can be calculated from:

$$\langle dP \rangle = \frac{dI_{peak}^2}{2} R \quad (15)$$

and is given for each voxel of the tract, see Fig. 3-e for the 8m ROI. The total  
 265 average power  $\langle P \rangle$  was taken by summing the  $\langle dP \rangle$  of all the voxels within the white matter tract, see Fig. 3-e for the 8m ROI.

This procedure was done for all five ROIs and the total steady state maximum and average current and power, induced steady state maximum and average current and power for the first three voxels (closest to the ROI) and last  
 270 three voxels (closest to ACC) are given as spider graphs in Fig. 4.

### 3. Discussion

Building on the original observation of flexoelectricity in liquid crystals, Petrov hypothesised that phospholipid membranes could also exhibit flexoelectricity [62]. Supporting this, his work and others' demonstrated that a change  
 275 in the curvature of these membranes could alter the membrane polarisation



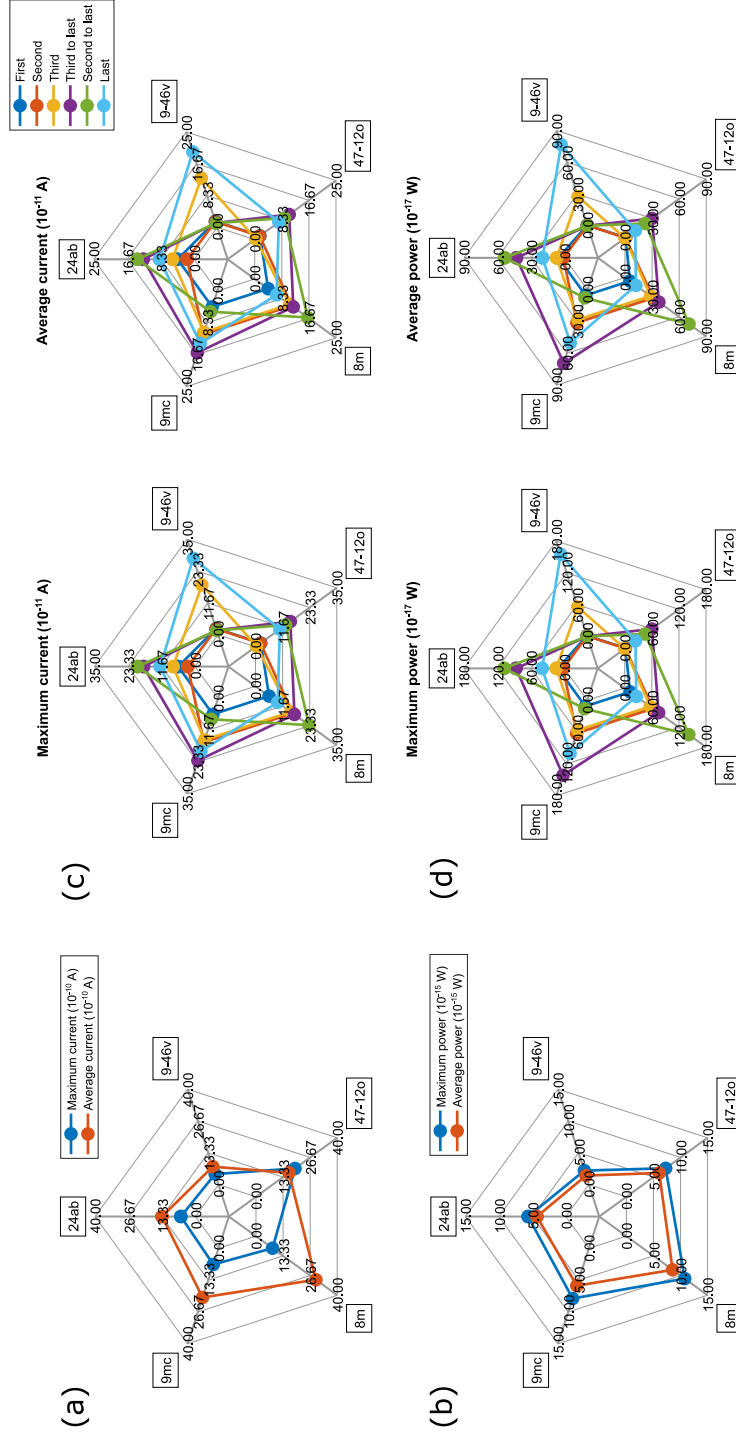


Figure 4: (a) Total steady state maximum and average current for the white matter tracts, (b) total steady state maximum and average power for the tracts, (c) induced steady state maximum and average current for each voxel showing the first three voxels and last three voxels within each tract, and (d) corresponding induced steady state maximum and average power for each voxel.

[63, 64]. Flexoelectricity was found to be likely to play a role in several biological membrane functions involving changes in the curvature of a membrane, e.g., exocytosis, endocytosis or even cell migration [65]. Whether in the context of biological membrane or more generally liquid crystals, flexoelectricity inherently  
280 requires any model to focus on the deformation of the underlying microstructure, which naturally precludes a straightforward upscaling of the phenomenon, e.g., from axonal membrane to white matter brain tissue.

In this paper, a theoretical framework for homogenised bulk flexoelectricity was proposed and validated by focussing on cylindrical representations of axons. The resulting formulation only requires the knowledge of axonal density  
285 and orientation readily accessible through DTI to compute the resulting current increment in the element of interest when submitted to a given deformation. Depending on the state of deformation, current can then be generated (maximum when the strain gradient in the underlying axons is maximised, e.g., pure bending) or not (when the deformation does not lead to any strain gradient, e.g.,  
290 uniaxial tension or compression in the axonal direction). For the sake of providing a calibration strategy, the model was calibrated on a micromechanical model of flexoelectricity developed by Chen *et al.* [40] where the local deformation of the membrane induces a membrane polarisation through flexoelectricity in a 2D problem. It is important to emphasise that the proposed approach does  
295 *not* however require flexoelectricity to be the main driving phenomenon at the membrane level. Instead, the proposed approach can be used as a phenomenological model for any system whose time-varying strain gradient deformation is observed to lead to current generation. This is in particular in line with the electromechanical coupling phenomena observed in the context of action potential generation [36]. Indeed, whether mechanosensitive ion channels, membrane  
300 movement through phase transition [66] or flexoelectricity [28], among others, are at the origin of this coupling, all these hypotheses do lead to the same observation at the mesoscale, which is phenomenologically captured by the proposed model. This approach has important implications in the context of ultrasound  
305 neuromodulation, as it does not necessarily need to postulate the exact nature

of the underlying mechanisms, and thus, by working at the tissue scale, benefits from an enhanced scalability. This has direct implications in problems requiring hundreds or thousands of simulations, such as the optimisation of sonication parameters for a given disease and subject.

Here, we leverage the model to explore the possibility that ultrasound mediated white matter tract stimulation could be responsible for discrepancies observed in the connectivity fingerprint of sonicated ACC in macaque monkeys [13]. In this experiment, both the ACC and amygdala of macaque monkeys were targeted with TUS. The measured BOLD signal activities from both the left and right hemispheres of the brain were obtained from 9 monkeys for the control, 4 monkeys post amygdala TUS and 3 monkeys post ACC TUS. The BOLD signal measurements were averaged and used to create the functional connectivity fingerprints of the ACC and amygdala [13]. The connectivity fingerprint is defined as a pattern of activity coupling that reflects a unique constellation of projections and interactions of a specific brain area, e.g., ACC and/or amygdala [67]. These connectivity fingerprints were normalised, where a value of 0 was given to the weakest connection of a given ROI with the target area, and a value of 1 was given to the strongest connection with the target area [68]. Note that it is only a relative measure of activity change in that specific area in regards to external activity or activity recorded from other brain areas. Therefore, it can only correlate the BOLD activity of a specific target area, e.g., ACC and/or amygdala with the BOLD activity in other areas, the ROIs [69].

As mentioned previously, the relatively low resolution of the macaque diffusion data used in this model was a limitation of this work, constraining the capability of the tractographic algorithms to reconstruct tracts brain areas with a high degree of crossing fibers such as in the white matter close to the amygdala. For this reason, amygdala connections could not be reliably recreated in silico. Because of this, only the tracts from the ACC to Brodmann areas 8m, 9mc, 24ab, 9-46v and 47-12o for the left hemisphere were recreated. To compare the model to the experiment, a relative change (see Fig. 5-a) and an absolute change (see Fig. 5-b) were obtained from the connectivity fingerprint of the

ACC using the control and ACC TUS results for Brodmann areas 8m, 9mc, 24ab, 9-46v and 47-12o. Fig. 5 shows how much the activity coupling between the ACC and other brain regions have changed or decreased due to the loss of coupling after ACC TUS. Simply, these spider graphs quantify the degree of change in correlation between the neural activity within the ACC and the 5 ROIs of interest, between the non-sonicated and the sonicated areas. The relative and absolute change both show a very similar trend. Brodmann area 8m had the highest relative and absolute change, followed by Brodmann area 9mc, 24ab, 47-12o and 9-46v, respectively. Specifically, from Fig. 5-a, the relative change in activity coupling was 49% for area 8m, 28% for area 9mc, 25% for area 24ab, 20% for area 47-12o, and 18% for area 9-46v. From Fig. 5-b, the absolute change in activity coupling was 0.16 for area 8m, 0.14 for area 9mc, 0.06 for area 24ab, 0.05 for area 47-12o, and 0.03 for area 9-46v. Note that the regions that were observed to have an enhanced correlation could not be captured for the issues of resolution mentioned above.

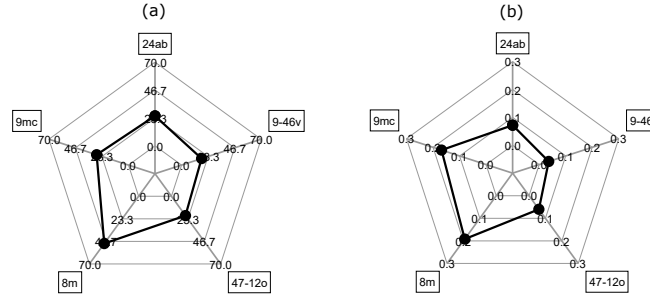


Figure 5: (a) Relative change between the experimental control and ACC TUS in the connectivity fingerprint of ACC, (b) Absolute change between the experimental control and ACC TUS in the connectivity fingerprint of ACC.

Maybe the most important property of white matter is its intrinsic anisotropy, i.e., the fibre orientation. This has obvious electrophysiological implications—the current is mainly flowing in this direction—but also mechanical—the tissue’s stiffness differs depending on the loading direction [70]. This duality means that any attempt at coupling electrophysiology and mechanics in the white matter

needs to account for this anisotropy [71]. Accordingly, the proposed methodology assumes that current generation solely occurs when strain gradient occurs and is time-varying (strain gradient phenomenologically polarises the tissue, but current is only generated when the polarisation is changing with time). This leads to the observation that a pressure wave in the direction of the fibre is less likely to generate current than when at an angle with it, where the axon can thus vibrate in bending mode. As can be seen in Fig. 2, three ROIs (8m, 9m and 24ab) are relatively close to ACC, while 9-46v and 47-12o are further away. However, the fact the pressure field is non-zero outside of the target region (because of, e.g., tissue inhomogeneity or skull morphology) does not necessarily mean that the white matter tracts around the distal ROIs should be less sonicated than around the closest ones. The additional effect of fibre orientation with respect to the pressure wave further impedes any straightforward prediction. Indeed, whether focussing on the current or power (maximum or average), the model predicts very little current generation in the white matter tract immediately leaving the ACC, but some activity in the second voxel for the tracts going to the 9-46v, 8m and 9mc, see Figures 3-b, 3-c, 4-c and 4-d. This is directly linked to the fibre orientation change from the first to the second voxel along with potential change in pressure level. More generally, this figure also shows that there is no obvious relation between the level of induced current or power in a voxel and its distance to the target or ROI, e.g., see the few occurrences of abrupt change of current or power between one voxel and its neighbour (e.g., second and third for 9-46v). Again, the non-straightforward combination of rotation of the fibre when going from one voxel to another (sometime abrupt, see Fig. 3-b) along with pressure level changes are driving these trends (or lack thereof). This further highlights the fact that outside of the targeted grey matter region, the level of white matter current generation cannot be straightforwardly estimated without numerical prediction, especially if indeed it is fibre orientation dependent, such as proposed here. Instead, we thus proposed to focus on averaged or maximum cumulated values across the entire tract.

When comparing the experimental results in Fig. 5 with the numerical

predictions in Figures 4-a and 4-b, higher mediated total current and power  
 390 contributions do seem correlate with a higher observed loss of activity coupling  
 between the ACC and other ROIs. This correlation however, is less obvious  
 for 47-12o. In particular, in the attempt of finding a simple qualitative relation  
 between the numerical predictions and the experimental observations a linear  
 regression was done between all simulations and both experimental measure-  
 395 ments (absolute and relative differences). Both experimental measures were  
 found to be roughly equivalent, but a strong correlation with an  $R^2$  of 0.85 was  
 found when comparing against the average induced current in the entire tract,  
 the lowest being when using maximum current with an  $R^2$  of 0.02. The power  
 was found to be slightly less predictive than the average current (with values of  
 400  $R^2$  in the region of 0.64-0.73). A possible explanation for this is that a higher  
 current generated within the tract heading towards a particular ROI may be  
 causing a greater disruption in the electrical activity of that brain region. This  
 could potentially cause a greater change in the BOLD signal activity being mea-  
 sured in the ROIs after TUS, which causes a greater loss of activity coupling  
 405 between the ACC and these regions. Such observation feeds directly into the  
 wider discussion of the use of neuromodulation for pain management, where a  
 current is understood to block the signal in a similar fashion [72, 73].

Neuromodulation studies on treatment-resistant depression have shown that  
 using DBS to stimulate the white matter tracts adjacent to the subcallosal cin-  
 410 gulate (SCC) region can lead to antidepressant effects [74, 75, 76] similar to  
 when targeting the immediately adjacent grey matter [77, 75]. In particular,  
 SCC DBS can normalise the activity abnormalities at the SCC and other of  
 brain regions connected to the SCC [76]. This suggests that DBS drives focal  
 activity at the SCC, which then leads to the inhibition or excitation of the con-  
 415 nected adjacent and remote regions [75]. This, in turn, disrupts the pathological  
 activity in limbic-cortical circuits, which underlies depression, thus allowing for  
 more normal cerebral function and behaviour [77]. It was also demonstrated  
 that the response to SCC DBS could be mediated by the direct impact in three  
 specific distinct fibre bundles on the SCC white matter (the bilateral forceps

420 minor of the anterior corpus callosum, the bilateral cingulum bundles, and the  
 medial branch of the uncinate fasciculus) [78, 79]. Taken together, such results  
 point towards a more important role for white matter sonication than generally  
 considered in TUS. These results on the DBS neuromodulation of the SCC and  
 adjacent white matter [75] also confirm that the differences observed here in the  
 425 magnitude of loss of coupling between the ROIs and the sonicated ACC (see  
 Fig. 5) may indeed arise from the “spill-out” sonication of the neighbouring  
 white matter tracts adjacent to the target area. This means that white matter  
 density and orientation for the different ROI tracts leaving the ACC need to  
 be accounted for when sonicating the ACC. The complexity of the head mor-  
 430 phology, material properties of the different brain regions and TUS setup thus  
 require the use of in silico predictions, such as proposed here.

To conclude, despite the limited number of ROIs (only five could be used  
 from the original experiments), the results show a strong correlation between  
 the induced maximum current in the entire tracts leaving the sonicated region,  
 435 the ACC, and the change in connectivity with the corresponding ROIs, where  
 more current leads to a stronger loss of connectivity. The model is, however,  
 not without limitations. Its validation would benefit from additional experi-  
 ments. Other sonicated regions and other ROIs would be required. Validation  
 on different brain/skull morphologies would also ensure that these changes can  
 440 acquire a patient-specific dimension. It is also very qualitative in nature and,  
 while the linear regression used here can predict the connectivity loss between  
 the ACC and the ROIs, the resulting relation is not necessarily conserved in  
 another setup. More work is thus needed in this respect. Overall though, the  
 adaptation of the theoretical framework in 3D can be further used to study  
 445 TUS to examine the connectivities within the brain as well as the important  
 role of white matter tracts in disrupting brain activity within circuits. This  
 work contributes to the advancement of knowledge on the use of ultrasound as  
 a neuromodulation tool as it can potentially help with the establishment of TUS  
 safety protocol, e.g., by identifying the optimum ultrasound protocol or param-  
 450 eters for the successful treatment of neurological and psychiatric disorders. In

particular, it will help identifying how the connectivity to distal cortical regions is affected during the sonication of a specific region. Future work shall aim at confirming such approach by, e.g., sonicating the white matter with the same protocol used in Ref. [13], but in the white matter tracts proximal to the ACC, and studying the effect on the connectivity fingerprint of the ACC.

#### 4. Conflict of interest

The authors declare that there is no conflict of interest.

#### 5. Acknowledgment

C.F and A.J. acknowledge funding from the EPSRC Healthcare Technologies Challenge Award No. EP/N020987/1.

#### 6. Supplementary information

##### 6.1. Finite element formulation

In a finite element approximation, the polarisation gradient is obtained from

$$\nabla \cdot \tilde{\mathbf{P}} = \nabla \cdot \left( \tilde{\mathbf{f}} \cdot \mathbf{B} \cdot \mathbf{d}^e \right) \quad (16)$$

where  $\mathbf{B}$  is the shape function second derivative matrix and  $\mathbf{d}^e$  is the displacement vector for a bulk element  $e$ .  $\mathbf{B}$  is obtained by making use of the gradient matrices  $\mathbf{L}_1$  and  $\mathbf{L}_2$ , and shape function matrix  $\mathbf{N}$  [80]:

$$\mathbf{B} = \mathbf{L}_2 \cdot \mathbf{L}_1 \cdot \mathbf{N} \quad (17)$$

##### 6.1.1. 2D model

For the 2D formulation, 8-node elements are used, see Fig. 6.



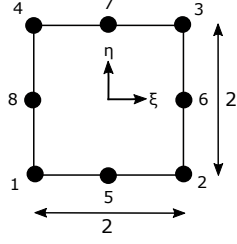


Figure 6: 8-node 2D quadrilateral element in the isoparametric reference frame  $(\xi, \eta)$ .

The displacement vector  $\mathbf{d}^e$  for one element is thus written as

$$\mathbf{d}^e = \begin{bmatrix} d_x^1 \\ d_y^1 \\ d_x^2 \\ d_y^2 \\ d_x^3 \\ d_y^3 \\ d_x^4 \\ d_y^4 \\ d_x^5 \\ d_y^5 \\ d_x^6 \\ d_y^6 \\ d_x^7 \\ d_y^7 \\ d_x^8 \\ d_y^8 \end{bmatrix}^T \quad (18)$$

The shape function tensor  $\mathbf{N}$  is:

$$\mathbf{N} = \begin{bmatrix} N_1 & 0 & N_2 & 0 & N_3 & 0 & \cdot & \cdot & N_8 & 0 \\ 0 & N_1 & 0 & N_2 & 0 & N_3 & \cdot & \cdot & 0 & N_8 \end{bmatrix} \quad (19)$$

The first derivative gradient tensor  $\mathbf{L}_1$  is:

$$\mathbf{L}_1 = \begin{bmatrix} \frac{\partial}{\partial x} & 0 \\ 0 & \frac{\partial}{\partial y} \\ \frac{\partial}{\partial y} & \frac{\partial}{\partial x} \end{bmatrix} \quad (20)$$

The second derivative gradient tensor  $\mathbf{L}_2$  is:

$$\mathbf{L}_2 = \begin{bmatrix} \frac{\partial}{\partial x} & 0 & 0 \\ \frac{\partial}{\partial y} & 0 & 0 \\ 0 & \frac{\partial}{\partial x} & 0 \\ 0 & \frac{\partial}{\partial y} & 0 \\ 0 & 0 & \frac{\partial}{\partial x} \\ 0 & 0 & \frac{\partial}{\partial y} \end{bmatrix} \quad (21)$$

Making use of (19), (20), and (21), (17) becomes:

$$\mathbf{B} = \begin{bmatrix} \frac{\partial^2 N_1}{\partial x^2} & 0 & \frac{\partial^2 N_2}{\partial x^2} & 0 & \frac{\partial^2 N_3}{\partial x^2} & 0 & \cdot & \cdot & \frac{\partial^2 N_8}{\partial x^2} & 0 \\ \frac{\partial^2 N_1}{\partial x \partial y} & 0 & \frac{\partial^2 N_2}{\partial x \partial y} & 0 & \frac{\partial^2 N_3}{\partial x \partial y} & 0 & \cdot & \cdot & \frac{\partial^2 N_8}{\partial x \partial y} & 0 \\ 0 & \frac{\partial^2 N_1}{\partial x \partial y} & 0 & \frac{\partial^2 N_2}{\partial x \partial y} & 0 & \frac{\partial^2 N_3}{\partial x \partial y} & \cdot & \cdot & 0 & \frac{\partial^2 N_8}{\partial x \partial y} \\ 0 & \frac{\partial^2 N_1}{\partial y^2} & 0 & \frac{\partial^2 N_2}{\partial y^2} & 0 & \frac{\partial^2 N_3}{\partial y^2} & \cdot & \cdot & 0 & \frac{\partial^2 N_8}{\partial y^2} \\ \frac{\partial^2 N_1}{\partial x \partial y} & \frac{\partial^2 N_1}{\partial x^2} & \frac{\partial^2 N_2}{\partial x \partial y} & \frac{\partial^2 N_2}{\partial x^2} & \frac{\partial^2 N_3}{\partial x \partial y} & \frac{\partial^2 N_3}{\partial x^2} & \cdot & \cdot & \frac{\partial^2 N_8}{\partial x \partial y} & \frac{\partial^2 N_8}{\partial x^2} \\ \frac{\partial^2 N_1}{\partial y^2} & \frac{\partial^2 N_1}{\partial x \partial y} & \frac{\partial^2 N_2}{\partial y^2} & \frac{\partial^2 N_2}{\partial x \partial y} & \frac{\partial^2 N_3}{\partial y^2} & \frac{\partial^2 N_3}{\partial x \partial y} & \cdot & \cdot & \frac{\partial^2 N_8}{\partial y^2} & \frac{\partial^2 N_8}{\partial x \partial y} \end{bmatrix} \quad (22)$$

The shape functions of the 8-noded quadratic element expressed in the local

natural coordinates are (see Fig. 6):

$$\begin{aligned}
N_1 &= \frac{1}{4}(1 - \xi)(1 - \eta)(-1 - \xi - \eta) \\
N_2 &= \frac{1}{4}(1 + \xi)(1 - \eta)(-1 + \xi - \eta) \\
N_3 &= \frac{1}{4}(1 + \xi)(1 + \eta)(-1 + \xi + \eta) \\
N_4 &= \frac{1}{4}(1 - \xi)(1 + \eta)(-1 - \xi + \eta) \\
N_5 &= \frac{1}{2}(1 - \xi^2)(1 - \eta) \\
N_6 &= \frac{1}{2}(1 + \xi)(1 - \eta^2) \\
N_7 &= \frac{1}{2}(1 - \xi^2)(1 + \eta) \\
N_8 &= \frac{1}{2}(1 - \xi)(1 - \eta^2)
\end{aligned} \tag{23}$$

From (23), the third derivatives of the shape functions are:

$$\begin{aligned}
\frac{\partial^3 N_1}{\partial \xi^3} &= 0 \\
\frac{\partial^3 N_2}{\partial \xi^3} &= 0 \\
\frac{\partial^3 N_3}{\partial \xi^3} &= 0 \\
\frac{\partial^3 N_4}{\partial \xi^3} &= 0 \\
\frac{\partial^3 N_5}{\partial \xi^3} &= 0 \\
\frac{\partial^3 N_6}{\partial \xi^3} &= 0 \\
\frac{\partial^3 N_7}{\partial \xi^3} &= 0 \\
\frac{\partial^3 N_8}{\partial \xi^3} &= 0
\end{aligned}$$

$$\frac{\partial^3 N_1}{\partial \eta^3} = 0$$

$$\frac{\partial^3 N_2}{\partial \eta^3} = 0$$

$$\frac{\partial^3 N_3}{\partial \eta^3} = 0$$

$$\frac{\partial^3 N_4}{\partial \eta^3} = 0$$

$$\frac{\partial^3 N_5}{\partial \eta^3} = 0$$

$$\frac{\partial^3 N_6}{\partial \eta^3} = 0$$

$$\frac{\partial^3 N_7}{\partial \eta^3} = 0$$

$$\frac{\partial^3 N_8}{\partial \eta^3} = 0$$

$$\frac{\partial^3 N_1}{\partial \xi^2 \partial \eta} = -\frac{1}{2}$$

$$\frac{\partial^3 N_2}{\partial \xi^2 \partial \eta} = -\frac{1}{2}$$

$$\frac{\partial^3 N_3}{\partial \xi^2 \partial \eta} = \frac{1}{2}$$

$$\frac{\partial^3 N_4}{\partial \xi^2 \partial \eta} = \frac{1}{2}$$

$$\frac{\partial^3 N_5}{\partial \xi^2 \partial \eta} = 1$$

$$\frac{\partial^3 N_6}{\partial \xi^2 \partial \eta} = 0$$

$$\frac{\partial^3 N_7}{\partial \xi^2 \partial \eta} = -1$$

$$\frac{\partial^3 N_8}{\partial \xi^2 \partial \eta} = 0$$

$$\begin{aligned}
\frac{\partial^3 N_1}{\partial \xi \partial \eta^2} &= -\frac{1}{2} \\
\frac{\partial^3 N_2}{\partial \xi \partial \eta^2} &= \frac{1}{2} \\
\frac{\partial^3 N_3}{\partial \xi \partial \eta^2} &= \frac{1}{2} \\
\frac{\partial^3 N_4}{\partial \xi \partial \eta^2} &= -\frac{1}{2} \\
\frac{\partial^3 N_5}{\partial \xi \partial \eta^2} &= 0 \\
\frac{\partial^3 N_6}{\partial \xi \partial \eta^2} &= -1 \\
\frac{\partial^3 N_7}{\partial \xi \partial \eta^2} &= 0 \\
\frac{\partial^3 N_8}{\partial \xi \partial \eta^2} &= 1
\end{aligned} \tag{24}$$

The unrotated transversely isotropic volumetric flexoelectric tensor  $\tilde{\mathbf{f}}$  ( $\tilde{f}_{ijkl}$  in the manuscript) follows the same notation as its surface counterpart [81]

$$\tilde{\mathbf{f}} = \begin{bmatrix} \tilde{f}_{1111} & 0 & \tilde{f}_{1221} & 0 & 0 & \tilde{f}_{1122} \\ 0 & \tilde{f}_{2112} & 0 & \tilde{f}_{2222} & \tilde{f}_{2121} & 0 \end{bmatrix} \tag{25}$$

or, by virtue of symmetry [50, 82],

$$\tilde{\mathbf{f}} = \begin{bmatrix} \tilde{f}_{11} & 0 & \tilde{f}_{55} & 0 & 0 & \tilde{f}_{55} \\ 0 & \tilde{f}_{44} & 0 & \tilde{f}_{22} & \tilde{f}_{44} & 0 \end{bmatrix} \tag{26}$$

465 where  $\tilde{f}_{11} = \tilde{f}_{1111}$ ,  $\tilde{f}_{22} = \tilde{f}_{2222}$ ,  $\tilde{f}_{44} = \tilde{f}_{2112} = \tilde{f}_{2121}$  and  $\tilde{f}_{55} = \tilde{f}_{1221} = \tilde{f}_{1122}$ .

To change the orientation of the fibre, the 2D coordinate system rotation matrix used to rotate  $\tilde{\mathbf{f}}$  through a clockwise angle  $\theta$  is:

$$\mathbf{Q} = \begin{bmatrix} \cos \theta & -\sin \theta \\ \sin \theta & \cos \theta \end{bmatrix} \tag{27}$$

This rotation gives the resulting rotated  $\tilde{\mathbf{f}}$  ( $\tilde{f}_{rmns}$  in the manuscript) [81]:

$$\tilde{\mathbf{f}} = \begin{bmatrix} \tilde{f}_{1111} & \tilde{f}_{1112} & \tilde{f}_{1221} & \tilde{f}_{1222} & \tilde{f}_{1121} & \tilde{f}_{1122} \\ \tilde{f}_{2111} & \tilde{f}_{2112} & \tilde{f}_{2221} & \tilde{f}_{2222} & \tilde{f}_{2121} & \tilde{f}_{2122} \end{bmatrix} \tag{28}$$

Note that, while a compact form for the rotated flexoelectric tensor can still be used, the symmetry of (26) cannot be assumed and the full compact tensor needs to be considered.

For a quadrilateral element of size  $2a \times 2b$ , the Jacobian matrix  $\mathbf{J}$  between the original reference frame and the isoparametric reference frame is given by:

$$\mathbf{J} = \begin{bmatrix} \frac{\partial x}{\partial \xi} & \frac{\partial y}{\partial \xi} \\ \frac{\partial x}{\partial \eta} & \frac{\partial y}{\partial \eta} \end{bmatrix} = \begin{bmatrix} a & 0 \\ 0 & b \end{bmatrix} \quad (29)$$

The polarisation gradient in (16) can be obtained by multiplying (28), (21),

(20), (19), and (18) together, and taking its divergence:

$$\begin{aligned}
\nabla \cdot \tilde{\mathbf{P}} = & \tilde{f}_{1111} \left[ (d_x^1) \frac{\partial^3 N_1}{\partial x^3} + (d_x^2) \frac{\partial^3 N_2}{\partial x^3} + (d_x^3) \frac{\partial^3 N_3}{\partial x^3} + (d_x^4) \frac{\partial^3 N_4}{\partial x^3} + \right. \\
& \left. (d_x^5) \frac{\partial^3 N_5}{\partial x^3} + (d_x^6) \frac{\partial^3 N_6}{\partial x^3} + (d_x^7) \frac{\partial^3 N_7}{\partial x^3} + (d_x^8) \frac{\partial^3 N_8}{\partial x^3} \right] + \\
& \tilde{f}_{1112} \left[ (d_x^1) \frac{\partial^3 N_1}{\partial x^2 \partial y} + (d_x^2) \frac{\partial^3 N_2}{\partial x^2 \partial y} + (d_x^3) \frac{\partial^3 N_3}{\partial x^2 \partial y} + (d_x^4) \frac{\partial^3 N_4}{\partial x^2 \partial y} + \right. \\
& \left. (d_x^5) \frac{\partial^3 N_5}{\partial x^2 \partial y} + (d_x^6) \frac{\partial^3 N_6}{\partial x^2 \partial y} + (d_x^7) \frac{\partial^3 N_7}{\partial x^2 \partial y} + (d_x^8) \frac{\partial^3 N_8}{\partial x^2 \partial y} \right] + \\
& \tilde{f}_{1221} \left[ (d_y^1) \frac{\partial^3 N_1}{\partial x^2 \partial y} + (d_y^2) \frac{\partial^3 N_2}{\partial x^2 \partial y} + (d_y^3) \frac{\partial^3 N_3}{\partial x^2 \partial y} + (d_y^4) \frac{\partial^3 N_4}{\partial x^2 \partial y} + \right. \\
& \left. (d_y^5) \frac{\partial^3 N_5}{\partial x^2 \partial y} + (d_y^6) \frac{\partial^3 N_6}{\partial x^2 \partial y} + (d_y^7) \frac{\partial^3 N_7}{\partial x^2 \partial y} + (d_y^8) \frac{\partial^3 N_8}{\partial x^2 \partial y} \right] + \\
& \tilde{f}_{1222} \left[ (d_y^1) \frac{\partial^3 N_1}{\partial x \partial y^2} + (d_y^2) \frac{\partial^3 N_2}{\partial x \partial y^2} + (d_y^3) \frac{\partial^3 N_3}{\partial x \partial y^2} + (d_y^4) \frac{\partial^3 N_4}{\partial x \partial y^2} + \right. \\
& \left. (d_y^5) \frac{\partial^3 N_5}{\partial x \partial y^2} + (d_y^6) \frac{\partial^3 N_6}{\partial x \partial y^2} + (d_y^7) \frac{\partial^3 N_7}{\partial x \partial y^2} + (d_y^8) \frac{\partial^3 N_8}{\partial x \partial y^2} \right] + \\
& \tilde{f}_{1121} \left[ (d_x^1) \frac{\partial^3 N_1}{\partial x^2 \partial y} + (d_y^1) \frac{\partial^3 N_1}{\partial x^3} + (d_x^2) \frac{\partial^3 N_2}{\partial x^2 \partial y} + (d_y^2) \frac{\partial^3 N_2}{\partial x^3} + \right. \\
& (d_x^3) \frac{\partial^3 N_3}{\partial x^2 \partial y} + (d_y^3) \frac{\partial^3 N_3}{\partial x^3} + (d_x^4) \frac{\partial^3 N_4}{\partial x^2 \partial y} + (d_y^4) \frac{\partial^3 N_4}{\partial x^3} + \\
& (d_x^5) \frac{\partial^3 N_5}{\partial x^2 \partial y} + (d_y^5) \frac{\partial^3 N_5}{\partial x^3} + (d_x^6) \frac{\partial^3 N_6}{\partial x^2 \partial y} + (d_y^6) \frac{\partial^3 N_6}{\partial x^3} + \\
& \left. (d_x^7) \frac{\partial^3 N_7}{\partial x^2 \partial y} + (d_y^7) \frac{\partial^3 N_7}{\partial x^3} + (d_x^8) \frac{\partial^3 N_8}{\partial x^2 \partial y} + (d_y^8) \frac{\partial^3 N_8}{\partial x^3} \right] +
\end{aligned}$$

[illegible]



Making use of (29), (24) and (30) leads to:

$$\begin{aligned}
\nabla \cdot \tilde{\mathbf{P}} = & \tilde{f}_{1112} \left[ (d_x^1) \frac{-1}{2a^2b} + (d_x^2) \frac{-1}{2a^2b} + (d_x^3) \frac{1}{2a^2b} + (d_x^4) \frac{1}{2a^2b} + (d_x^5) \frac{1}{a^2b} + (d_x^7) \frac{-1}{a^2b} \right] + \\
& \tilde{f}_{1221} \left[ (d_y^1) \frac{-1}{2a^2b} + (d_y^2) \frac{-1}{2a^2b} + (d_y^3) \frac{1}{2a^2b} + (d_y^4) \frac{1}{2a^2b} + (d_y^5) \frac{1}{a^2b} + (d_y^7) \frac{-1}{a^2b} \right] + \\
& \tilde{f}_{1222} \left[ (d_y^1) \frac{-1}{2ab^2} + (d_y^2) \frac{1}{2ab^2} + (d_y^3) \frac{1}{2ab^2} + (d_y^4) \frac{-1}{2ab^2} + (d_y^6) \frac{-1}{ab^2} + (d_y^8) \frac{1}{ab^2} \right] + \\
& \tilde{f}_{1121} \left[ (d_x^1) \frac{-1}{2a^2b} + (d_x^2) \frac{-1}{2a^2b} + (d_x^3) \frac{1}{2a^2b} + (d_x^4) \frac{1}{2a^2b} + (d_x^5) \frac{1}{a^2b} + (d_x^7) \frac{-1}{a^2b} \right] + \\
& \tilde{f}_{1122} \left[ (d_x^1) \frac{-1}{2ab^2} + (d_y^1) \frac{-1}{2a^2b} + (d_x^2) \frac{1}{2ab^2} + (d_y^2) \frac{-1}{2a^2b} + (d_x^3) \frac{1}{2ab^2} + (d_y^3) \frac{1}{2a^2b} + \right. \\
& \quad \left. (d_x^4) \frac{-1}{2ab^2} + (d_y^4) \frac{1}{2a^2b} + (d_y^5) \frac{1}{a^2b} + (d_x^6) \frac{-1}{ab^2} + (d_y^7) \frac{-1}{a^2b} + (d_x^8) \frac{1}{ab^2} \right] + \\
& \tilde{f}_{2111} \left[ (d_x^1) \frac{-1}{2a^2b} + (d_x^2) \frac{-1}{2a^2b} + (d_x^3) \frac{1}{2a^2b} + (d_x^4) \frac{1}{2a^2b} + (d_x^5) \frac{1}{a^2b} + (d_x^7) \frac{-1}{a^2b} \right] + \\
& \tilde{f}_{2112} \left[ (d_x^1) \frac{-1}{2ab^2} + (d_x^2) \frac{1}{2ab^2} + (d_x^3) \frac{1}{2ab^2} + (d_x^4) \frac{-1}{2ab^2} + (d_x^6) \frac{-1}{ab^2} + (d_x^8) \frac{1}{ab^2} \right] + \\
& \tilde{f}_{2221} \left[ (d_y^1) \frac{-1}{2ab^2} + (d_y^2) \frac{1}{2ab^2} + (d_y^3) \frac{1}{2ab^2} + (d_y^4) \frac{-1}{2ab^2} + (d_y^6) \frac{-1}{ab^2} + (d_y^8) \frac{1}{ab^2} \right] + \\
& \tilde{f}_{2121} \left[ (d_x^1) \frac{-1}{2ab^2} + (d_y^1) \frac{-1}{2a^2b} + (d_x^2) \frac{1}{2ab^2} + (d_y^2) \frac{-1}{2a^2b} + (d_x^3) \frac{1}{2ab^2} + (d_y^3) \frac{1}{2a^2b} + \right. \\
& \quad \left. (d_x^4) \frac{-1}{2ab^2} + (d_y^4) \frac{1}{2a^2b} + (d_y^5) \frac{1}{a^2b} + (d_x^6) \frac{-1}{ab^2} + (d_y^7) \frac{-1}{a^2b} + (d_x^8) \frac{1}{ab^2} \right] + \\
& \tilde{f}_{2122} \left[ (d_y^1) \frac{-1}{2ab^2} + (d_y^2) \frac{1}{2ab^2} + (d_y^3) \frac{1}{2ab^2} + (d_y^4) \frac{-1}{2ab^2} + (d_y^6) \frac{-1}{ab^2} + (d_y^8) \frac{1}{ab^2} \right]
\end{aligned} \tag{31}$$

The calculation of the induced current is then given by:

$$dI = \frac{\partial \iint \nabla \cdot \tilde{\mathbf{P}} dx dy}{\partial t} = \frac{\partial \iint \nabla \cdot (\tilde{\mathbf{f}} \cdot \mathbf{B} \cdot \mathbf{d}^e) dx dy}{\partial t} \tag{32}$$

As the integrand is constant within the element (because  $\mathbf{B}$  is), and after time

discretisation, one then has:

$$dI = v_e \rho_a \frac{\nabla \cdot (\tilde{\mathbf{f}} \cdot \mathbf{B} \cdot \mathbf{d}^e)^{n+1} - \nabla \cdot (\tilde{\mathbf{f}} \cdot \mathbf{B} \cdot \mathbf{d}^e)^n}{\Delta t} \quad (33)$$

where  $\rho_a$  is the density of fibres,  $v_e$  is the total volume (area in 2D) of the  
470 element,  $\Delta t$  is the time step and, the superscripts  $n$  and  $n+1$  refer to the value  
at time steps  $n$  and  $n+1$ , respectively.

### 6.1.2. 3D model

For the 3D formulation, 20-node brick elements are used, see Fig. 7.

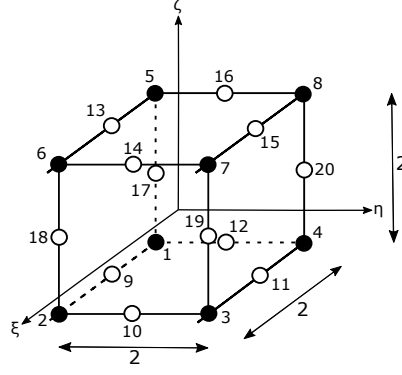


Figure 7: 20-node 3D brick element in the isoparametric reference frame  $(\xi, \eta, \zeta)$ .

Similarly, the displacement vector  $\mathbf{d}^e$  is written as:

$$\mathbf{d}^e = \begin{bmatrix} d_x^1 \\ d_y^1 \\ d_z^1 \\ d_x^2 \\ d_y^2 \\ d_z^2 \\ d_x^3 \\ d_y^3 \\ d_z^3 \\ \cdot \\ \cdot \\ \cdot \\ d_x^{20} \\ d_y^{20} \\ d_z^{20} \end{bmatrix}^T \quad (34)$$

The shape function tensor  $\mathbf{N}$  is:

$$\mathbf{N} = \begin{bmatrix} N_1 & 0 & 0 & \cdot & \cdot & \cdot & N_{20} & 0 & 0 \\ 0 & N_1 & 0 & \cdot & \cdot & \cdot & 0 & N_{20} & 0 \\ 0 & 0 & N_1 & \cdot & \cdot & \cdot & 0 & 0 & N_{20} \end{bmatrix} \quad (35)$$

The first derivative gradient tensor is given by:

$$\mathbf{L}_1 = \begin{bmatrix} \frac{\partial}{\partial x} & 0 & 0 \\ 0 & \frac{\partial}{\partial y} & 0 \\ 0 & 0 & \frac{\partial}{\partial z} \\ \frac{\partial}{\partial y} & \frac{\partial}{\partial x} & 0 \\ \frac{\partial}{\partial z} & 0 & \frac{\partial}{\partial x} \\ 0 & \frac{\partial}{\partial z} & \frac{\partial}{\partial y} \end{bmatrix} \quad (36)$$

The second derivative gradient tensor is given by:

$$\mathbf{L}_2 = \begin{bmatrix} \frac{\partial}{\partial x} & 0 & 0 & 0 & 0 & 0 \\ \frac{\partial}{\partial y} & 0 & 0 & 0 & 0 & 0 \\ \frac{\partial}{\partial z} & 0 & 0 & 0 & 0 & 0 \\ 0 & \frac{\partial}{\partial x} & 0 & 0 & 0 & 0 \\ 0 & \frac{\partial}{\partial y} & 0 & 0 & 0 & 0 \\ 0 & \frac{\partial}{\partial z} & 0 & 0 & 0 & 0 \\ 0 & 0 & \frac{\partial}{\partial x} & 0 & 0 & 0 \\ 0 & 0 & \frac{\partial}{\partial y} & 0 & 0 & 0 \\ 0 & 0 & \frac{\partial}{\partial z} & 0 & 0 & 0 \\ 0 & 0 & 0 & \frac{\partial}{\partial x} & 0 & 0 \\ 0 & 0 & 0 & \frac{\partial}{\partial y} & 0 & 0 \\ 0 & 0 & 0 & \frac{\partial}{\partial z} & 0 & 0 \\ 0 & 0 & 0 & 0 & \frac{\partial}{\partial x} & 0 \\ 0 & 0 & 0 & 0 & \frac{\partial}{\partial y} & 0 \\ 0 & 0 & 0 & 0 & \frac{\partial}{\partial z} & 0 \\ 0 & 0 & 0 & 0 & 0 & \frac{\partial}{\partial x} \\ 0 & 0 & 0 & 0 & 0 & \frac{\partial}{\partial y} \\ 0 & 0 & 0 & 0 & 0 & \frac{\partial}{\partial z} \end{bmatrix} \quad (37)$$

Making use of (35), (36), and (37), (17) becomes:

$$\mathbf{B} = \begin{bmatrix} \frac{\partial^2 N_1}{\partial x^2} & 0 & 0 & \cdot & \cdot & \cdot & \frac{\partial^2 N_{20}}{\partial x^2} & 0 & 0 \\ \frac{\partial^2 N_1}{\partial x \partial y} & 0 & 0 & \cdot & \cdot & \cdot & \frac{\partial^2 N_{20}}{\partial x \partial y} & 0 & 0 \\ \frac{\partial^2 N_1}{\partial x \partial z} & 0 & 0 & \cdot & \cdot & \cdot & \frac{\partial^2 N_{20}}{\partial x \partial z} & 0 & 0 \\ 0 & \frac{\partial^2 N_1}{\partial x \partial y} & 0 & \cdot & \cdot & \cdot & 0 & \frac{\partial^2 N_{20}}{\partial x \partial y} & 0 \\ 0 & \frac{\partial^2 N_1}{\partial y^2} & 0 & \cdot & \cdot & \cdot & 0 & \frac{\partial^2 N_{20}}{\partial y^2} & 0 \\ 0 & \frac{\partial^2 N_1}{\partial y \partial z} & 0 & \cdot & \cdot & \cdot & 0 & \frac{\partial^2 N_{20}}{\partial y \partial z} & 0 \\ 0 & 0 & \frac{\partial^2 N_1}{\partial x \partial z} & \cdot & \cdot & \cdot & 0 & 0 & \frac{\partial^2 N_{20}}{\partial x \partial z} \\ 0 & 0 & \frac{\partial^2 N_1}{\partial y \partial z} & \cdot & \cdot & \cdot & 0 & 0 & \frac{\partial^2 N_{20}}{\partial y \partial z} \\ 0 & 0 & \frac{\partial^2 N_1}{\partial z^2} & \cdot & \cdot & \cdot & 0 & 0 & \frac{\partial^2 N_{20}}{\partial z^2} \\ \frac{\partial^2 N_1}{\partial x \partial y} & \frac{\partial^2 N_1}{\partial x^2} & 0 & \cdot & \cdot & \cdot & \frac{\partial^2 N_{20}}{\partial x \partial y} & \frac{\partial^2 N_{20}}{\partial x^2} & 0 \\ \frac{\partial^2 N_1}{\partial y^2} & \frac{\partial^2 N_1}{\partial x \partial y} & 0 & \cdot & \cdot & \cdot & \frac{\partial^2 N_{20}}{\partial y^2} & \frac{\partial^2 N_{20}}{\partial x \partial y} & 0 \\ \frac{\partial^2 N_1}{\partial y \partial z} & \frac{\partial^2 N_1}{\partial x \partial z} & 0 & \cdot & \cdot & \cdot & \frac{\partial^2 N_{20}}{\partial y \partial z} & \frac{\partial^2 N_{20}}{\partial x \partial z} & 0 \\ \frac{\partial^2 N_1}{\partial x \partial z} & 0 & \frac{\partial^2 N_1}{\partial x^2} & \cdot & \cdot & \frac{\partial^2 N_{20}}{\partial x \partial z} & 0 & \frac{\partial^2 N_{20}}{\partial x^2} & \\ \frac{\partial^2 N_1}{\partial y \partial z} & 0 & \frac{\partial^2 N_1}{\partial x \partial y} & \cdot & \cdot & \cdot & \frac{\partial^2 N_{20}}{\partial y \partial z} & 0 & \frac{\partial^2 N_{20}}{\partial x \partial y} \\ \frac{\partial^2 N_1}{\partial z^2} & 0 & \frac{\partial^2 N_1}{\partial x \partial z} & \cdot & \cdot & \cdot & \frac{\partial^2 N_{20}}{\partial z^2} & 0 & \frac{\partial^2 N_{20}}{\partial x \partial z} \\ 0 & \frac{\partial^2 N_1}{\partial x \partial z} & \frac{\partial^2 N_1}{\partial x \partial y} & \cdot & \cdot & \cdot & 0 & \frac{\partial^2 N_{20}}{\partial x \partial z} & \frac{\partial^2 N_{20}}{\partial x \partial y} \\ 0 & \frac{\partial^2 N_1}{\partial y \partial z} & \frac{\partial^2 N_1}{\partial y^2} & \cdot & \cdot & \cdot & 0 & \frac{\partial^2 N_{20}}{\partial y \partial z} & \frac{\partial^2 N_{20}}{\partial y^2} \\ 0 & \frac{\partial^2 N_1}{\partial z^2} & \frac{\partial^2 N_1}{\partial y \partial z} & \cdot & \cdot & \cdot & 0 & \frac{\partial^2 N_{20}}{\partial z^2} & \frac{\partial^2 N_{20}}{\partial y \partial z} \end{bmatrix} \quad (38)$$

The shape functions of the 20-noded quadratic element expressed in the local

natural coordinates are (see Fig. 7):

$$\begin{aligned}
N_1 &= \frac{1}{8}(1-\xi)(1-\eta)(1-\zeta)(-2-\xi-\eta-\zeta) \\
N_2 &= \frac{1}{8}(1+\xi)(1-\eta)(1-\zeta)(-2+\xi-\eta-\zeta) \\
N_3 &= \frac{1}{8}(1+\xi)(1+\eta)(1-\zeta)(-2+\xi+\eta-\zeta) \\
N_4 &= \frac{1}{8}(1-\xi)(1+\eta)(1-\zeta)(-2-\xi+\eta-\zeta) \\
N_5 &= \frac{1}{8}(1-\xi)(1-\eta)(1+\zeta)(-2-\xi-\eta+\zeta) \\
N_6 &= \frac{1}{8}(1+\xi)(1-\eta)(1+\zeta)(-2+\xi-\eta+\zeta) \\
N_7 &= \frac{1}{8}(1+\xi)(1+\eta)(1+\zeta)(-2+\xi+\eta+\zeta) \\
N_8 &= \frac{1}{8}(1-\xi)(1+\eta)(1+\zeta)(-2-\xi+\eta+\zeta) \\
N_9 &= \frac{1}{4}(1-\xi^2)(1-\eta)(1-\zeta) \\
N_{10} &= \frac{1}{4}(1+\xi)(1-\eta^2)(1-\zeta) \\
N_{11} &= \frac{1}{4}(1-\xi^2)(1+\eta)(1-\zeta) \\
N_{12} &= \frac{1}{4}(1-\xi)(1-\eta^2)(1-\zeta) \\
N_{13} &= \frac{1}{4}(1-\xi^2)(1-\eta)(1+\zeta) \\
N_{14} &= \frac{1}{4}(1+\xi)(1-\eta^2)(1+\zeta) \\
N_{15} &= \frac{1}{4}(1-\xi^2)(1+\eta)(1+\zeta) \\
N_{16} &= \frac{1}{4}(1-\xi)(1-\eta^2)(1+\zeta) \\
N_{17} &= \frac{1}{4}(1-\xi)(1-\eta)(1-\zeta^2) \\
N_{18} &= \frac{1}{4}(1+\xi)(1-\eta)(1-\zeta^2) \\
N_{19} &= \frac{1}{4}(1+\xi)(1+\eta)(1-\zeta^2) \\
N_{20} &= \frac{1}{4}(1-\xi)(1+\eta)(1-\zeta^2)
\end{aligned} \tag{39}$$

The third derivative of the shape functions are:

$$\frac{\partial^3 N_1}{\partial \xi^3} = 0$$

$$\frac{\partial^3 N_2}{\partial \xi^3} = 0$$

$$\frac{\partial^3 N_3}{\partial \xi^3} = 0$$

$$\frac{\partial^3 N_4}{\partial \xi^3} = 0$$

$$\frac{\partial^3 N_5}{\partial \xi^3} = 0$$

$$\frac{\partial^3 N_6}{\partial \xi^3} = 0$$

$$\frac{\partial^3 N_7}{\partial \xi^3} = 0$$

$$\frac{\partial^3 N_8}{\partial \xi^3} = 0$$

$$\frac{\partial^3 N_9}{\partial \xi^3} = 0$$

$$\frac{\partial^3 N_{10}}{\partial \xi^3} = 0$$

$$\frac{\partial^3 N_{11}}{\partial \xi^3} = 0$$

$$\frac{\partial^3 N_{12}}{\partial \xi^3} = 0$$

$$\frac{\partial^3 N_{13}}{\partial \xi^3} = 0$$

$$\frac{\partial^3 N_{14}}{\partial \xi^3} = 0$$

$$\frac{\partial^3 N_{15}}{\partial \xi^3} = 0$$

$$\frac{\partial^3 N_{16}}{\partial \xi^3} = 0$$

$$\frac{\partial^3 N_{17}}{\partial \xi^3} = 0$$

$$\frac{\partial^3 N_{18}}{\partial \xi^3} = 0$$

$$\frac{\partial^3 N_{19}}{\partial \xi^3} = 0$$

$$\frac{\partial^3 N_{20}}{\partial \xi^3} = 0$$

$$\begin{aligned}
\frac{\partial^3 N_1}{\partial \eta^3} &= 0 \\
\frac{\partial^3 N_2}{\partial \eta^3} &= 0 \\
\frac{\partial^3 N_3}{\partial \eta^3} &= 0 \\
\frac{\partial^3 N_4}{\partial \eta^3} &= 0 \\
\frac{\partial^3 N_5}{\partial \eta^3} &= 0 \\
\frac{\partial^3 N_6}{\partial \eta^3} &= 0 \\
\frac{\partial^3 N_7}{\partial \eta^3} &= 0 \\
\frac{\partial^3 N_8}{\partial \eta^3} &= 0 \\
\frac{\partial^3 N_9}{\partial \eta^3} &= 0 \\
\frac{\partial^3 N_{10}}{\partial \eta^3} &= 0 \\
\frac{\partial^3 N_{11}}{\partial \eta^3} &= 0 \\
\frac{\partial^3 N_{12}}{\partial \eta^3} &= 0 \\
\frac{\partial^3 N_{13}}{\partial \eta^3} &= 0 \\
\frac{\partial^3 N_{14}}{\partial \eta^3} &= 0 \\
\frac{\partial^3 N_{15}}{\partial \eta^3} &= 0 \\
\frac{\partial^3 N_{16}}{\partial \eta^3} &= 0 \\
\frac{\partial^3 N_{17}}{\partial \eta^3} &= 0 \\
\frac{\partial^3 N_{18}}{\partial \eta^3} &= 0 \\
\frac{\partial^3 N_{19}}{\partial \eta^3} &= 0 \\
\frac{\partial^3 N_{20}}{\partial \eta^3} &= 0
\end{aligned}$$



$$\begin{aligned}
\frac{\partial^3 N_1}{\partial \zeta^3} &= 0 \\
\frac{\partial^3 N_2}{\partial \zeta^3} &= 0 \\
\frac{\partial^3 N_3}{\partial \zeta^3} &= 0 \\
\frac{\partial^3 N_4}{\partial \zeta^3} &= 0 \\
\frac{\partial^3 N_5}{\partial \zeta^3} &= 0 \\
\frac{\partial^3 N_6}{\partial \zeta^3} &= 0 \\
\frac{\partial^3 N_7}{\partial \zeta^3} &= 0 \\
\frac{\partial^3 N_8}{\partial \zeta^3} &= 0 \\
\frac{\partial^3 N_9}{\partial \zeta^3} &= 0 \\
\frac{\partial^3 N_{10}}{\partial \zeta^3} &= 0 \\
\frac{\partial^3 N_{11}}{\partial \zeta^3} &= 0 \\
\frac{\partial^3 N_{12}}{\partial \zeta^3} &= 0 \\
\frac{\partial^3 N_{13}}{\partial \zeta^3} &= 0 \\
\frac{\partial^3 N_{14}}{\partial \zeta^3} &= 0 \\
\frac{\partial^3 N_{15}}{\partial \zeta^3} &= 0 \\
\frac{\partial^3 N_{16}}{\partial \zeta^3} &= 0 \\
\frac{\partial^3 N_{17}}{\partial \zeta^3} &= 0 \\
\frac{\partial^3 N_{18}}{\partial \zeta^3} &= 0 \\
\frac{\partial^3 N_{19}}{\partial \zeta^3} &= 0 \\
\frac{\partial^3 N_{20}}{\partial \zeta^3} &= 0
\end{aligned}$$

$$\begin{aligned}
\frac{\partial^3 N_1}{\partial \xi^2 \eta} &= \frac{1}{4}(-1 + \zeta) \\
\frac{\partial^3 N_2}{\partial \xi^2 \eta} &= \frac{1}{4}(-1 + \zeta) \\
\frac{\partial^3 N_3}{\partial \xi^2 \eta} &= \frac{1}{4}(1 - \zeta) \\
\frac{\partial^3 N_4}{\partial \xi^2 \eta} &= \frac{1}{4}(1 - \zeta) \\
\frac{\partial^3 N_5}{\partial \xi^2 \eta} &= \frac{1}{4}(-1 - \zeta) \\
\frac{\partial^3 N_6}{\partial \xi^2 \eta} &= \frac{1}{4}(-1 - \zeta) \\
\frac{\partial^3 N_7}{\partial \xi^2 \eta} &= \frac{1}{4}(1 + \zeta) \\
\frac{\partial^3 N_8}{\partial \xi^2 \eta} &= \frac{1}{4}(1 + \zeta) \\
\frac{\partial^3 N_9}{\partial \xi^2 \eta} &= \frac{1}{2}(1 - \zeta) \\
\frac{\partial^3 N_{10}}{\partial \xi^2 \eta} &= 0 \\
\frac{\partial^3 N_{11}}{\partial \xi^2 \eta} &= \frac{1}{2}(-1 + \zeta) \\
\frac{\partial^3 N_{12}}{\partial \xi^2 \eta} &= 0 \\
\frac{\partial^3 N_{13}}{\partial \xi^2 \eta} &= \frac{1}{2}(1 + \zeta) \\
\frac{\partial^3 N_{14}}{\partial \xi^2 \eta} &= 0 \\
\frac{\partial^3 N_{15}}{\partial \xi^2 \eta} &= \frac{1}{2}(-1 - \zeta) \\
\frac{\partial^3 N_{16}}{\partial \xi^2 \eta} &= 0 \\
\frac{\partial^3 N_{17}}{\partial \xi^2 \eta} &= 0 \\
\frac{\partial^3 N_{18}}{\partial \xi^2 \eta} &= 0 \\
\frac{\partial^3 N_{19}}{\partial \xi^2 \eta} &= 0 \\
\frac{\partial^3 N_{20}}{\partial \xi^2 \eta} &= 0
\end{aligned}$$

$$\begin{aligned}
\frac{\partial^3 N_1}{\partial \xi^2 \zeta} &= \frac{1}{4}(-1 + \eta) \\
\frac{\partial^3 N_2}{\partial \xi^2 \zeta} &= \frac{1}{4}(-1 + \eta) \\
\frac{\partial^3 N_3}{\partial \xi^2 \zeta} &= \frac{1}{4}(-1 - \eta) \\
\frac{\partial^3 N_4}{\partial \xi^2 \zeta} &= \frac{1}{4}(-1 - \eta) \\
\frac{\partial^3 N_5}{\partial \xi^2 \zeta} &= \frac{1}{4}(1 - \eta) \\
\frac{\partial^3 N_6}{\partial \xi^2 \zeta} &= \frac{1}{4}(1 - \eta) \\
\frac{\partial^3 N_7}{\partial \xi^2 \zeta} &= \frac{1}{4}(1 + \eta) \\
\frac{\partial^3 N_8}{\partial \xi^2 \zeta} &= \frac{1}{4}(1 + \eta) \\
\frac{\partial^3 N_9}{\partial \xi^2 \zeta} &= \frac{1}{2}(1 - \eta) \\
\frac{\partial^3 N_{10}}{\partial \xi^2 \zeta} &= 0 \\
\frac{\partial^3 N_{11}}{\partial \xi^2 \zeta} &= \frac{1}{2}(1 + \eta) \\
\frac{\partial^3 N_{12}}{\partial \xi^2 \zeta} &= 0 \\
\frac{\partial^3 N_{13}}{\partial \xi^2 \zeta} &= \frac{1}{2}(-1 + \eta) \\
\frac{\partial^3 N_{14}}{\partial \xi^2 \zeta} &= 0 \\
\frac{\partial^3 N_{15}}{\partial \xi^2 \zeta} &= \frac{1}{2}(-1 - \eta) \\
\frac{\partial^3 N_{16}}{\partial \xi^2 \zeta} &= 0 \\
\frac{\partial^3 N_{17}}{\partial \xi^2 \zeta} &= 0 \\
\frac{\partial^3 N_{18}}{\partial \xi^2 \zeta} &= 0 \\
\frac{\partial^3 N_{19}}{\partial \xi^2 \zeta} &= 0 \\
\frac{\partial^3 N_{20}}{\partial \xi^2 \zeta} &= 0
\end{aligned}$$

$$\begin{aligned}
\frac{\partial^3 N_1}{\partial \eta^2 \xi} &= \frac{1}{4}(-1 + \zeta) \\
\frac{\partial^3 N_2}{\partial \eta^2 \xi} &= \frac{1}{4}(1 - \zeta) \\
\frac{\partial^3 N_3}{\partial \eta^2 \xi} &= \frac{1}{4}(1 - \zeta) \\
\frac{\partial^3 N_4}{\partial \eta^2 \xi} &= \frac{1}{4}(-1 + \zeta) \\
\frac{\partial^3 N_5}{\partial \eta^2 \xi} &= \frac{1}{4}(-1 - \zeta) \\
\frac{\partial^3 N_6}{\partial \eta^2 \xi} &= \frac{1}{4}(1 + \zeta) \\
\frac{\partial^3 N_7}{\partial \eta^2 \xi} &= \frac{1}{4}(1 + \zeta) \\
\frac{\partial^3 N_8}{\partial \eta^2 \xi} &= \frac{1}{4}(-1 - \zeta) \\
\frac{\partial^3 N_9}{\partial \eta^2 \xi} &= 0 \\
\frac{\partial^3 N_{10}}{\partial \eta^2 \xi} &= \frac{1}{2}(-1 + \zeta) \\
\frac{\partial^3 N_{11}}{\partial \eta^2 \xi} &= 0 \\
\frac{\partial^3 N_{12}}{\partial \eta^2 \xi} &= \frac{1}{2}(1 - \zeta) \\
\frac{\partial^3 N_{13}}{\partial \eta^2 \xi} &= 0 \\
\frac{\partial^3 N_{14}}{\partial \eta^2 \xi} &= \frac{1}{2}(-1 - \zeta) \\
\frac{\partial^3 N_{15}}{\partial \eta^2 \xi} &= 0 \\
\frac{\partial^3 N_{16}}{\partial \eta^2 \xi} &= \frac{1}{2}(1 + \zeta) \\
\frac{\partial^3 N_{17}}{\partial \eta^2 \xi} &= 0 \\
\frac{\partial^3 N_{18}}{\partial \eta^2 \xi} &= 0 \\
\frac{\partial^3 N_{19}}{\partial \eta^2 \xi} &= 0 \\
\frac{\partial^3 N_{20}}{\partial \eta^2 \xi} &= 0
\end{aligned}$$

$$\begin{aligned}
\frac{\partial^3 N_1}{\partial \eta^2 \zeta} &= \frac{1}{4}(-1 + \xi) \\
\frac{\partial^3 N_2}{\partial \eta^2 \zeta} &= \frac{1}{4}(-1 - \xi) \\
\frac{\partial^3 N_3}{\partial \eta^2 \zeta} &= \frac{1}{4}(-1 - \xi) \\
\frac{\partial^3 N_4}{\partial \eta^2 \zeta} &= \frac{1}{4}(-1 + \xi) \\
\frac{\partial^3 N_5}{\partial \eta^2 \zeta} &= \frac{1}{4}(1 - \xi) \\
\frac{\partial^3 N_6}{\partial \eta^2 \zeta} &= \frac{1}{4}(1 + \xi) \\
\frac{\partial^3 N_7}{\partial \eta^2 \zeta} &= \frac{1}{4}(1 + \xi) \\
\frac{\partial^3 N_8}{\partial \eta^2 \zeta} &= \frac{1}{4}(1 - \xi) \\
\frac{\partial^3 N_9}{\partial \eta^2 \zeta} &= 0 \\
\frac{\partial^3 N_{10}}{\partial \eta^2 \zeta} &= \frac{1}{2}(1 + \xi) \\
\frac{\partial^3 N_{11}}{\partial \eta^2 \zeta} &= 0 \\
\frac{\partial^3 N_{12}}{\partial \eta^2 \zeta} &= \frac{1}{2}(1 - \xi) \\
\frac{\partial^3 N_{13}}{\partial \eta^2 \zeta} &= 0 \\
\frac{\partial^3 N_{14}}{\partial \eta^2 \zeta} &= \frac{1}{2}(-1 - \xi) \\
\frac{\partial^3 N_{15}}{\partial \eta^2 \zeta} &= 0 \\
\frac{\partial^3 N_{16}}{\partial \eta^2 \zeta} &= \frac{1}{2}(-1 + \xi) \\
\frac{\partial^3 N_{17}}{\partial \eta^2 \zeta} &= 0 \\
\frac{\partial^3 N_{18}}{\partial \eta^2 \zeta} &= 0 \\
\frac{\partial^3 N_{19}}{\partial \eta^2 \zeta} &= 0 \\
\frac{\partial^3 N_{20}}{\partial \eta^2 \zeta} &= 0
\end{aligned}$$

$$\frac{\partial^3 N_1}{\partial \zeta^2 \xi} = \frac{1}{4}(-1 + \eta)$$

$$\frac{\partial^3 N_2}{\partial \zeta^2 \xi} = \frac{1}{4}(1 - \eta)$$

$$\frac{\partial^3 N_3}{\partial \zeta^2 \xi} = \frac{1}{4}(1 + \eta)$$

$$\frac{\partial^3 N_4}{\partial \zeta^2 \xi} = \frac{1}{4}(-1 - \eta)$$

$$\frac{\partial^3 N_5}{\partial \zeta^2 \xi} = \frac{1}{4}(-1 + \eta)$$

$$\frac{\partial^3 N_6}{\partial \zeta^2 \xi} = \frac{1}{4}(1 - \eta)$$

$$\frac{\partial^3 N_7}{\partial \zeta^2 \xi} = \frac{1}{4}(1 + \eta)$$

$$\frac{\partial^3 N_8}{\partial \zeta^2 \xi} = \frac{1}{4}(-1 - \eta)$$

$$\frac{\partial^3 N_9}{\partial \zeta^2 \xi} = 0$$

$$\frac{\partial^3 N_{10}}{\partial \zeta^2 \xi} = 0$$

$$\frac{\partial^3 N_{11}}{\partial \zeta^2 \xi} = 0$$

$$\frac{\partial^3 N_{12}}{\partial \zeta^2 \xi} = 0$$

$$\frac{\partial^3 N_{13}}{\partial \zeta^2 \xi} = 0$$

$$\frac{\partial^3 N_{14}}{\partial \zeta^2 \xi} = 0$$

$$\frac{\partial^3 N_{15}}{\partial \zeta^2 \xi} = 0$$

$$\frac{\partial^3 N_{16}}{\partial \zeta^2 \xi} = 0$$

$$\frac{\partial^3 N_{17}}{\partial \zeta^2 \xi} = \frac{1}{2}(1 - \eta)$$

$$\frac{\partial^3 N_{18}}{\partial \zeta^2 \xi} = \frac{1}{2}(-1 + \eta)$$

$$\frac{\partial^3 N_{19}}{\partial \zeta^2 \xi} = \frac{1}{2}(-1 - \eta)$$

$$\frac{\partial^3 N_{20}}{\partial \zeta^2 \xi} = \frac{1}{2}(1 + \eta)$$

$$\begin{aligned}
\frac{\partial^3 N_1}{\partial \zeta^2 \eta} &= \frac{1}{4}(-1 + \xi) \\
\frac{\partial^3 N_2}{\partial \zeta^2 \eta} &= \frac{1}{4}(-1 - \xi) \\
\frac{\partial^3 N_3}{\partial \zeta^2 \eta} &= \frac{1}{4}(1 + \xi) \\
\frac{\partial^3 N_4}{\partial \zeta^2 \eta} &= \frac{1}{4}(1 - \xi) \\
\frac{\partial^3 N_5}{\partial \zeta^2 \eta} &= \frac{1}{4}(-1 + \xi) \\
\frac{\partial^3 N_6}{\partial \zeta^2 \eta} &= \frac{1}{4}(-1 - \xi) \\
\frac{\partial^3 N_7}{\partial \zeta^2 \eta} &= \frac{1}{4}(1 + \xi) \\
\frac{\partial^3 N_8}{\partial \zeta^2 \eta} &= \frac{1}{4}(1 - \xi) \\
\frac{\partial^3 N_9}{\partial \zeta^2 \eta} &= 0 \\
\frac{\partial^3 N_{10}}{\partial \zeta^2 \eta} &= 0 \\
\frac{\partial^3 N_{11}}{\partial \zeta^2 \eta} &= 0 \\
\frac{\partial^3 N_{12}}{\partial \zeta^2 \eta} &= 0 \\
\frac{\partial^3 N_{13}}{\partial \zeta^2 \eta} &= 0 \\
\frac{\partial^3 N_{14}}{\partial \zeta^2 \eta} &= 0 \\
\frac{\partial^3 N_{15}}{\partial \zeta^2 \eta} &= 0 \\
\frac{\partial^3 N_{16}}{\partial \zeta^2 \eta} &= 0 \\
\frac{\partial^3 N_{17}}{\partial \zeta^2 \eta} &= \frac{1}{2}(1 - \xi) \\
\frac{\partial^3 N_{18}}{\partial \zeta^2 \eta} &= \frac{1}{2}(1 + \xi) \\
\frac{\partial^3 N_{19}}{\partial \zeta^2 \eta} &= \frac{1}{2}(-1 - \xi) \\
\frac{\partial^3 N_{20}}{\partial \zeta^2 \eta} &= \frac{1}{2}(-1 + \xi)
\end{aligned} \tag{40}$$

By analogy with the 2D case, the unrotated transversely isotropic volumetric flexoelectric tensor ( $\tilde{f}_{ijkl}$  in the manuscript) is given by [81]

$$\tilde{\mathbf{f}} = \begin{bmatrix} \tilde{f}_{1111} & 0 & 0 & \tilde{f}_{1221} & 0 & 0 & \tilde{f}_{1331} & 0 & 0 \\ 0 & \tilde{f}_{2112} & 0 & 0 & \tilde{f}_{2222} & 0 & 0 & \tilde{f}_{2332} & 0 \\ 0 & 0 & \tilde{f}_{3113} & 0 & 0 & \tilde{f}_{3223} & 0 & 0 & \tilde{f}_{3333} \\ 0 & \tilde{f}_{1122} & 0 & 0 & 0 & \tilde{f}_{1133} & 0 & 0 & 0 \\ \tilde{f}_{2121} & 0 & 0 & 0 & 0 & 0 & 0 & 0 & \tilde{f}_{2233} \\ 0 & 0 & 0 & \tilde{f}_{3131} & 0 & 0 & 0 & \tilde{f}_{3232} & 0 \end{bmatrix} \quad (41)$$

or

$$\tilde{\mathbf{f}} = \begin{bmatrix} \tilde{f}_{11} & 0 & 0 & \tilde{f}_{55} & 0 & 0 & \tilde{f}_{55} & 0 & 0 \\ 0 & \tilde{f}_{44} & 0 & 0 & \tilde{f}_{22} & 0 & 0 & \tilde{f}_{33} & 0 \\ 0 & 0 & \tilde{f}_{44} & 0 & 0 & \tilde{f}_{33} & 0 & 0 & \tilde{f}_{22} \\ 0 & \tilde{f}_{55} & 0 & 0 & 0 & \tilde{f}_{55} & 0 & 0 & 0 \\ \tilde{f}_{44} & 0 & 0 & 0 & 0 & 0 & 0 & 0 & \tilde{f}_{33} \\ 0 & 0 & 0 & \tilde{f}_{44} & 0 & 0 & 0 & \tilde{f}_{33} & 0 \end{bmatrix} \quad (42)$$

where  $\tilde{f}_{11} = \tilde{f}_{1111}$ ,  $\tilde{f}_{22} = \tilde{f}_{2222} = \tilde{f}_{3333}$ ,  $\tilde{f}_{33} = \tilde{f}_{2233} = \tilde{f}_{2332} = \tilde{f}_{2323} = \tilde{f}_{3322} = \tilde{f}_{3223} = \tilde{f}_{3232}$ ,  $\tilde{f}_{44} = \tilde{f}_{2211} = \tilde{f}_{2121} = \tilde{f}_{2112} = \tilde{f}_{3311} = \tilde{f}_{3131} = \tilde{f}_{3113}$  and  $\tilde{f}_{55} = \tilde{f}_{1122} = \tilde{f}_{1212} = \tilde{f}_{1221} = \tilde{f}_{1133} = \tilde{f}_{1313} = \tilde{f}_{1331}$  [82], with the equivalent symmetries to the 2D case.

To change the orientation of the fibre, a combination of 3D coordinate system rotation matrices is used to rotate  $\tilde{\mathbf{f}}$  through a clockwise direction where

$$\mathbf{Q} = \mathbf{R}_{y'} \cdot \mathbf{R}_z \quad (43)$$

with the fibre assumed to be originally oriented in the  $x$ -direction, then rotated around the  $z$ -axis by an angle  $\gamma$ , then by  $\beta$  around the  $y'$ -axis which is the  $y$ -axis rotated by  $\mathbf{R}_z$ .



The rotation matrices used are

$$\begin{aligned}\mathbf{R}_{y'}(\beta) &= \begin{bmatrix} \cos \beta & 0 & \sin \beta \\ 0 & 1 & 0 \\ -\sin \beta & 0 & \cos \beta \end{bmatrix} \\ \mathbf{R}_z(\gamma) &= \begin{bmatrix} \cos \gamma & -\sin \gamma & 0 \\ \sin \gamma & \cos \gamma & 0 \\ 0 & 0 & 1 \end{bmatrix}\end{aligned}\quad (44)$$

This rotation gives the resulting rotated tensor  $\tilde{\mathbf{f}}$  ( $\tilde{f}_{rmns}$  in the manuscript) [81]:

$$\tilde{\mathbf{f}} = \begin{bmatrix} \tilde{f}_{1111} & \tilde{f}_{1112} & \tilde{f}_{1113} & \tilde{f}_{1221} & \tilde{f}_{1222} & \tilde{f}_{1223} & \tilde{f}_{1331} & \tilde{f}_{1332} & \tilde{f}_{1333} & \tilde{f}_{1121} \\ \tilde{f}_{2111} & \tilde{f}_{2112} & \tilde{f}_{2113} & \tilde{f}_{2221} & \tilde{f}_{2222} & \tilde{f}_{2223} & \tilde{f}_{2331} & \tilde{f}_{2332} & \tilde{f}_{2333} & \tilde{f}_{2121} \\ \tilde{f}_{3111} & \tilde{f}_{3112} & \tilde{f}_{3113} & \tilde{f}_{3221} & \tilde{f}_{3222} & \tilde{f}_{3223} & \tilde{f}_{3331} & \tilde{f}_{3332} & \tilde{f}_{3333} & \tilde{f}_{3121} \\ & & & & & & & & & \\ & & & & \tilde{f}_{1122} & \tilde{f}_{1123} & \tilde{f}_{1131} & \tilde{f}_{1132} & \tilde{f}_{1133} & \tilde{f}_{1231} & \tilde{f}_{1232} & \tilde{f}_{1233} \\ & & & & \tilde{f}_{2122} & \tilde{f}_{2123} & \tilde{f}_{2131} & \tilde{f}_{2132} & \tilde{f}_{2133} & \tilde{f}_{2231} & \tilde{f}_{2232} & \tilde{f}_{2233} \\ & & & & \tilde{f}_{3122} & \tilde{f}_{3123} & \tilde{f}_{3131} & \tilde{f}_{3132} & \tilde{f}_{3133} & \tilde{f}_{3231} & \tilde{f}_{3232} & \tilde{f}_{3233} \end{bmatrix} \quad (45)$$

Again, after rotation, the symmetries of (42) do not necessarily apply to the rotated flexoelectric tensor, and a full tensor needs to be considered.

For a brick element of size  $2a \times 2b \times 2c$ , the Jacobian matrix  $\mathbf{J}$  between the original reference frame and the isoparametric reference frame is given by:

$$\mathbf{J} = \begin{bmatrix} \frac{\partial x}{\partial \xi} & \frac{\partial y}{\partial \xi} & \frac{\partial z}{\partial \xi} \\ \frac{\partial x}{\partial \eta} & \frac{\partial y}{\partial \eta} & \frac{\partial z}{\partial \eta} \\ \frac{\partial x}{\partial \zeta} & \frac{\partial y}{\partial \zeta} & \frac{\partial z}{\partial \zeta} \end{bmatrix} = \begin{bmatrix} a & 0 & 0 \\ 0 & b & 0 \\ 0 & 0 & c \end{bmatrix} \quad (46)$$

Note that, unlike the 2D case, the  $\mathbf{B}$  matrix in 3D (see (38)) is not constant within the element but linear in  $\xi$ ,  $\eta$  and  $\zeta$ .

The polarisation gradient in (16) can be obtained by multiplying (45), (37),

[illegible]

[illegible]

[illegible]

[illegible]

[illegible]

[illegible]

[illegible]



[illegible]

[illegible]

[illegible]

[illegible]

[illegible]

[illegible]

[illegible]

which, making use of (46), leads to:

$$\begin{aligned}
\nabla \cdot \tilde{\mathbf{P}} = & \tilde{f}_{1112} \left[ (d_x^1) \frac{-1+\zeta}{4a^2b} + (d_x^2) \frac{-1+\zeta}{4a^2b} + (d_x^3) \frac{1-\zeta}{4a^2b} + (d_x^4) \frac{1-\zeta}{4a^2b} + \right. \\
& (d_x^5) \frac{-1-\zeta}{4a^2b} + (d_x^6) \frac{-1-\zeta}{4a^2b} + (d_x^7) \frac{1+\zeta}{4a^2b} + (d_x^8) \frac{1+\zeta}{4a^2b} + \\
& \left. (d_x^9) \frac{1-\zeta}{2a^2b} + (d_x^{11}) \frac{-1+\zeta}{2a^2b} + (d_x^{13}) \frac{1+\zeta}{2a^2b} + (d_x^{15}) \frac{-1-\zeta}{2a^2b} \right] + \\
& \tilde{f}_{1113} \left[ (d_x^1) \frac{-1+\eta}{4a^2c} + (d_x^2) \frac{-1+\eta}{4a^2c} + (d_x^3) \frac{-1-\eta}{4a^2c} + (d_x^4) \frac{-1-\eta}{4a^2c} + \right. \\
& (d_x^5) \frac{1-\eta}{4a^2c} + (d_x^6) \frac{1-\eta}{4a^2c} + (d_x^7) \frac{1+\eta}{4a^2c} + (d_x^8) \frac{1+\eta}{4a^2c} + \\
& \left. (d_x^9) \frac{1-\eta}{2a^2c} + (d_x^{11}) \frac{1+\eta}{2a^2c} + (d_x^{13}) \frac{-1+\eta}{2a^2c} + (d_x^{15}) \frac{-1-\eta}{2a^2c} \right] + \\
& \tilde{f}_{1221} \left[ (d_y^1) \frac{-1+\zeta}{4a^2b} + (d_y^2) \frac{-1+\zeta}{4a^2b} + (d_y^3) \frac{1-\zeta}{4a^2b} + (d_y^4) \frac{1-\zeta}{4a^2b} + \right. \\
& (d_y^5) \frac{-1-\zeta}{4a^2b} + (d_y^6) \frac{-1-\zeta}{4a^2b} + (d_y^7) \frac{1+\zeta}{4a^2b} + (d_y^8) \frac{1+\zeta}{4a^2b} + \\
& \left. (d_y^9) \frac{1-\zeta}{2a^2b} + (d_y^{11}) \frac{-1+\zeta}{2a^2b} + (d_y^{13}) \frac{1+\zeta}{2a^2b} + (d_y^{15}) \frac{-1-\zeta}{2a^2b} \right] + \\
& \tilde{f}_{1222} \left[ (d_y^1) \frac{-1+\zeta}{4ab^2} + (d_y^2) \frac{1-\zeta}{4ab^2} + (d_y^3) \frac{1-\zeta}{4ab^2} + (d_y^4) \frac{-1+\zeta}{4ab^2} + \right. \\
& (d_y^5) \frac{-1-\zeta}{4ab^2} + (d_y^6) \frac{1+\zeta}{4ab^2} + (d_y^7) \frac{1+\zeta}{4ab^2} + (d_y^8) \frac{-1-\zeta}{4ab^2} + \\
& \left. (d_y^{10}) \frac{-1+\zeta}{2ab^2} + (d_y^{12}) \frac{1-\zeta}{2ab^2} + (d_y^{14}) \frac{-1-\zeta}{2ab^2} + (d_y^{16}) \frac{1+\zeta}{2ab^2} \right] + \\
& \tilde{f}_{1223} \left[ (d_y^1) \frac{-1+2\xi+2\eta+2\zeta}{8abc} + (d_y^2) \frac{1+2\xi-2\eta-2\zeta}{8abc} + \right. \\
& (d_y^3) \frac{-1-2\xi-2\eta+2\zeta}{8abc} + (d_y^4) \frac{1-2\xi+2\eta-2\zeta}{8abc} + \\
& (d_y^5) \frac{1-2\xi-2\eta+2\zeta}{8abc} + (d_y^6) \frac{-1-2\xi+2\eta-2\zeta}{8abc} + \\
& (d_y^7) \frac{1+2\xi+2\eta+2\zeta}{8abc} + (d_y^8) \frac{-1+2\xi-2\eta-2\zeta}{8abc} + \\
& (d_y^9) \frac{-\xi}{2abc} + (d_y^{10}) \frac{\eta}{2abc} + (d_y^{11}) \frac{\xi}{2abc} + (d_y^{12}) \frac{-\eta}{2abc} + \\
& (d_y^{13}) \frac{\xi}{2abc} + (d_y^{14}) \frac{-\eta}{2abc} + (d_y^{15}) \frac{-\xi}{2abc} + (d_y^{16}) \frac{\eta}{2abc} + \\
& \left. (d_y^{17}) \frac{-\zeta}{2abc} + (d_y^{18}) \frac{\zeta}{2abc} + (d_y^{19}) \frac{-\zeta}{2abc} + (d_y^{20}) \frac{\zeta}{2abc} \right] + \\
& \tilde{f}_{1331} \left[ (d_z^1) \frac{-1+\eta}{4a^2c} + (d_z^2) \frac{-1+\eta}{4a^2c} + (d_z^3) \frac{-1-\eta}{4a^2c} + (d_z^4) \frac{-1-\eta}{4a^2c} + \right. \\
& (d_z^5) \frac{1-\eta}{4a^2c} + (d_z^6) \frac{1-\eta}{4a^2c} + (d_z^7) \frac{1+\eta}{4a^2c} + (d_z^8) \frac{1+\eta}{4a^2c} + \\
& \left. (d_z^9) \frac{1-\eta}{2a^2c} + (d_z^{11}) \frac{1+\eta}{2a^2c} + (d_z^{13}) \frac{-1+\eta}{2a^2c} + (d_z^{15}) \frac{-1-\eta}{2a^2c} \right] +
\end{aligned}$$



$$\begin{aligned}
& \tilde{f}_{1332} \left[ (d_z^1) \frac{-1+2\xi+2\eta+2\zeta}{8abc} + (d_z^2) \frac{1+2\xi-2\eta-2\zeta}{8abc} + \right. \\
& (d_z^3) \frac{-1-2\xi-2\eta+2\zeta}{8abc} + (d_z^4) \frac{1-2\xi+2\eta-2\zeta}{8abc} + \\
& (d_z^5) \frac{1-2\xi-2\eta+2\zeta}{8abc} + (d_z^6) \frac{-1-2\xi+2\eta-2\zeta}{8abc} + \\
& (d_z^7) \frac{1+2\xi+2\eta+2\zeta}{8abc} + (d_z^8) \frac{-1+2\xi-2\eta-2\zeta}{8abc} + \\
& (d_z^9) \frac{-\xi}{2abc} + (d_z^{10}) \frac{\eta}{2abc} + (d_z^{11}) \frac{\xi}{2abc} + (d_z^{12}) \frac{-\eta}{2abc} + \\
& (d_z^{13}) \frac{\xi}{2abc} + (d_z^{14}) \frac{-\eta}{2abc} + (d_z^{15}) \frac{-\xi}{2abc} + (d_z^{16}) \frac{\eta}{2abc} + \\
& \left. (d_z^{17}) \frac{-\zeta}{2abc} + (d_z^{18}) \frac{\zeta}{2abc} + (d_z^{19}) \frac{-\zeta}{2abc} + (d_z^{20}) \frac{\zeta}{2abc} \right] + \\
& \tilde{f}_{1333} \left[ (d_z^1) \frac{-1+\eta}{4ac^2} + (d_z^2) \frac{1-\eta}{4ac^2} + (d_z^3) \frac{1+\eta}{4ac^2} + (d_z^4) \frac{-1-\eta}{4ac^2} + \right. \\
& (d_z^5) \frac{-1+\eta}{4ac^2} + (d_z^6) \frac{1-\eta}{4ac^2} + (d_z^7) \frac{1+\eta}{4ac^2} + (d_z^8) \frac{-1-\eta}{4ac^2} + \\
& \left. (d_z^{17}) \frac{1-\eta}{2ac^2} + (d_z^{18}) \frac{-1+\eta}{2ac^2} + (d_z^{19}) \frac{-1-\eta}{2ac^2} + (d_z^{20}) \frac{1+\eta}{2ac^2} \right] + \\
& \tilde{f}_{1121} \left[ (d_x^1) \frac{-1+\zeta}{4a^2b} + (d_x^2) \frac{-1+\zeta}{4a^2b} + (d_x^3) \frac{1-\zeta}{4a^2b} + (d_x^4) \frac{1-\zeta}{4a^2b} + \right. \\
& (d_x^5) \frac{-1-\zeta}{4a^2b} + (d_x^6) \frac{-1-\zeta}{4a^2b} + (d_x^7) \frac{1+\zeta}{4a^2b} + (d_x^8) \frac{1+\zeta}{4a^2b} + \\
& \left. (d_x^9) \frac{1-\zeta}{2a^2b} + (d_x^{11}) \frac{-1+\zeta}{2a^2b} + (d_x^{13}) \frac{1+\zeta}{2a^2b} + (d_x^{15}) \frac{-1-\zeta}{2a^2b} \right] + \\
& \tilde{f}_{1122} \left[ (d_x^1) \frac{-1+\zeta}{4ab^2} + (d_y^1) \frac{-1+\zeta}{4a^2b} + (d_x^2) \frac{1-\zeta}{4ab^2} + (d_y^2) \frac{-1+\zeta}{4a^2b} + \right. \\
& (d_x^3) \frac{1-\zeta}{4ab^2} + (d_y^3) \frac{1-\zeta}{4a^2b} + (d_x^4) \frac{-1+\zeta}{4ab^2} + (d_y^4) \frac{1-\zeta}{4a^2b} + \\
& (d_x^5) \frac{-1-\zeta}{4ab^2} + (d_y^5) \frac{-1-\zeta}{4a^2b} + (d_x^6) \frac{1+\zeta}{4ab^2} + (d_y^6) \frac{-1-\zeta}{4a^2b} + \\
& (d_x^7) \frac{1+\zeta}{4ab^2} + (d_y^7) \frac{1+\zeta}{4a^2b} + (d_x^8) \frac{-1-\zeta}{4ab^2} + (d_y^8) \frac{1+\zeta}{4a^2b} + \\
& (d_y^9) \frac{1-\zeta}{2a^2b} + (d_x^{10}) \frac{-1+\zeta}{2ab^2} + (d_y^{11}) \frac{-1+\zeta}{2a^2b} + (d_x^{12}) \frac{1-\zeta}{2ab^2} + \\
& \left. (d_y^{13}) \frac{1+\zeta}{2a^2b} + (d_x^{14}) \frac{-1-\zeta}{2ab^2} + (d_y^{15}) \frac{-1-\zeta}{2a^2b} + (d_x^{16}) \frac{1+\zeta}{2ab^2} \right] +
\end{aligned}$$

$$\begin{aligned}
& \tilde{f}_{1123} \left[ (d_x^1) \frac{-1+2\xi+2\eta+2\zeta}{8abc} + (d_y^1) \frac{-1+\eta}{4a^2c} + (d_x^2) \frac{1+2\xi-2\eta-2\zeta}{8abc} + \right. \\
& (d_y^2) \frac{-1+\eta}{4a^2c} + (d_x^3) \frac{-1-2\xi-2\eta+2\zeta}{8abc} + (d_y^3) \frac{-1-\eta}{4a^2c} + \\
& (d_x^4) \frac{1-2\xi+2\eta-2\zeta}{8abc} + (d_y^4) \frac{-1-\eta}{4a^2c} + (d_x^5) \frac{1-2\xi-2\eta+2\zeta}{8abc} + \\
& (d_y^5) \frac{1-\eta}{4a^2c} + (d_x^6) \frac{-1-2\xi+2\eta-2\zeta}{8abc} + (d_y^6) \frac{1-\eta}{4a^2c} + \\
& (d_x^7) \frac{1+2\xi+2\eta+2\zeta}{8abc} + (d_y^7) \frac{1+\eta}{4a^2c} + (d_x^8) \frac{-1+2\xi-2\eta-2\zeta}{8abc} + \\
& (d_y^8) \frac{1+\eta}{4a^2c} + (d_x^9) \frac{-\xi}{2abc} + (d_y^9) \frac{1-\eta}{2a^2c} + (d_x^{10}) \frac{\eta}{2abc} + \\
& (d_x^{11}) \frac{\xi}{2abc} + (d_y^{11}) \frac{1+\eta}{2a^2c} + (d_x^{12}) \frac{-\eta}{2abc} + (d_x^{13}) \frac{\xi}{2abc} + \\
& (d_y^{13}) \frac{-1+\eta}{2a^2c} + (d_x^{14}) \frac{-\eta}{2abc} + (d_x^{15}) \frac{-\xi}{2abc} + (d_y^{15}) \frac{-1-\eta}{2a^2c} + \\
& (d_x^{16}) \frac{\eta}{2abc} + (d_x^{17}) \frac{-\zeta}{2abc} + (d_x^{18}) \frac{\zeta}{2abc} + (d_x^{19}) \frac{-\zeta}{2abc} + (d_x^{20}) \frac{\zeta}{2abc} \Big] + \\
& \tilde{f}_{1131} \left[ (d_x^1) \frac{-1+\eta}{4a^2c} + (d_x^2) \frac{-1+\eta}{4a^2c} + (d_x^3) \frac{-1-\eta}{4a^2c} + (d_x^4) \frac{-1-\eta}{4a^2c} + \right. \\
& (d_x^5) \frac{1-\eta}{4a^2c} + (d_x^6) \frac{1-\eta}{4a^2c} + (d_x^7) \frac{1+\eta}{4a^2c} + (d_x^8) \frac{1+\eta}{4a^2c} + \\
& (d_x^9) \frac{1-\eta}{2a^2c} + (d_x^{11}) \frac{1+\eta}{2a^2c} + (d_x^{13}) \frac{-1+\eta}{2a^2c} + (d_x^{15}) \frac{-1-\eta}{2a^2c} \Big] + \\
& \tilde{f}_{1132} \left[ (d_x^1) \frac{-1+2\xi+2\eta+2\zeta}{8abc} + (d_z^1) \frac{-1+\zeta}{4a^2b} + (d_x^2) \frac{1+2\xi-2\eta-2\zeta}{8abc} + \right. \\
& (d_z^2) \frac{-1+\zeta}{4a^2b} + (d_x^3) \frac{-1-2\xi-2\eta+2\zeta}{8abc} + (d_z^3) \frac{1-\zeta}{4a^2b} + \\
& (d_x^4) \frac{1-2\xi+2\eta-2\zeta}{8abc} + (d_z^4) \frac{1-\zeta}{4a^2b} + (d_x^5) \frac{1-2\xi-2\eta+2\zeta}{8abc} + \\
& (d_z^5) \frac{-1-\zeta}{4a^2b} + (d_x^6) \frac{-1-2\xi+2\eta-2\zeta}{8abc} + (d_z^6) \frac{-1-\zeta}{4a^2b} + \\
& (d_x^7) \frac{1+2\xi+2\eta+2\zeta}{8abc} + (d_z^7) \frac{1+\zeta}{4a^2b} + (d_x^8) \frac{-1+2\xi-2\eta-2\zeta}{8abc} + \\
& (d_z^8) \frac{1+\zeta}{4a^2b} + (d_x^9) \frac{-\xi}{2abc} + (d_z^9) \frac{1-\zeta}{2a^2b} + (d_x^{10}) \frac{\eta}{2abc} + \\
& (d_x^{11}) \frac{\xi}{2abc} + (d_z^{11}) \frac{-1+\zeta}{2a^2b} + (d_x^{12}) \frac{-\eta}{2abc} + (d_x^{13}) \frac{\xi}{2abc} + \\
& (d_z^{13}) \frac{1+\zeta}{2a^2b} + (d_x^{14}) \frac{-\eta}{2abc} + (d_x^{15}) \frac{-\xi}{2abc} + (d_z^{15}) \frac{-1-\zeta}{2a^2b} + \\
& (d_x^{16}) \frac{\eta}{2abc} + (d_x^{17}) \frac{-\zeta}{2abc} + (d_x^{18}) \frac{\zeta}{2abc} + (d_x^{19}) \frac{-\zeta}{2abc} + (d_x^{20}) \frac{\zeta}{2abc} \Big] + \\
& \tilde{f}_{1133} \left[ (d_x^1) \frac{-1+\eta}{4ac^2} + (d_z^1) \frac{-1+\eta}{4a^2c} + (d_x^2) \frac{1-\eta}{4ac^2} + (d_z^2) \frac{-1+\eta}{4a^2c} + \right. \\
& (d_x^3) \frac{1+\eta}{4ac^2} + (d_z^3) \frac{-1-\eta}{4a^2c} + (d_x^4) \frac{-1-\eta}{4ac^2} + (d_z^4) \frac{-1-\eta}{4a^2c} + \\
& (d_x^5) \frac{-1+\eta}{4ac^2} + (d_z^5) \frac{1-\eta}{4a^2c} + (d_x^6) \frac{1-\eta}{4ac^2} + (d_z^6) \frac{1-\eta}{4a^2c} + \\
& (d_x^7) \frac{1+\eta}{4ac^2} + (d_z^7) \frac{1+\eta}{4a^2c} + (d_x^8) \frac{-1-\eta}{4ac^2} + (d_z^8) \frac{1+\eta}{4a^2c} +
\end{aligned}$$

$$\begin{aligned}
& \tilde{f}_{1231} \left[ (d_y^1) \frac{-1+\eta}{4a^2c} + (d_z^1) \frac{-1+\zeta}{4a^2b} + (d_y^2) \frac{-1+\eta}{4a^2c} + (d_z^2) \frac{-1+\zeta}{4a^2b} + \right. \\
& (d_y^3) \frac{-1-\eta}{4a^2c} + (d_z^3) \frac{1-\zeta}{4a^2b} + (d_y^4) \frac{-1-\eta}{4a^2c} + (d_z^4) \frac{1-\zeta}{4a^2b} + \\
& (d_y^5) \frac{1-\eta}{4a^2c} + (d_z^5) \frac{-1-\zeta}{4a^2b} + (d_y^6) \frac{1-\eta}{4a^2c} + (d_z^6) \frac{-1-\zeta}{4a^2b} + \\
& (d_y^7) \frac{1+\eta}{4a^2c} + (d_z^7) \frac{1+\zeta}{4a^2b} + (d_y^8) \frac{1+\eta}{4a^2c} + (d_z^8) \frac{1+\zeta}{4a^2b} + \\
& (d_y^9) \frac{1-\eta}{2a^2c} + (d_z^9) \frac{1-\zeta}{2a^2b} + (d_y^{11}) \frac{1+\eta}{2a^2c} + (d_z^{11}) \frac{-1+\zeta}{2a^2b} + \\
& \left. (d_y^{13}) \frac{-1+\eta}{2a^2c} + (d_z^{13}) \frac{1+\zeta}{2a^2b} + (d_y^{15}) \frac{-1-\eta}{2a^2c} + (d_z^{15}) \frac{-1-\zeta}{2a^2b} \right] + \\
& \tilde{f}_{1232} \left[ (d_y^1) \frac{-1+2\xi+2\eta+2\zeta}{8abc} + (d_z^1) \frac{-1+\zeta}{4ab^2} + (d_y^2) \frac{1+2\xi-2\eta-2\zeta}{8abc} + \right. \\
& (d_z^2) \frac{1-\zeta}{4ab^2} + (d_y^3) \frac{-1-2\xi-2\eta+2\zeta}{8abc} + (d_z^3) \frac{1-\zeta}{4ab^2} + \\
& (d_y^4) \frac{1-2\xi+2\eta-2\zeta}{8abc} + (d_z^4) \frac{-1+\zeta}{4ab^2} + (d_y^5) \frac{1-2\xi-2\eta+2\zeta}{8abc} + \\
& (d_z^5) \frac{-1-\zeta}{4ab^2} + (d_y^6) \frac{-1-2\xi+2\eta-2\zeta}{8abc} + (d_z^6) \frac{1+\zeta}{4ab^2} + \\
& (d_y^7) \frac{1+2\xi+2\eta+2\zeta}{8abc} + (d_z^7) \frac{1+\zeta}{4ab^2} + (d_y^8) \frac{-1+2\xi-2\eta-2\zeta}{8abc} + \\
& (d_z^8) \frac{-1-\zeta}{4ab^2} + (d_y^9) \frac{-\xi}{2abc} + (d_y^{10}) \frac{\eta}{2abc} + (d_z^{10}) \frac{-1+\zeta}{2ab^2} + \\
& (d_y^{11}) \frac{\xi}{2abc} + (d_y^{12}) \frac{-\eta}{2abc} + (d_z^{12}) \frac{1-\zeta}{2ab^2} + (d_y^{13}) \frac{\xi}{2abc} + \\
& (d_y^{14}) \frac{-\eta}{2abc} + (d_z^{14}) \frac{-1-\zeta}{2ab^2} + (d_y^{15}) \frac{-\xi}{2abc} + (d_y^{16}) \frac{\eta}{2abc} + \\
& (d_z^{16}) \frac{1+\zeta}{2ab^2} + (d_y^{17}) \frac{-\zeta}{2abc} + (d_y^{18}) \frac{\zeta}{2abc} + (d_y^{19}) \frac{-\zeta}{2abc} + (d_y^{20}) \frac{\zeta}{2abc} \left. \right] + \\
& \tilde{f}_{1233} \left[ (d_y^1) \frac{-1+\eta}{4ac^2} + (d_z^1) \frac{-1+2\xi+2\eta+2\zeta}{8abc} + (d_y^2) \frac{1-\eta}{4ac^2} + \right. \\
& (d_z^2) \frac{1+2\xi-2\eta-2\zeta}{8abc} + (d_y^3) \frac{1+\eta}{4ac^2} + (d_z^3) \frac{-1-2\xi-2\eta+2\zeta}{8abc} + \\
& (d_y^4) \frac{-1-\eta}{4ac^2} + (d_z^4) \frac{1-2\xi+2\eta-2\zeta}{8abc} + (d_y^5) \frac{-1+\eta}{4ac^2} + \\
& (d_z^5) \frac{1-2\xi-2\eta+2\zeta}{8abc} + (d_y^6) \frac{1-\eta}{4ac^2} + (d_z^6) \frac{-1-2\xi+2\eta-2\zeta}{8abc} + \\
& (d_y^7) \frac{1+\eta}{4ac^2} + (d_z^7) \frac{1+2\xi+2\eta+2\zeta}{8abc} + (d_y^8) \frac{-1-\eta}{4ac^2} + \\
& (d_z^8) \frac{-1+2\xi-2\eta-2\zeta}{8abc} + (d_y^9) \frac{-\xi}{2abc} + (d_z^9) \frac{\eta}{2abc} + (d_z^{11}) \frac{\xi}{2abc} + \\
& (d_z^{12}) \frac{-\eta}{2abc} + (d_z^{13}) \frac{\xi}{2abc} + (d_z^{14}) \frac{-\eta}{2abc} + (d_z^{15}) \frac{-\xi}{2abc} + \\
& (d_z^{16}) \frac{\eta}{2abc} + (d_y^{17}) \frac{1-\eta}{2ac^2} + (d_z^{17}) \frac{-\zeta}{2abc} + (d_y^{18}) \frac{-1+\eta}{2ac^2} + \\
& \left. (d_z^{18}) \frac{\zeta}{2abc} + (d_y^{19}) \frac{-1-\eta}{2ac^2} + (d_z^{19}) \frac{-\zeta}{2abc} + (d_y^{20}) \frac{1+\eta}{2ac^2} + (d_z^{20}) \frac{\zeta}{2abc} \right] +
\end{aligned}$$

$$\begin{aligned}
& \tilde{f}_{2111} \left[ (d_x^1) \frac{-1+\zeta}{4a^2b} + (d_x^2) \frac{-1+\zeta}{4a^2b} + (d_x^3) \frac{1-\zeta}{4a^2b} + (d_x^4) \frac{1-\zeta}{4a^2b} + \right. \\
& \quad (d_x^5) \frac{-1-\zeta}{4a^2b} + (d_x^6) \frac{-1-\zeta}{4a^2b} + (d_x^7) \frac{1+\zeta}{4a^2b} + (d_x^8) \frac{1+\zeta}{4a^2b} + \\
& \quad \left. (d_x^9) \frac{1-\zeta}{2a^2b} + (d_x^{11}) \frac{-1+\zeta}{2a^2b} + (d_x^{13}) \frac{1+\zeta}{2a^2b} + (d_x^{15}) \frac{-1-\zeta}{2a^2b} \right] + \\
& \tilde{f}_{2112} \left[ (d_x^1) \frac{-1+\zeta}{4ab^2} + (d_x^2) \frac{1-\zeta}{4ab^2} + (d_x^3) \frac{1-\zeta}{4ab^2} + (d_x^4) \frac{-1+\zeta}{4ab^2} + \right. \\
& \quad (d_x^5) \frac{-1-\zeta}{4ab^2} + (d_x^6) \frac{1+\zeta}{4ab^2} + (d_x^7) \frac{1+\zeta}{4ab^2} + (d_x^8) \frac{-1-\zeta}{4ab^2} + \\
& \quad \left. (d_x^{10}) \frac{-1+\zeta}{2ab^2} + (d_x^{12}) \frac{1-\zeta}{2ab^2} + (d_x^{14}) \frac{-1-\zeta}{2ab^2} + (d_x^{16}) \frac{1+\zeta}{2ab^2} \right] + \\
& \tilde{f}_{2113} \left[ (d_x^1) \frac{-1+2\xi+2\eta+2\zeta}{8abc} + (d_x^2) \frac{1+2\xi-2\eta-2\zeta}{8abc} + \right. \\
& \quad (d_x^3) \frac{-1-2\xi-2\eta+2\zeta}{8abc} + (d_x^4) \frac{1-2\xi+2\eta-2\zeta}{8abc} + \\
& \quad (d_x^5) \frac{1-2\xi-2\eta+2\zeta}{8abc} + (d_x^6) \frac{-1-2\xi+2\eta-2\zeta}{8abc} + \\
& \quad (d_x^7) \frac{1+2\xi+2\eta+2\zeta}{8abc} + (d_x^8) \frac{-1+2\xi-2\eta-2\zeta}{8abc} + \\
& \quad (d_x^9) \frac{-\xi}{2abc} + (d_x^{10}) \frac{\eta}{2abc} + (d_x^{11}) \frac{\xi}{2abc} + (d_x^{12}) \frac{-\eta}{2abc} + \\
& \quad (d_x^{13}) \frac{\xi}{2abc} + (d_x^{14}) \frac{-\eta}{2abc} + (d_x^{15}) \frac{-\xi}{2abc} + (d_x^{16}) \frac{\eta}{2abc} + \\
& \quad \left. (d_x^{17}) \frac{-\zeta}{2abc} + (d_x^{18}) \frac{\zeta}{2abc} + (d_x^{19}) \frac{-\zeta}{2abc} + (d_x^{20}) \frac{\zeta}{2abc} \right] + \\
& \tilde{f}_{2221} \left[ (d_y^1) \frac{-1+\zeta}{4ab^2} + (d_y^2) \frac{1-\zeta}{4ab^2} + (d_y^3) \frac{1-\zeta}{4ab^2} + (d_y^4) \frac{-1+\zeta}{4ab^2} + \right. \\
& \quad (d_y^5) \frac{-1-\zeta}{4ab^2} + (d_y^6) \frac{1+\zeta}{4ab^2} + (d_y^7) \frac{1+\zeta}{4ab^2} + (d_y^8) \frac{-1-\zeta}{4ab^2} + \\
& \quad \left. (d_y^{10}) \frac{-1+\zeta}{2ab^2} + (d_y^{12}) \frac{1-\zeta}{2ab^2} + (d_y^{14}) \frac{-1-\zeta}{2ab^2} + (d_y^{16}) \frac{-1-\zeta}{2ab^2} \right] + \\
& \tilde{f}_{2223} \left[ (d_y^1) \frac{-1+\xi}{4b^2c} + (d_y^2) \frac{-1-\xi}{4b^2c} + (d_y^3) \frac{-1-\xi}{4b^2c} + (d_y^4) \frac{-1+\xi}{4b^2c} + \right. \\
& \quad (d_y^5) \frac{1-\xi}{4b^2c} + (d_y^6) \frac{1+\xi}{4b^2c} + (d_y^7) \frac{1+\xi}{4b^2c} + (d_y^8) \frac{1-\xi}{4b^2c} + \\
& \quad \left. (d_y^{10}) \frac{1+\xi}{2b^2c} + (d_y^{12}) \frac{1-\xi}{2b^2c} + (d_y^{14}) \frac{-1-\xi}{2b^2c} + (d_y^{16}) \frac{-1+\xi}{2b^2c} \right] +
\end{aligned}$$

$$\begin{aligned}
& \tilde{f}_{2331} \left[ (d_z^1) \frac{-1+2\xi+2\eta+2\zeta}{8abc} + (d_z^2) \frac{1+2\xi-2\eta-2\zeta}{8abc} + \right. \\
& (d_z^3) \frac{-1-2\xi-2\eta+2\zeta}{8abc} + (d_z^4) \frac{1-2\xi+2\eta-2\zeta}{8abc} + \\
& (d_z^5) \frac{1-2\xi-2\eta+2\zeta}{8abc} + (d_z^6) \frac{-1-2\xi+2\eta-2\zeta}{8abc} + \\
& (d_z^7) \frac{1+2\xi+2\eta+2\zeta}{8abc} + (d_z^8) \frac{-1+2\xi-2\eta-2\zeta}{8abc} + \\
& (d_z^9) \frac{-\xi}{2abc} + (d_z^{10}) \frac{\eta}{2abc} + (d_z^{11}) \frac{\xi}{2abc} + (d_z^{12}) \frac{-\eta}{2abc} + \\
& (d_z^{13}) \frac{\xi}{2abc} + (d_z^{14}) \frac{-\eta}{2abc} + (d_z^{15}) \frac{-\xi}{2abc} + (d_z^{16}) \frac{\eta}{2abc} + \\
& \left. (d_z^{17}) \frac{-\zeta}{2abc} + (d_z^{18}) \frac{\zeta}{2abc} + (d_z^{19}) \frac{-\zeta}{2abc} + (d_z^{20}) \frac{\zeta}{2abc} \right] + \\
& \tilde{f}_{2332} \left[ (d_z^1) \frac{-1+\xi}{4b^2c} + (d_z^2) \frac{-1-\xi}{4b^2c} + (d_z^3) \frac{-1-\xi}{4b^2c} + (d_z^4) \frac{-1+\xi}{4b^2c} + \right. \\
& (d_z^5) \frac{1-\xi}{4b^2c} + (d_z^6) \frac{1+\xi}{4b^2c} + (d_z^7) \frac{1+\xi}{4b^2c} + (d_z^8) \frac{1-\xi}{4b^2c} + \\
& \left. (d_z^{10}) \frac{1+\xi}{2b^2c} + (d_z^{12}) \frac{1-\xi}{2b^2c} + (d_z^{14}) \frac{-1-\xi}{2b^2c} + (d_z^{16}) \frac{-1+\xi}{2b^2c} \right] + \\
& \tilde{f}_{2333} \left[ (d_z^1) \frac{-1+\xi}{4bc^2} + (d_z^2) \frac{-1-\xi}{4bc^2} + (d_z^3) \frac{1+\xi}{4bc^2} + (d_z^4) \frac{1-\xi}{4bc^2} + \right. \\
& (d_z^5) \frac{-1+\xi}{4bc^2} + (d_z^6) \frac{-1-\xi}{4bc^2} + (d_z^7) \frac{1+\xi}{4bc^2} + (d_z^8) \frac{1-\xi}{4bc^2} + \\
& \left. (d_z^{17}) \frac{1-\xi}{2bc^2} + (d_z^{18}) \frac{1+\xi}{2bc^2} + (d_z^{19}) \frac{-1-\xi}{2bc^2} + (d_z^{20}) \frac{-1+\xi}{2bc^2} \right] + \\
& \tilde{f}_{2121} \left[ (d_x^1) \frac{-1+\zeta}{4ab^2} + (d_y^1) \frac{-1+\zeta}{4a^2b} + (d_x^2) \frac{1-\zeta}{4ab^2} + (d_y^2) \frac{-1+\zeta}{4a^2b} + \right. \\
& (d_x^3) \frac{1-\zeta}{4ab^2} + (d_y^3) \frac{1-\zeta}{4a^2b} + (d_x^4) \frac{-1+\zeta}{4ab^2} + (d_y^4) \frac{1-\zeta}{4a^2b} + \\
& (d_x^5) \frac{-1-\zeta}{4ab^2} + (d_y^5) \frac{-1-\zeta}{4a^2b} + (d_x^6) \frac{1+\zeta}{4ab^2} + (d_y^6) \frac{-1-\zeta}{4a^2b} + \\
& (d_x^7) \frac{1+\zeta}{4ab^2} + (d_y^7) \frac{1+\zeta}{4a^2b} + (d_x^8) \frac{-1-\zeta}{4ab^2} + (d_y^8) \frac{1+\zeta}{4a^2b} + \\
& (d_y^9) \frac{1-\zeta}{2a^2b} + (d_x^{10}) \frac{-1+\zeta}{2ab^2} + (d_y^{11}) \frac{-1+\zeta}{2a^2b} + (d_x^{12}) \frac{1-\zeta}{2ab^2} + \\
& (d_y^{13}) \frac{1+\zeta}{2a^2b} + (d_x^{14}) \frac{-1-\zeta}{2ab^2} + (d_y^{15}) \frac{-1-\zeta}{2a^2b} + (d_x^{16}) \frac{1+\zeta}{2ab^2} \left. \right] + \\
& \tilde{f}_{2122} \left[ (d_y^1) \frac{-1+\zeta}{4ab^2} + (d_y^2) \frac{1-\zeta}{4ab^2} + (d_y^3) \frac{1-\zeta}{4ab^2} + (d_y^4) \frac{-1+\zeta}{4ab^2} + \right. \\
& (d_y^5) \frac{-1-\zeta}{4ab^2} + (d_y^6) \frac{1+\zeta}{4ab^2} + (d_y^7) \frac{1+\zeta}{4ab^2} + (d_y^8) \frac{-1-\zeta}{4ab^2} + \\
& \left. (d_y^{10}) \frac{-1+\zeta}{2ab^2} + (d_y^{12}) \frac{1-\zeta}{2ab^2} + (d_y^{14}) \frac{-1-\zeta}{2ab^2} + (d_y^{16}) \frac{1+\zeta}{2ab^2} \right] +
\end{aligned}$$

$$\begin{aligned}
& \tilde{f}_{2123} \left[ (d_x^1) \frac{-1+\xi}{4b^2c} + (d_y^1) \frac{-1+2\xi+2\eta+2\zeta}{8abc} + (d_x^2) \frac{-1-\xi}{4ab^2c} + \right. \\
& (d_y^2) \frac{1+2\xi-2\eta-2\zeta}{8abc} + (d_x^3) \frac{-1-\xi}{4b^2c} + (d_y^3) \frac{-1-2\xi-2\eta+2\zeta}{8abc} + \\
& (d_x^4) \frac{-1+\xi}{4b^2c} + (d_y^4) \frac{1-2\xi+2\eta-2\zeta}{8abc} + (d_x^5) \frac{1-\xi}{4b^2c} + \\
& (d_y^5) \frac{1-2\xi-2\eta+2\zeta}{8abc} + (d_x^6) \frac{1+\xi}{4b^2c} + (d_y^6) \frac{-1-2\xi+2\eta-2\zeta}{8abc} + \\
& (d_x^7) \frac{1+\xi}{4b^2c} + (d_y^7) \frac{1+2\xi+2\eta+2\zeta}{8abc} + (d_x^8) \frac{1-\xi}{4b^2c} + \\
& (d_y^8) \frac{-1+2\xi-2\eta-2\zeta}{8abc} + (d_y^9) \frac{-\xi}{2abc} + (d_x^{10}) \frac{1+\xi}{2b^2c} + (d_y^{10}) \frac{\eta}{2abc} + \\
& (d_y^{11}) \frac{\xi}{2abc} + (d_x^{12}) \frac{1-\xi}{2b^2c} + (d_y^{12}) \frac{-\eta}{2abc} + (d_y^{13}) \frac{\xi}{2abc} + \\
& (d_x^{14}) \frac{-1-\xi}{2b^2c} + (d_y^{14}) \frac{-\eta}{2abc} + (d_y^{15}) \frac{-\xi}{2abc} + (d_x^{16}) \frac{-1+\xi}{2b^2c} + \\
& (d_y^{16}) \frac{\eta}{2abc} + (d_y^{17}) \frac{-\zeta}{2abc} + (d_y^{18}) \frac{\zeta}{2abc} + (d_y^{19}) \frac{-\zeta}{2abc} + (d_y^{20}) \frac{\zeta}{2abc} \left. \right] + \\
& \tilde{f}_{2131} \left[ (d_x^1) \frac{-1+2\xi+2\eta+2\zeta}{8abc} + (d_z^1) \frac{-1+\zeta}{4a^2b} + (d_x^2) \frac{1+2\xi-2\eta-2\zeta}{8abc} + \right. \\
& (d_z^2) \frac{-1+\zeta}{4a^2b} + (d_x^3) \frac{-1-2\xi-2\eta+2\zeta}{8abc} + (d_z^3) \frac{1-\zeta}{4a^2b} + \\
& (d_x^4) \frac{1-2\xi+2\eta-2\zeta}{8abc} + (d_z^4) \frac{1-\zeta}{4a^2b} + (d_x^5) \frac{1-2\xi-2\eta+2\zeta}{8abc} + \\
& (d_z^5) \frac{-1-\zeta}{4a^2b} + (d_x^6) \frac{-1-2\xi+2\eta-2\zeta}{8abc} + (d_z^6) \frac{-1-\zeta}{4a^2b} + \\
& (d_x^7) \frac{1+2\xi+2\eta+2\zeta}{8abc} + (d_z^7) \frac{1+\zeta}{4a^2b} + (d_x^8) \frac{-1+2\xi-2\eta-2\zeta}{8abc} + \\
& (d_z^8) \frac{1+\zeta}{4a^2b} + (d_x^9) \frac{-\xi}{2abc} + (d_z^9) \frac{1-\zeta}{2a^2b} + (d_x^{10}) \frac{\eta}{2abc} + \\
& (d_x^{11}) \frac{\xi}{2abc} + (d_z^{11}) \frac{-1+\zeta}{2a^2b} + (d_x^{12}) \frac{-\eta}{2abc} + (d_x^{13}) \frac{\xi}{2abc} + \\
& (d_z^{13}) \frac{1+\zeta}{2a^2b} + (d_x^{14}) \frac{-\eta}{2abc} + (d_x^{15}) \frac{-\xi}{2abc} + (d_z^{15}) \frac{-1-\zeta}{2a^2b} + \\
& (d_x^{16}) \frac{\eta}{2abc} + (d_x^{17}) \frac{-\zeta}{2abc} + (d_x^{18}) \frac{\zeta}{2abc} + (d_x^{19}) \frac{-\zeta}{2abc} + (d_x^{20}) \frac{\zeta}{2abc} \left. \right] + \\
& \tilde{f}_{2132} \left[ (d_x^1) \frac{-1+\xi}{4b^2c} + (d_z^1) \frac{-1+\zeta}{4ab^2} + (d_x^2) \frac{-1-\xi}{4b^2c} + (d_z^2) \frac{1-\zeta}{4ab^2} + \right. \\
& (d_x^3) \frac{-1-\xi}{4b^2c} + (d_z^3) \frac{1-\zeta}{4ab^2} + (d_x^4) \frac{-1+\xi}{4b^2c} + (d_z^4) \frac{-1+\zeta}{4ab^2} + \\
& (d_x^5) \frac{1-\xi}{4b^2c} + (d_z^5) \frac{-1-\zeta}{4ab^2} + (d_x^6) \frac{1+\xi}{4b^2c} + (d_z^6) \frac{1+\zeta}{4ab^2} + \\
& (d_x^7) \frac{1+\xi}{4b^2c} + (d_z^7) \frac{1+\zeta}{4ab^2} + (d_x^8) \frac{1-\xi}{4b^2c} + (d_z^8) \frac{-1-\zeta}{4ab^2} + \\
& (d_x^{10}) \frac{1+\xi}{2b^2c} + (d_z^{10}) \frac{-1+\zeta}{2ab^2} + (d_x^{12}) \frac{1-\xi}{2b^2c} + (d_z^{12}) \frac{1-\zeta}{2ab^2} + \\
& (d_x^{14}) \frac{-1-\xi}{2b^2c} + (d_z^{14}) \frac{-1-\zeta}{2ab^2} + (d_x^{16}) \frac{-1+\xi}{2b^2c} + (d_z^{16}) \frac{1+\zeta}{2ab^2} \left. \right] +
\end{aligned}$$

$$\begin{aligned} \tilde{f}_{2133} & \left[ (d_x^1) \frac{-1+\xi}{4bc^2} + (d_z^1) \frac{-1+2\xi+2\eta+2\zeta}{8abc} + (d_x^2) \frac{-1-\xi}{4bc^2} + \right. \\ & (d_z^2) \frac{1+2\xi-2\eta-2\zeta}{8abc} + (d_x^3) \frac{1+\xi}{4bc^2} + (d_z^3) \frac{-1-2\xi-2\eta+2\zeta}{8abc} + \\ & (d_x^4) \frac{1-\xi}{4bc^2} + (d_z^4) \frac{1-2\xi+2\eta-2\zeta}{8abc} + (d_x^5) \frac{-1+\xi}{4bc^2} + \\ & (d_z^5) \frac{1-2\xi-2\eta+2\zeta}{8abc} + (d_x^6) \frac{-1-\xi}{4bc^2} + (d_z^6) \frac{-1-2\xi+2\eta-2\zeta}{8abc} + \\ & (d_x^7) \frac{1+\xi}{4bc^2} + (d_z^7) \frac{1+2\xi+2\eta+2\zeta}{8abc} + (d_x^8) \frac{1-\xi}{4bc^2} + \\ & (d_z^8) \frac{-1+2\xi-2\eta-2\zeta}{8abc} + (d_z^9) \frac{-\xi}{2abc} + (d_z^{10}) \frac{\eta}{2abc} + (d_z^{11}) \frac{\xi}{2abc} + \\ & (d_z^{12}) \frac{-\eta}{2abc} + (d_z^{13}) \frac{\xi}{2abc} + (d_z^{14}) \frac{-\eta}{2abc} + (d_z^{15}) \frac{-\xi}{2abc} + \\ & (d_z^{16}) \frac{\eta}{2abc} + (d_x^{17}) \frac{1-\xi}{2bc^2} + (d_z^{17}) \frac{-\zeta}{2abc} + (d_x^{18}) \frac{1+\xi}{2bc^2} + \\ & \left. (d_z^{18}) \frac{\zeta}{2abc} + (d_x^{19}) \frac{-1-\xi}{2bc^2} + (d_z^{19}) \frac{-\zeta}{2abc} + (d_x^{20}) \frac{-1+\xi}{2bc^2} + (d_z^{20}) \frac{\zeta}{2abc} \right] + \end{aligned}$$

$$\begin{aligned} \tilde{f}_{2231} & \left[ (d_y^1) \frac{-1+2\xi+2\eta+2\zeta}{8abc} + (d_z^1) \frac{-1+\zeta}{4ab^2} + (d_y^2) \frac{1+2\xi-2\eta-2\zeta}{8abc} + \right. \\ & (d_z^2) \frac{1-\zeta}{4ab^2} + (d_y^3) \frac{-1-2\xi-2\eta+2\zeta}{8abc} + (d_z^3) \frac{1-\zeta}{4ab^2} + \\ & (d_y^4) \frac{1-2\xi+2\eta-2\zeta}{8abc} + (d_z^4) \frac{-1+\zeta}{4ab^2} + (d_y^5) \frac{1-2\xi-2\eta+2\zeta}{8abc} + \\ & (d_z^5) \frac{-1-\zeta}{4ab^2} + (d_y^6) \frac{-1-2\xi+2\eta-2\zeta}{8abc} + (d_z^6) \frac{1+\zeta}{4ab^2} + \\ & (d_y^7) \frac{1+2\xi+2\eta+2\zeta}{8abc} + (d_z^7) \frac{1+\zeta}{4ab^2} + (d_y^8) \frac{-1+2\xi-2\eta-2\zeta}{8abc} + \\ & (d_z^8) \frac{-1-\zeta}{4ab^2} + (d_y^9) \frac{-\xi}{2abc} + (d_y^{10}) \frac{\eta}{2abc} + (d_z^{10}) \frac{-1+\zeta}{2ab^2} + \\ & (d_y^{11}) \frac{\xi}{2abc} + (d_y^{12}) \frac{-\eta}{2abc} + (d_z^{12}) \frac{1-\zeta}{2ab^2} + (d_y^{13}) \frac{\xi}{2abc} + \\ & (d_y^{14}) \frac{-\eta}{2abc} + (d_z^{14}) \frac{-1-\zeta}{2ab^2} + (d_y^{15}) \frac{-\xi}{2abc} + (d_y^{16}) \frac{\eta}{2abc} + \\ & \left. (d_z^{16}) \frac{1+\zeta}{2ab^2} + (d_y^{17}) \frac{-\zeta}{2abc} + (d_y^{18}) \frac{\zeta}{2abc} + (d_y^{19}) \frac{-\zeta}{2abc} + (d_y^{20}) \frac{\zeta}{2abc} \right] + \end{aligned}$$

$$\begin{aligned} \tilde{f}_{2232} & \left[ (d_y^1) \frac{-1+\xi}{4b^2c} + (d_y^2) \frac{-1-\xi}{4b^2c} + (d_y^3) \frac{-1-\xi}{4b^2c} + (d_y^4) \frac{-1+\xi}{4b^2c} + \right. \\ & (d_y^5) \frac{1-\xi}{4b^2c} + (d_y^6) \frac{1+\xi}{4b^2c} + (d_y^7) \frac{1+\xi}{4b^2c} + (d_y^8) \frac{1-\xi}{4b^2c} + \\ & \left. (d_y^{10}) \frac{1+\xi}{2b^2c} + (d_y^{12}) \frac{1-\xi}{2b^2c} + (d_y^{14}) \frac{-1-\xi}{2b^2c} + (d_y^{16}) \frac{-1+\xi}{2b^2c} \right] + \end{aligned}$$

$$\begin{aligned} \tilde{f}_{2233} & \left[ (d_y^1) \frac{-1+\xi}{4bc^2} + (d_z^1) \frac{-1+\xi}{4b^2c} + (d_y^2) \frac{-1-\xi}{4bc^2} + (d_z^2) \frac{-1-\xi}{4b^2c} + \right. \\ & (d_y^3) \frac{1+\xi}{4bc^2} + (d_z^3) \frac{-1-\xi}{4b^2c} + (d_y^4) \frac{1-\xi}{4bc^2} + (d_z^4) \frac{-1+\xi}{4b^2c} + \\ & (d_y^5) \frac{-1+\xi}{4bc^2} + (d_z^5) \frac{1-\xi}{4b^2c} + (d_y^6) \frac{-1-\xi}{4bc^2} + (d_z^6) \frac{1+\xi}{4b^2c} + \\ & \left. (d_y^7) \frac{1+\xi}{4bc^2} + (d_z^7) \frac{1+\xi}{4b^2c} + (d_y^8) \frac{1-\xi}{4bc^2} + (d_z^8) \frac{1-\xi}{4b^2c} + \right. \end{aligned}$$

$$\begin{aligned}
& \tilde{f}_{3111} \left[ (d_x^1) \frac{-1+\eta}{4a^2c} + (d_x^2) \frac{-1+\eta}{4a^2c} + (d_x^3) \frac{-1-\eta}{4a^2c} + (d_x^4) \frac{-1-\eta}{4a^2c} + \right. \\
& \quad (d_x^5) \frac{1-\eta}{4a^2c} + (d_x^6) \frac{1-\eta}{4a^2c} + (d_x^7) \frac{1+\eta}{4a^2c} + (d_x^8) \frac{1+\eta}{4a^2c} + \\
& \quad \left. (d_x^9) \frac{1-\eta}{2a^2c} + (d_x^{11}) \frac{1+\eta}{2a^2c} + (d_x^{13}) \frac{-1+\eta}{2a^2c} + (d_x^{15}) \frac{-1-\eta}{2a^2c} \right] + \\
& \tilde{f}_{3112} \left[ (d_x^1) \frac{-1+2\xi+2\eta+2\zeta}{8abc} + (d_x^2) \frac{1+2\xi-2\eta-2\zeta}{8abc} + \right. \\
& \quad (d_x^3) \frac{-1-2\xi-2\eta+2\zeta}{8abc} + (d_x^4) \frac{1-2\xi+2\eta-2\zeta}{8abc} + \\
& \quad (d_x^5) \frac{1-2\xi-2\eta+2\zeta}{8abc} + (d_x^6) \frac{-1-2\xi+2\eta-2\zeta}{8abc} + \\
& \quad (d_x^7) \frac{1+2\xi+2\eta+2\zeta}{8abc} + (d_x^8) \frac{-1+2\xi-2\eta-2\zeta}{8abc} + \\
& \quad (d_x^9) \frac{-\xi}{2abc} + (d_x^{10}) \frac{\eta}{2abc} + (d_x^{11}) \frac{\xi}{2abc} + (d_x^{12}) \frac{-\eta}{2abc} + \\
& \quad (d_x^{13}) \frac{\xi}{2abc} + (d_x^{14}) \frac{-\eta}{2abc} + (d_x^{15}) \frac{-\xi}{2abc} + (d_x^{16}) \frac{\eta}{2abc} + \\
& \quad \left. (d_x^{17}) \frac{-\zeta}{2abc} + (d_x^{18}) \frac{\zeta}{2abc} + (d_x^{19}) \frac{-\zeta}{2abc} + (d_x^{20}) \frac{\zeta}{2abc} \right] + \\
& \tilde{f}_{3113} \left[ (d_x^1) \frac{-1+\eta}{4ac^2} + (d_x^2) \frac{1-\eta}{4ac^2} + (d_x^3) \frac{1+\eta}{4ac^2} + (d_x^4) \frac{-1-\eta}{4ac^2} + \right. \\
& \quad (d_x^5) \frac{-1+\eta}{4ac^2} + (d_x^6) \frac{1-\eta}{4ac^2} + (d_x^7) \frac{1+\eta}{4ac^2} + (d_x^8) \frac{-1-\eta}{4ac^2} + \\
& \quad \left. (d_x^{17}) \frac{1-\eta}{2ac^2} + (d_x^{18}) \frac{-1+\eta}{2ac^2} + (d_x^{19}) \frac{-1-\eta}{2ac^2} + (d_x^{20}) \frac{1+\eta}{2ac^2} \right] + \\
& \tilde{f}_{3221} \left[ (d_y^1) \frac{-1+2\xi+2\eta+2\zeta}{8abc} + (d_y^2) \frac{1+2\xi-2\eta-2\zeta}{8abc} + \right. \\
& \quad (d_y^3) \frac{-1-2\xi-2\eta+2\zeta}{8abc} + (d_y^4) \frac{1-2\xi+2\eta-2\zeta}{8abc} + \\
& \quad (d_y^5) \frac{1-2\xi-2\eta+2\zeta}{8abc} + (d_y^6) \frac{-1-2\xi+2\eta-2\zeta}{8abc} + \\
& \quad (d_y^7) \frac{1+2\xi+2\eta+2\zeta}{8abc} + (d_y^8) \frac{-1+2\xi-2\eta-2\zeta}{8abc} + \\
& \quad (d_y^9) \frac{-\xi}{2abc} + (d_y^{10}) \frac{\eta}{2abc} + (d_y^{11}) \frac{\xi}{2abc} + (d_y^{12}) \frac{-\eta}{2abc} + \\
& \quad (d_y^{13}) \frac{\xi}{2abc} + (d_y^{14}) \frac{-\eta}{2abc} + (d_y^{15}) \frac{-\xi}{2abc} + (d_y^{16}) \frac{\eta}{2abc} + \\
& \quad \left. (d_y^{17}) \frac{-\zeta}{2abc} + (d_y^{18}) \frac{\zeta}{2abc} + (d_y^{19}) \frac{-\zeta}{2abc} + (d_y^{20}) \frac{\zeta}{2abc} \right] + \\
& \tilde{f}_{3222} \left[ (d_y^1) \frac{-1+\xi}{4b^2c} + (d_y^2) \frac{-1-\xi}{4b^2c} + (d_y^3) \frac{-1-\xi}{4b^2c} + (d_y^4) \frac{-1+\xi}{4b^2c} + \right. \\
& \quad (d_y^5) \frac{1-\xi}{4b^2c} + (d_y^6) \frac{1+\xi}{4b^2c} + (d_y^7) \frac{1+\xi}{4b^2c} + (d_y^8) \frac{1-\xi}{4b^2c} + \\
& \quad \left. (d_y^{10}) \frac{1+\xi}{2b^2c} + (d_y^{12}) \frac{1-\xi}{2b^2c} + (d_y^{14}) \frac{-1-\xi}{2b^2c} + (d_y^{16}) \frac{-1+\xi}{2b^2c} \right] +
\end{aligned}$$



$$\begin{aligned}
& \tilde{f}_{3223} \left[ (d_y^1) \frac{-1+\xi}{4bc^2} + (d_y^2) \frac{-1-\xi}{4bc^2} + (d_y^3) \frac{1+\xi}{4bc^2} + (d_y^4) \frac{1-\xi}{4bc^2} + \right. \\
& \quad (d_y^5) \frac{-1+\xi}{4bc^2} + (d_y^6) \frac{-1-\xi}{4bc^2} + (d_y^7) \frac{1+\xi}{4bc^2} + (d_y^8) \frac{1-\xi}{4bc^2} + \\
& \quad \left. (d_y^{17}) \frac{1-\xi}{2bc^2} + (d_y^{18}) \frac{1+\xi}{2bc^2} + (d_y^{19}) \frac{-1-\xi}{2bc^2} + (d_y^{20}) \frac{-1+\xi}{2bc^2} \right] + \\
& \tilde{f}_{3331} \left[ (d_z^1) \frac{-1+\eta}{4ac^2} + (d_z^2) \frac{1-\eta}{4ac^2} + (d_z^3) \frac{1+\eta}{4ac^2} + (d_z^4) \frac{-1-\eta}{4ac^2} + \right. \\
& \quad (d_z^5) \frac{-1+\eta}{4ac^2} + (d_z^6) \frac{1-\eta}{4ac^2} + (d_z^7) \frac{1+\eta}{4ac^2} + (d_z^8) \frac{-1-\eta}{4ac^2} + \\
& \quad \left. (d_z^{17}) \frac{1-\eta}{2ac^2} + (d_z^{18}) \frac{-1+\eta}{2ac^2} + (d_z^{19}) \frac{-1-\eta}{2ac^2} + (d_z^{20}) \frac{1+\eta}{2ac^2} \right] + \\
& \tilde{f}_{3332} \left[ (d_z^1) \frac{-1+\xi}{4bc^2} + (d_z^2) \frac{-1-\xi}{4bc^2} + (d_z^3) \frac{1+\xi}{4bc^2} + (d_z^4) \frac{1-\xi}{4bc^2} + \right. \\
& \quad (d_z^5) \frac{-1+\xi}{4bc^2} + (d_z^6) \frac{-1-\xi}{4bc^2} + (d_z^7) \frac{1+\xi}{4bc^2} + (d_z^8) \frac{1-\xi}{4bc^2} + \\
& \quad \left. (d_z^{17}) \frac{1-\xi}{2bc^2} + (d_z^{18}) \frac{1+\xi}{2bc^2} + (d_z^{19}) \frac{-1-\xi}{2bc^2} + (d_z^{20}) \frac{-1+\xi}{2bc^2} \right] + \\
& \tilde{f}_{3121} \left[ (d_x^1) \frac{-1+2\xi+2\eta+2\zeta}{8abc} + (d_y^1) \frac{-1+\eta}{4a^2c} + (d_x^2) \frac{1+2\xi-2\eta-2\zeta}{8abc} + \right. \\
& \quad (d_y^2) \frac{-1+\eta}{4a^2c} + (d_x^3) \frac{-1-2\xi-2\eta+2\zeta}{8abc} + (d_y^3) \frac{-1-\eta}{4a^2c} + \\
& \quad (d_x^4) \frac{1-2\xi+2\eta-2\zeta}{8abc} + (d_y^4) \frac{-1-\eta}{4a^2c} + (d_x^5) \frac{1-2\xi-2\eta+2\zeta}{8abc} + \\
& \quad (d_y^5) \frac{1-\eta}{4a^2c} + (d_x^6) \frac{-1-2\xi+2\eta-2\zeta}{8abc} + (d_y^6) \frac{1-\eta}{4a^2c} + \\
& \quad (d_x^7) \frac{1+2\xi+2\eta+2\zeta}{8abc} + (d_y^7) \frac{1+\eta}{4a^2c} + (d_x^8) \frac{-1+2\xi-2\eta-2\zeta}{8abc} + \\
& \quad (d_y^8) \frac{1+\eta}{4a^2c} + (d_x^9) \frac{-\xi}{2abc} + (d_y^9) \frac{1-\eta}{2a^2c} + (d_x^{10}) \frac{\eta}{2abc} + \\
& \quad (d_x^{11}) \frac{\xi}{2abc} + (d_y^{11}) \frac{1+\eta}{2a^2c} + (d_x^{12}) \frac{-\eta}{2abc} + (d_x^{13}) \frac{\xi}{2abc} + \\
& \quad (d_y^{13}) \frac{-1+\eta}{2a^2c} + (d_x^{14}) \frac{-\eta}{2abc} + (d_x^{15}) \frac{-\xi}{2abc} + (d_y^{15}) \frac{-1-\eta}{2a^2c} + \\
& \quad \left. (d_x^{16}) \frac{\eta}{2abc} + (d_x^{17}) \frac{-\zeta}{2abc} + (d_x^{18}) \frac{\zeta}{2abc} + (d_x^{19}) \frac{-\zeta}{2abc} + (d_x^{20}) \frac{\zeta}{2abc} \right] +
\end{aligned}$$

$$\begin{aligned}
& \tilde{f}_{3122} \left[ (d_x^1) \frac{-1+\xi}{4b^2c} + (d_y^1) \frac{-1+2\xi+2\eta+2\zeta}{8abc} + (d_x^2) \frac{-1-\xi}{4b^2c} + \right. \\
& (d_y^2) \frac{1+2\xi-2\eta-2\zeta}{8abc} + (d_x^3) \frac{-1-\xi}{4b^2c} + (d_y^3) \frac{-1-2\xi-2\eta+2\zeta}{8abc} + \\
& (d_x^4) \frac{-1+\xi}{4b^2c} + (d_y^4) \frac{1-2\xi+2\eta-2\zeta}{8abc} + (d_x^5) \frac{1-\xi}{4b^2c} + \\
& (d_y^5) \frac{1-2\xi-2\eta+2\zeta}{8abc} + (d_x^6) \frac{1+\xi}{4b^2c} + (d_y^6) \frac{-1-2\xi+2\eta-2\zeta}{8abc} + \\
& (d_x^7) \frac{1+\xi}{4b^2c} + (d_y^7) \frac{1+2\xi+2\eta+2\zeta}{8abc} + (d_x^8) \frac{1-\xi}{4b^2c} + \\
& (d_y^8) \frac{-1+2\xi-2\eta-2\zeta}{8abc} + (d_y^9) \frac{-\xi}{2abc} + (d_x^{10}) \frac{1+\xi}{2b^2c} + (d_y^{10}) \frac{\eta}{2abc} + \\
& (d_y^{11}) \frac{\xi}{2abc} + (d_x^{12}) \frac{1-\xi}{2b^2c} + (d_y^{12}) \frac{-\eta}{2abc} + (d_y^{13}) \frac{\xi}{2abc} + \\
& (d_x^{14}) \frac{-1-\xi}{2b^2c} + (d_y^{14}) \frac{-\eta}{2abc} + (d_y^{15}) \frac{-\xi}{2abc} + (d_x^{16}) \frac{-1+\xi}{2b^2c} + \\
& (d_y^{16}) \frac{\eta}{2abc} + (d_y^{17}) \frac{-\zeta}{2abc} + (d_y^{18}) \frac{\zeta}{2abc} + (d_y^{19}) \frac{-\zeta}{2abc} + (d_y^{20}) \frac{\zeta}{2abc} \Big] + \\
& \tilde{f}_{3123} \left[ (d_x^1) \frac{-1+\xi}{4bc^2} + (d_y^1) \frac{-1+\eta}{4ac^2} + (d_x^2) \frac{-1-\xi}{4bc^2} + (d_y^2) \frac{1-\eta}{4ac^2} + \right. \\
& (d_x^3) \frac{1+\xi}{4bc^2} + (d_y^3) \frac{1+\eta}{4ac^2} + (d_x^4) \frac{1-\xi}{4bc^2} + (d_y^4) \frac{-1-\eta}{4ac^2} + \\
& (d_x^5) \frac{-1+\xi}{4bc^2} + (d_y^5) \frac{-1+\eta}{4ac^2} + (d_x^6) \frac{-1-\xi}{4bc^2} + (d_y^6) \frac{1-\eta}{4ac^2} + \\
& (d_x^7) \frac{1+\xi}{4bc^2} + (d_y^7) \frac{1+\eta}{4ac^2} + (d_x^8) \frac{1-\xi}{4bc^2} + (d_y^8) \frac{-1-\eta}{4ac^2} + \\
& (d_x^{17}) \frac{1-\xi}{2bc^2} + (d_y^{17}) \frac{1-\eta}{2ac^2} + (d_x^{18}) \frac{1+\xi}{2bc^2} + (d_y^{18}) \frac{-1+\eta}{2ac^2} + \\
& (d_x^{19}) \frac{-1-\xi}{2bc^2} + (d_y^{19}) \frac{-1-\eta}{2ac^2} + (d_x^{20}) \frac{-1+\xi}{2bc^2} + (d_y^{20}) \frac{1+\eta}{2ac^2} \Big] + \\
& \tilde{f}_{3131} \left[ (d_x^1) \frac{-1+\eta}{4ac^2} + (d_z^1) \frac{-1+\eta}{4a^2c} + (d_x^2) \frac{1-\eta}{4ac^2} + (d_z^2) \frac{-1+\eta}{4a^2c} + \right. \\
& (d_x^3) \frac{1+\eta}{4ac^2} + (d_z^3) \frac{-1-\eta}{4a^2c} + (d_x^4) \frac{-1-\eta}{4ac^2} + (d_z^4) \frac{-1-\eta}{4a^2c} + \\
& (d_x^5) \frac{-1+\eta}{4ac^2} + (d_z^5) \frac{1-\eta}{4a^2c} + (d_x^6) \frac{1-\eta}{4ac^2} + (d_z^6) \frac{1-\eta}{4a^2c} + \\
& (d_x^7) \frac{1+\eta}{4ac^2} + (d_z^7) \frac{1+\eta}{4a^2c} + (d_x^8) \frac{-1-\eta}{4ac^2} + (d_z^8) \frac{1+\eta}{4a^2c} + \\
& (d_z^9) \frac{1-\eta}{2a^2c} + (d_z^{11}) \frac{1+\eta}{2a^2c} + (d_z^{13}) \frac{-1+\eta}{2a^2c} + (d_z^{15}) \frac{-1-\eta}{2a^2c} + \\
& (d_x^{17}) \frac{1-\eta}{2ac^2} + (d_x^{18}) \frac{-1+\eta}{2ac^2} + (d_x^{19}) \frac{-1-\eta}{2ac^2} + (d_x^{20}) \frac{1+\eta}{2ac^2} \Big] +
\end{aligned}$$

$$\begin{aligned} \tilde{f}_{3132} & \left[ (d_x^1) \frac{-1+\xi}{4bc^2} + (d_z^1) \frac{-1+2\xi+2\eta+2\zeta}{8abc} + (d_x^2) \frac{-1-\xi}{4bc^2} + \right. \\ & (d_z^2) \frac{1+2\xi-2\eta-2\zeta}{8abc} + (d_x^3) \frac{1+\xi}{4bc^2} + (d_z^3) \frac{-1-2\xi-2\eta+2\zeta}{8abc} + \\ & (d_x^4) \frac{1-\xi}{4bc^2} + (d_z^4) \frac{1-2\xi+2\eta-2\zeta}{8abc} + (d_x^5) \frac{-1+\xi}{4bc^2} + \\ & (d_z^5) \frac{1-2\xi-2\eta+2\zeta}{8abc} + (d_x^6) \frac{-1-\xi}{4bc^2} + (d_z^6) \frac{-1-2\xi+2\eta-2\zeta}{8abc} + \\ & (d_x^7) \frac{1+\xi}{4bc^2} + (d_z^7) \frac{1+2\xi+2\eta+2\zeta}{8abc} + (d_x^8) \frac{1-\xi}{4bc^2} + \\ & (d_z^8) \frac{-1+2\xi-2\eta-2\zeta}{8abc} + (d_z^9) \frac{-\xi}{2abc} + (d_z^{10}) \frac{\eta}{2abc} + (d_z^{11}) \frac{\xi}{2abc} + \\ & (d_z^{12}) \frac{-\eta}{2abc} + (d_z^{13}) \frac{\xi}{2abc} + (d_z^{14}) \frac{-\eta}{2abc} + (d_z^{15}) \frac{-\xi}{2abc} + \\ & (d_z^{16}) \frac{\eta}{2abc} + (d_x^{17}) \frac{1-\xi}{2bc^2} + (d_z^{17}) \frac{-\zeta}{2abc} + (d_x^{18}) \frac{1+\xi}{2bc^2} + \\ & \left. (d_z^{18}) \frac{\zeta}{2abc} + (d_x^{19}) \frac{-1-\xi}{2bc^2} + (d_z^{19}) \frac{-\zeta}{2abc} + (d_x^{20}) \frac{-1+\xi}{2bc^2} + (d_z^{20}) \frac{\zeta}{2abc} \right] + \end{aligned}$$

$$\begin{aligned} \tilde{f}_{3133} & \left[ (d_z^1) \frac{-1+\eta}{4ac^2} + (d_z^2) \frac{1-\eta}{4ac^2} + (d_z^3) \frac{1+\eta}{4ac^2} + (d_z^4) \frac{-1-\eta}{4ac^2} + \right. \\ & (d_z^5) \frac{-1+\eta}{4ac^2} + (d_z^6) \frac{1-\eta}{4ac^2} + (d_z^7) \frac{1+\eta}{4ac^2} + (d_z^8) \frac{-1-\eta}{4ac^2} + \\ & \left. (d_z^{17}) \frac{1-\eta}{1ac^2} + (d_z^{18}) \frac{-1+\eta}{2ac^2} + (d_z^{19}) \frac{-1-\eta}{2ac^2} + (d_z^{20}) \frac{1+\eta}{2ac^2} \right] + \end{aligned}$$

$$\begin{aligned} \tilde{f}_{3231} & \left[ (d_y^1) \frac{-1+\eta}{4ac^2} + (d_z^1) \frac{-1+2\xi+2\eta+2\zeta}{8abc} + (d_y^2) \frac{1-\eta}{4ac^2} + \right. \\ & (d_z^2) \frac{1+2\xi-2\eta-2\zeta}{8abc} + (d_y^3) \frac{1+\eta}{4ac^2} + (d_z^3) \frac{-1-2\xi-2\eta+2\zeta}{8abc} + \\ & (d_y^4) \frac{-1-\eta}{4ac^2} + (d_z^4) \frac{1-2\xi+2\eta-2\zeta}{8abc} + (d_y^5) \frac{-1+\eta}{4ac^2} + \\ & (d_z^5) \frac{1-2\xi-2\eta+2\zeta}{8abc} + (d_y^6) \frac{1-\eta}{4ac^2} + (d_z^6) \frac{-1-2\xi+2\eta-2\zeta}{8abc} + \\ & (d_y^7) \frac{1+\eta}{4ac^2} + (d_z^7) \frac{1+2\xi+2\eta+2\zeta}{8abc} + (d_y^8) \frac{-1-\eta}{4ac^2} + \\ & (d_z^8) \frac{-1+2\xi-2\eta-2\zeta}{8abc} + (d_z^9) \frac{-\xi}{2abc} + (d_z^{10}) \frac{\eta}{2abc} + (d_z^{11}) \frac{\xi}{2abc} + \\ & (d_z^{12}) \frac{-\eta}{2abc} + (d_z^{13}) \frac{\xi}{2abc} + (d_z^{14}) \frac{-\eta}{2abc} + (d_z^{15}) \frac{-\xi}{2abc} + \\ & (d_z^{16}) \frac{\eta}{2abc} + (d_y^{17}) \frac{1-\eta}{2ac^2} + (d_z^{17}) \frac{-\zeta}{2abc} + (d_y^{18}) \frac{-1+\eta}{2ac^2} + \\ & \left. (d_z^{18}) \frac{\zeta}{2abc} + (d_y^{19}) \frac{-1-\eta}{2ac^2} + (d_z^{19}) \frac{-\zeta}{2abc} + (d_y^{20}) \frac{1+\eta}{2ac^2} + (d_z^{20}) \frac{-\zeta}{2abc} \right] + \end{aligned}$$

$$\begin{aligned} \tilde{f}_{3232} & \left[ (d_y^1) \frac{-1+\xi}{4bc^2} + (d_z^1) \frac{-1+\xi}{4b^2c} + (d_y^2) \frac{-1-\xi}{4bc^2} + (d_z^2) \frac{-1-\xi}{4b^2c} + \right. \\ & (d_y^3) \frac{1+\xi}{4bc^2} + (d_z^3) \frac{-1-\xi}{4b^2c} + (d_y^4) \frac{1-\xi}{4bc^2} + (d_z^4) \frac{-1+\xi}{4b^2c} + \\ & (d_y^5) \frac{-1+\xi}{4bc^2} + (d_z^5) \frac{1-\xi}{4b^2c} + (d_y^6) \frac{-1-\xi}{4bc^2} + (d_z^6) \frac{1+\xi}{4b^2c} + \\ & (d_y^7) \frac{1+\xi}{4bc^2} + (d_z^7) \frac{1+\xi}{4b^2c} + (d_y^8) \frac{1-\xi}{4bc^2} + (d_z^8) \frac{1-\xi}{4b^2c} + \end{aligned}$$

$$\begin{aligned}
\tilde{f}_{3233} \left[ (d_z^1) \frac{-1+\xi}{4bc^2} + (d_z^2) \frac{-1-\xi}{4bc^2} + (d_z^3) \frac{1+\xi}{4bc^2} + (d_z^4) \frac{1-\xi}{4bc^2} + \right. \\
(d_z^5) \frac{-1+\xi}{4bc^2} + (d_z^6) \frac{-1-\xi}{4bc^2} + (d_z^7) \frac{1+\xi}{4bc^2} + (d_z^8) \frac{1-\xi}{4bc^2} + \\
\left. (d_z^{17}) \frac{1-\xi}{2bc^2} + (d_z^{18}) \frac{1+\xi}{2bc^2} + (d_z^{19}) \frac{-1-\xi}{2bc^2} + (d_z^{20}) \frac{-1+\xi}{2bc^2} \right] \quad (48)
\end{aligned}$$

Assuming an homogeneous axonal distribution within the volume, one can take the value of the integrand in the centre of the element, e.g., at  $(\xi, \eta, \zeta) =$

$(0, 0, 0)$ . This simplifies (48) to:

$$\begin{aligned}
\nabla \cdot \tilde{\mathbf{P}} = & \tilde{f}_{1112} \left[ (d_x^1) \frac{-1}{4a^2b} + (d_x^2) \frac{-1}{4a^2b} + (d_x^3) \frac{1}{4a^2b} + (d_x^4) \frac{1}{4a^2b} + \right. \\
& (d_x^5) \frac{-1}{4a^2b} + (d_x^6) \frac{-1}{4a^2b} + (d_x^7) \frac{1}{4a^2b} + (d_x^8) \frac{1}{4a^2b} + \\
& \left. (d_x^9) \frac{1}{2a^2b} + (d_x^{11}) \frac{-1}{2a^2b} + (d_x^{13}) \frac{1}{2a^2b} + (d_x^{15}) \frac{-1}{2a^2b} \right] + \\
& \tilde{f}_{1113} \left[ (d_x^1) \frac{-1}{4a^2c} + (d_x^2) \frac{-1}{4a^2c} + (d_x^3) \frac{-1}{4a^2c} + (d_x^4) \frac{-1}{4a^2c} + \right. \\
& (d_x^5) \frac{1}{4a^2c} + (d_x^6) \frac{1}{4a^2c} + (d_x^7) \frac{1}{4a^2c} + (d_x^8) \frac{1}{4a^2c} + \\
& \left. (d_x^9) \frac{1}{2a^2c} + (d_x^{11}) \frac{1}{2a^2c} + (d_x^{13}) \frac{-1}{2a^2c} + (d_x^{15}) \frac{-1}{2a^2c} \right] + \\
& \tilde{f}_{1221} \left[ (d_y^1) \frac{-1}{4a^2b} + (d_y^2) \frac{-1}{4a^2b} + (d_y^3) \frac{1}{4a^2b} + (d_y^4) \frac{1}{4a^2b} + \right. \\
& (d_y^5) \frac{-1}{4a^2b} + (d_y^6) \frac{-1}{4a^2b} + (d_y^7) \frac{1}{4a^2b} + (d_y^8) \frac{1}{4a^2b} + \\
& \left. (d_y^9) \frac{1}{2a^2b} + (d_y^{11}) \frac{-1}{2a^2b} + (d_y^{13}) \frac{1}{2a^2b} + (d_y^{15}) \frac{-1}{2a^2b} \right] + \\
& \tilde{f}_{1222} \left[ (d_y^1) \frac{-1}{4ab^2} + (d_y^2) \frac{1}{4ab^2} + (d_y^3) \frac{1}{4ab^2} + (d_y^4) \frac{-1}{4ab^2} + \right. \\
& (d_y^5) \frac{-1}{4ab^2} + (d_y^6) \frac{1}{4ab^2} + (d_y^7) \frac{1}{4ab^2} + (d_y^8) \frac{-1}{4ab^2} + \\
& \left. (d_y^{10}) \frac{-1}{2ab^2} + (d_y^{12}) \frac{1}{2ab^2} + (d_y^{14}) \frac{-1}{2ab^2} + (d_y^{16}) \frac{1}{2ab^2} \right] + \\
& \tilde{f}_{1223} \left[ (d_y^1) \frac{-1}{8abc} + (d_y^2) \frac{1}{8abc} + (d_y^3) \frac{-1}{8abc} + (d_y^4) \frac{1}{8abc} + \right. \\
& (d_y^5) \frac{1}{8abc} + (d_y^6) \frac{-1}{8abc} + (d_y^7) \frac{1}{8abc} + (d_y^8) \frac{-1}{8abc} \left. \right] + \\
& \tilde{f}_{1331} \left[ (d_z^1) \frac{-1}{4a^2c} + (d_z^2) \frac{-1}{4a^2c} + (d_z^3) \frac{-1}{4a^2c} + (d_z^4) \frac{-1}{4a^2c} + \right. \\
& (d_z^5) \frac{1}{4a^2c} + (d_z^6) \frac{1}{4a^2c} + (d_z^7) \frac{1}{4a^2c} + (d_z^8) \frac{1}{4a^2c} + \\
& \left. (d_z^9) \frac{1}{2a^2c} + (d_z^{11}) \frac{1}{2a^2c} + (d_z^{13}) \frac{-1}{2a^2c} + (d_z^{15}) \frac{-1}{2a^2c} \right] +
\end{aligned}$$

$$\begin{aligned}
& \tilde{f}_{1332} \left[ (d_z^1) \frac{-1}{8abc} + (d_z^2) \frac{1}{8abc} + (d_z^3) \frac{-1}{8abc} + (d_z^4) \frac{1}{8abc} + \right. \\
& \quad \left. (d_z^5) \frac{1}{8abc} + (d_z^6) \frac{-1}{8abc} + (d_z^7) \frac{1}{8abc} + (d_z^8) \frac{-1}{8abc} \right] + \\
& \tilde{f}_{1333} \left[ (d_z^1) \frac{-1}{4ac^2} + (d_z^2) \frac{1}{4ac^2} + (d_z^3) \frac{1}{4ac^2} + (d_z^4) \frac{-1}{4ac^2} + \right. \\
& \quad (d_z^5) \frac{-1}{4ac^2} + (d_z^6) \frac{1}{4ac^2} + (d_z^7) \frac{1}{4ac^2} + (d_z^8) \frac{-1}{4ac^2} + \\
& \quad \left. (d_z^{17}) \frac{1}{2ac^2} + (d_z^{18}) \frac{-1}{2ac^2} + (d_z^{19}) \frac{-1}{2ac^2} + (d_z^{20}) \frac{1}{2ac^2} \right] + \\
& \tilde{f}_{1121} \left[ (d_x^1) \frac{-1}{4a^2b} + (d_x^2) \frac{-1}{4a^2b} + (d_x^3) \frac{1}{4a^2b} + (d_x^4) \frac{1}{4a^2b} + \right. \\
& \quad (d_x^5) \frac{-1}{4a^2b} + (d_x^6) \frac{-1}{4a^2b} + (d_x^7) \frac{1}{4a^2b} + (d_x^8) \frac{1}{4a^2b} + \\
& \quad \left. (d_x^9) \frac{1}{2a^2b} + (d_x^{11}) \frac{-1}{2a^2b} + (d_x^{13}) \frac{1}{2a^2b} + (d_x^{15}) \frac{-1}{2a^2b} \right] + \\
& \tilde{f}_{1122} \left[ (d_x^1) \frac{-1}{4ab^2} + (d_y^1) \frac{-1}{4a^2b} + (d_x^2) \frac{1}{4ab^2} + (d_y^2) \frac{-1}{4a^2b} + \right. \\
& \quad (d_x^3) \frac{1}{4ab^2} + (d_y^3) \frac{1}{4a^2b} + (d_x^4) \frac{-1}{4ab^2} + (d_y^4) \frac{1}{4a^2b} + \\
& \quad (d_x^5) \frac{-1}{4ab^2} + (d_y^5) \frac{-1}{4a^2b} + (d_x^6) \frac{1}{4ab^2} + (d_y^6) \frac{-1}{4a^2b} + \\
& \quad (d_x^7) \frac{1}{4ab^2} + (d_y^7) \frac{1}{4a^2b} + (d_x^8) \frac{-1}{4ab^2} + (d_y^8) \frac{1}{4a^2b} + \\
& \quad (d_y^9) \frac{1}{2a^2b} + (d_x^{10}) \frac{-1}{2ab^2} + (d_y^{11}) \frac{-1}{2a^2b} + (d_x^{12}) \frac{1}{2ab^2} + \\
& \quad \left. (d_y^{13}) \frac{1}{2a^2b} + (d_x^{14}) \frac{-1}{2ab^2} + (d_y^{15}) \frac{-1}{2a^2b} + (d_x^{16}) \frac{1}{2ab^2} \right] + \\
& \tilde{f}_{1123} \left[ (d_x^1) \frac{-1}{8abc} + (d_y^1) \frac{-1}{4a^2c} + (d_x^2) \frac{1}{8abc} + (d_y^2) \frac{-1}{4a^2c} + \right. \\
& \quad (d_x^3) \frac{-1}{8abc} + (d_y^3) \frac{-1}{4a^2c} + (d_x^4) \frac{1}{8abc} + (d_y^4) \frac{-1}{4a^2c} + \\
& \quad (d_x^5) \frac{1}{8abc} + (d_y^5) \frac{1}{4a^2c} + (d_x^6) \frac{-1}{8abc} + (d_y^6) \frac{1}{4a^2c} + \\
& \quad (d_x^7) \frac{1}{8abc} + (d_y^7) \frac{1}{4a^2c} + (d_x^8) \frac{-1}{8abc} + (d_y^8) \frac{1}{4a^2c} + \\
& \quad \left. (d_y^9) \frac{1}{2a^2c} + (d_y^{11}) \frac{1}{2a^2c} + (d_y^{13}) \frac{-1}{2a^2c} + (d_y^{15}) \frac{-1}{2a^2c} \right] + \\
& \tilde{f}_{1131} \left[ (d_x^1) \frac{-1}{4a^2c} + (d_x^2) \frac{-1}{4a^2c} + (d_x^3) \frac{-1}{4a^2c} + (d_x^4) \frac{-1}{4a^2c} + \right. \\
& \quad (d_x^5) \frac{1}{4a^2c} + (d_x^6) \frac{1}{4a^2c} + (d_x^7) \frac{1}{4a^2c} + (d_x^8) \frac{1}{4a^2c} + \\
& \quad \left. (d_x^9) \frac{1}{2a^2c} + (d_x^{11}) \frac{1}{2a^2c} + (d_x^{13}) \frac{-1}{2a^2c} + (d_x^{15}) \frac{-1}{2a^2c} \right] +
\end{aligned}$$

$$\begin{aligned}
& \tilde{f}_{1132} \left[ (d_x^1) \frac{-1}{8abc} + (d_z^1) \frac{-1}{4a^2b} + (d_x^2) \frac{1}{8abc} + (d_z^2) \frac{-1}{4ab} + \right. \\
& \quad (d_x^3) \frac{-1}{8abc} + (d_z^3) \frac{1}{4a^2b} + (d_x^4) \frac{1}{8abc} + (d_z^4) \frac{1}{4a^2b} + \\
& \quad (d_x^5) \frac{1}{8abc} + (d_z^5) \frac{-1}{4a^2b} + (d_x^6) \frac{-1}{8abc} + (d_z^6) \frac{-1}{4a^2b} + \\
& \quad (d_x^7) \frac{1}{8abc} + (d_z^7) \frac{1}{4a^2b} + (d_x^8) \frac{-1}{8abc} + (d_z^8) \frac{1}{4a^2b} + \\
& \quad \left. (d_z^9) \frac{1}{2a^2b} + (d_z^{11}) \frac{-1}{2a^2b} + (d_z^{13}) \frac{1}{2a^2b} + (d_z^{15}) \frac{-1}{2a^2b} \right] + \\
& \tilde{f}_{1133} \left[ (d_x^1) \frac{-1}{4ac^2} + (d_z^1) \frac{-1}{4a^2c} + (d_x^2) \frac{1}{4ac^2} + (d_z^2) \frac{-1}{4a^2c} + \right. \\
& \quad (d_x^3) \frac{1}{4ac^2} + (d_z^3) \frac{-1}{4a^2c} + (d_x^4) \frac{-1}{4ac^2} + (d_z^4) \frac{-1}{4a^2c} + \\
& \quad (d_x^5) \frac{-1}{4ac^2} + (d_z^5) \frac{1}{4a^2c} + (d_x^6) \frac{1}{4ac^2} + (d_z^6) \frac{1}{4a^2c} + \\
& \quad (d_x^7) \frac{1}{4ac^2} + (d_z^7) \frac{1}{4a^2c} + (d_x^8) \frac{-1}{4ac^2} + (d_z^8) \frac{1}{4a^2c} + \\
& \quad (d_z^9) \frac{1}{2a^2c} + (d_z^{11}) \frac{1}{2a^2c} + (d_z^{13}) \frac{-1}{2a^2c} + (d_z^{15}) \frac{-1}{2a^2c} + \\
& \quad \left. (d_x^{17}) \frac{1}{2ac^2} + (d_x^{18}) \frac{-1}{2ac^2} + (d_x^{19}) \frac{-1}{2ac^2} + (d_x^{20}) \frac{1}{2ac^2} \right] + \\
& \tilde{f}_{1231} \left[ (d_y^1) \frac{-1}{4a^2c} + (d_z^1) \frac{-1}{4a^2b} + (d_y^2) \frac{-1}{4a^2c} + (d_z^2) \frac{-1}{4a^2b} + \right. \\
& \quad (d_y^3) \frac{-1}{4a^2c} + (d_z^3) \frac{1}{4a^2b} + (d_y^4) \frac{-1}{4a^2c} + (d_z^4) \frac{1}{4a^2b} + \\
& \quad (d_y^5) \frac{1}{4a^2c} + (d_z^5) \frac{-1}{4a^2b} + (d_y^6) \frac{1}{4a^2c} + (d_z^6) \frac{-1}{4a^2b} + \\
& \quad (d_y^7) \frac{1}{4a^2c} + (d_z^7) \frac{1}{4a^2b} + (d_y^8) \frac{1}{4a^2c} + (d_z^8) \frac{1}{4a^2b} + \\
& \quad (d_y^9) \frac{1}{2a^2c} + (d_z^9) \frac{1}{2a^2b} + (d_y^{11}) \frac{1}{2a^2c} + (d_z^{11}) \frac{-1}{2a^2b} + \\
& \quad \left. (d_y^{13}) \frac{-1}{2a^2c} + (d_z^{13}) \frac{1}{2a^2b} + (d_y^{15}) \frac{-1}{2a^2c} + (d_z^{15}) \frac{-1}{2a^2b} \right] + \\
& \tilde{f}_{1232} \left[ (d_y^1) \frac{-1}{8abc} + (d_z^1) \frac{-1}{4ab^2} + (d_y^2) \frac{1}{8abc} + (d_z^2) \frac{1}{4ab^2} + \right. \\
& \quad (d_y^3) \frac{-1}{8abc} + (d_z^3) \frac{1}{4ab^2} + (d_y^4) \frac{1}{8abc} + (d_z^4) \frac{-1}{4ab^2} + \\
& \quad (d_y^5) \frac{1}{8abc} + (d_z^5) \frac{-1}{4ab^2} + (d_y^6) \frac{-1}{8abc} + (d_z^6) \frac{1}{4ab^2} + \\
& \quad (d_y^7) \frac{1}{8abc} + (d_z^7) \frac{1}{4ab^2} + (d_y^8) \frac{-1}{8abc} + (d_z^8) \frac{-1}{4ab^2} + \\
& \quad \left. (d_z^{10}) \frac{-1}{2ab^2} + (d_z^{12}) \frac{1}{2ab^2} + (d_z^{14}) \frac{-1}{2ab^2} + (d_z^{16}) \frac{1}{2ab^2} \right] +
\end{aligned}$$

$$\begin{aligned}
& \tilde{f}_{1233} \left[ (d_y^1) \frac{-1}{4ac^2} + (d_z^1) \frac{-1}{8abc} + (d_y^2) \frac{1}{4ac^2} + (d_z^2) \frac{1}{8abc} + \right. \\
& \quad (d_y^3) \frac{1}{4ac^2} + (d_z^3) \frac{-1}{8abc} + (d_y^4) \frac{-1}{4ac^2} + (d_z^4) \frac{1}{8abc} + \\
& \quad (d_y^5) \frac{-1}{4ac^2} + (d_z^5) \frac{1}{8abc} + (d_y^6) \frac{1}{4ac^2} + (d_z^6) \frac{-1}{8abc} + \\
& \quad (d_y^7) \frac{1}{4ac^2} + (d_z^7) \frac{1}{8abc} + (d_y^8) \frac{-1}{4ac^2} + (d_z^8) \frac{-1}{8abc} + \\
& \quad \left. (d_y^{17}) \frac{1}{2ac^2} + (d_y^{18}) \frac{-1}{2ac^2} + (d_y^{19}) \frac{-1}{2ac^2} + (d_y^{20}) \frac{1}{2ac^2} \right] + \\
& \tilde{f}_{2111} \left[ (d_x^1) \frac{-1}{4a^2b} + (d_x^2) \frac{-1}{4a^2b} + (d_x^3) \frac{1}{4a^2b} + (d_x^4) \frac{1}{4a^2b} + \right. \\
& \quad (d_x^5) \frac{-1}{4a^2b} + (d_x^6) \frac{-1}{4a^2b} + (d_x^7) \frac{1}{4a^2b} + (d_x^8) \frac{1}{4a^2b} + \\
& \quad \left. (d_x^9) \frac{1}{2a^2b} + (d_x^{11}) \frac{-1}{2a^2b} + (d_x^{13}) \frac{1}{2a^2b} + (d_x^{15}) \frac{-1}{2a^2b} \right] + \\
& \tilde{f}_{2112} \left[ (d_x^1) \frac{-1}{4ab^2} + (d_x^2) \frac{1}{4ab^2} + (d_x^3) \frac{1}{4ab^2} + (d_x^4) \frac{-1}{4ab^2} + \right. \\
& \quad (d_x^5) \frac{-1}{4ab^2} + (d_x^6) \frac{1}{4ab^2} + (d_x^7) \frac{1}{4ab^2} + (d_x^8) \frac{-1}{4ab^2} + \\
& \quad \left. (d_x^{10}) \frac{-1}{2ab^2} + (d_x^{12}) \frac{1}{2ab^2} + (d_x^{14}) \frac{-1}{2ab^2} + (d_x^{16}) \frac{1}{2ab^2} \right] + \\
& \tilde{f}_{2113} \left[ (d_x^1) \frac{-1}{8abc} + (d_x^2) \frac{1}{8abc} + (d_x^3) \frac{-1}{8abc} + (d_x^4) \frac{1}{8abc} + \right. \\
& \quad (d_x^5) \frac{1}{8abc} + (d_x^6) \frac{-1}{8abc} + (d_x^7) \frac{1}{8abc} + (d_x^8) \frac{-1}{8abc} \left. \right] + \\
& \tilde{f}_{2221} \left[ (d_y^1) \frac{-1}{4ab^2} + (d_y^2) \frac{1}{4ab^2} + (d_y^3) \frac{1}{4ab^2} + (d_y^4) \frac{-1}{4ab^2} + \right. \\
& \quad (d_y^5) \frac{-1}{4ab^2} + (d_y^6) \frac{1}{4ab^2} + (d_y^7) \frac{1}{4ab^2} + (d_y^8) \frac{-1}{4ab^2} + \\
& \quad \left. (d_y^{10}) \frac{-1}{2ab^2} + (d_y^{12}) \frac{1}{2ab^2} + (d_y^{14}) \frac{-1}{2ab^2} + (d_y^{16}) \frac{-1}{2ab^2} \right] + \\
& \tilde{f}_{2223} \left[ (d_y^1) \frac{-1}{4b^2c} + (d_y^2) \frac{-1}{4b^2c} + (d_y^3) \frac{-1}{4b^2c} + (d_y^4) \frac{-1}{4b^2c} + \right. \\
& \quad (d_y^5) \frac{1}{4b^2c} + (d_y^6) \frac{1}{4b^2c} + (d_y^7) \frac{1}{4b^2c} + (d_y^8) \frac{1}{4b^2c} + \\
& \quad \left. (d_y^{10}) \frac{1}{2b^2c} + (d_y^{12}) \frac{1}{2b^2c} + (d_y^{14}) \frac{-1}{2b^2c} + (d_y^{16}) \frac{-1}{2b^2c} \right] + \\
& \tilde{f}_{2331} \left[ (d_z^1) \frac{-1}{8abc} + (d_z^2) \frac{1}{8abc} + (d_z^3) \frac{1}{8abc} + (d_z^4) \frac{1}{8abc} + \right. \\
& \quad \left. (d_z^5) \frac{1}{8abc} + (d_z^6) \frac{-1}{8abc} + (d_z^7) \frac{1}{8abc} + (d_z^8) \frac{-1}{8abc} \right] +
\end{aligned}$$



$$\begin{aligned}
& \tilde{f}_{2332} \left[ (d_z^1) \frac{-1}{4b^2c} + (d_z^2) \frac{-1}{4b^2c} + (d_z^3) \frac{-1}{4b^2c} + (d_z^4) \frac{-1}{4b^2c} + \right. \\
& \quad (d_z^5) \frac{1}{4b^2c} + (d_z^6) \frac{1}{4b^2c} + (d_z^7) \frac{1}{4b^2c} + (d_z^8) \frac{1}{4b^2c} + \\
& \quad \left. (d_z^{10}) \frac{1}{2b^2c} + (d_z^{12}) \frac{1}{2b^2c} + (d_z^{14}) \frac{-1}{2b^2c} + (d_z^{16}) \frac{-1}{2b^2c} \right] + \\
& \tilde{f}_{2333} \left[ (d_z^1) \frac{-1}{4bc^2} + (d_z^2) \frac{-1}{4bc^2} + (d_z^3) \frac{1}{4bc^2} + (d_z^4) \frac{1}{4bc^2} + \right. \\
& \quad (d_z^5) \frac{-1}{4bc^2} + (d_z^6) \frac{-1}{4bc^2} + (d_z^7) \frac{1}{4bc^2} + (d_z^8) \frac{1}{4bc^2} + \\
& \quad \left. (d_z^{17}) \frac{1}{2bc^2} + (d_z^{18}) \frac{1}{2bc^2} + (d_z^{19}) \frac{-1}{2bc^2} + (d_z^{20}) \frac{-1}{2bc^2} \right] + \\
& \tilde{f}_{2121} \left[ (d_x^1) \frac{-1}{4ab^2} + (d_y^1) \frac{-1}{4a^2b} + (d_x^2) \frac{1}{4ab^2} + (d_y^2) \frac{-1}{4a^2b} + \right. \\
& \quad (d_x^3) \frac{1}{4ab^2} + (d_y^3) \frac{1}{4a^2b} + (d_x^4) \frac{-1}{4ab^2} + (d_y^4) \frac{1}{4a^2b} + \\
& \quad (d_x^5) \frac{-1}{4ab^2} + (d_y^5) \frac{-1}{4a^2b} + (d_x^6) \frac{1}{4ab^2} + (d_y^6) \frac{-1}{4a^2b} + \\
& \quad (d_x^7) \frac{1}{4ab^2} + (d_y^7) \frac{1}{4a^2b} + (d_x^8) \frac{-1}{4ab^2} + (d_y^8) \frac{1}{4a^2b} + \\
& \quad (d_y^9) \frac{1}{2a^2b} + (d_x^{10}) \frac{-1}{2ab^2} + (d_y^{11}) \frac{-1}{2a^2b} + (d_x^{12}) \frac{1}{2ab^2} + \\
& \quad \left. (d_y^{13}) \frac{1}{2a^2b} + (d_x^{14}) \frac{-1}{2ab^2} + (d_y^{15}) \frac{-1}{2a^2b} + (d_x^{16}) \frac{1}{2ab^2} \right] + \\
& \tilde{f}_{2122} \left[ (d_y^1) \frac{-1}{4ab^2} + (d_y^2) \frac{1}{4ab^2} + (d_y^3) \frac{1}{4ab^2} + (d_y^4) \frac{-1}{4ab^2} + \right. \\
& \quad (d_y^5) \frac{-1}{4ab^2} + (d_y^6) \frac{1}{4ab^2} + (d_y^7) \frac{1}{4ab^2} + (d_y^8) \frac{-1}{4ab^2} + \\
& \quad \left. (d_y^{10}) \frac{-1}{2ab^2} + (d_y^{12}) \frac{1}{2ab^2} + (d_y^{14}) \frac{-1}{2ab^2} + (d_y^{16}) \frac{1}{2ab^2} \right] + \\
& \tilde{f}_{2123} \left[ (d_x^1) \frac{-1}{4b^2c} + (d_y^1) \frac{-1}{8abc} + (d_x^2) \frac{-1}{4ab^2c} + (d_y^2) \frac{1}{8abc} + \right. \\
& \quad (d_x^3) \frac{-1}{4b^2c} + (d_y^3) \frac{-1}{8abc} + (d_x^4) \frac{-1}{4b^2c} + (d_y^4) \frac{1}{8abc} + \\
& \quad (d_x^5) \frac{1}{4b^2c} + (d_y^5) \frac{1}{8abc} + (d_x^6) \frac{1}{4b^2c} + (d_y^6) \frac{-1}{8abc} + \\
& \quad (d_x^7) \frac{1}{4b^2c} + (d_y^7) \frac{1}{8abc} + (d_x^8) \frac{1}{4b^2c} + (d_y^8) \frac{-1}{8abc} + \\
& \quad \left. (d_x^{10}) \frac{1}{2b^2c} + (d_x^{12}) \frac{1}{2b^2c} + (d_x^{14}) \frac{-1}{2b^2c} + (d_x^{16}) \frac{-1}{2b^2c} \right] + \\
& \tilde{f}_{2131} \left[ (d_x^1) \frac{-1}{8abc} + (d_z^1) \frac{-1}{4a^2b} + (d_x^2) \frac{1}{8abc} + (d_z^2) \frac{-1}{4a^2b} + \right. \\
& \quad (d_x^3) \frac{-1}{8abc} + (d_z^3) \frac{1}{4a^2b} + (d_x^4) \frac{1}{8abc} + (d_z^4) \frac{1}{4a^2b} + \\
& \quad (d_x^5) \frac{1}{8abc} + (d_z^5) \frac{-1}{4a^2b} + (d_x^6) \frac{-1}{8abc} + (d_z^6) \frac{-1}{4a^2b} + \\
& \quad (d_x^7) \frac{1}{8abc} + (d_z^7) \frac{1}{4a^2b} + (d_x^8) \frac{-1}{8abc} + (d_z^8) \frac{1}{4a^2b} + \\
& \quad \left. (d_x^9) \frac{-1}{8abc} + (d_z^9) \frac{-1}{4a^2b} + (d_x^{10}) \frac{1}{8abc} + (d_z^{10}) \frac{1}{4a^2b} + \right. \\
& \quad (d_x^{11}) \frac{1}{8abc} + (d_z^{11}) \frac{1}{4a^2b} + (d_x^{12}) \frac{-1}{8abc} + (d_z^{12}) \frac{-1}{4a^2b} + \\
& \quad (d_x^{13}) \frac{-1}{8abc} + (d_z^{13}) \frac{-1}{4a^2b} + (d_x^{14}) \frac{1}{8abc} + (d_z^{14}) \frac{1}{4a^2b} + \\
& \quad (d_x^{15}) \frac{1}{8abc} + (d_z^{15}) \frac{1}{4a^2b} + (d_x^{16}) \frac{-1}{8abc} + (d_z^{16}) \frac{-1}{4a^2b} + \\
& \quad (d_x^{17}) \frac{-1}{8abc} + (d_z^{17}) \frac{-1}{4a^2b} + (d_x^{18}) \frac{1}{8abc} + (d_z^{18}) \frac{1}{4a^2b} + \\
& \quad (d_x^{19}) \frac{1}{8abc} + (d_z^{19}) \frac{1}{4a^2b} + (d_x^{20}) \frac{-1}{8abc} + (d_z^{20}) \frac{-1}{4a^2b} \left. \right] +
\end{aligned}$$

$$\begin{aligned}
& \tilde{f}_{2132} \left[ (d_x^1) \frac{-1}{4b^2c} + (d_z^1) \frac{-1}{4ab^2} + (d_x^2) \frac{-1}{4b^2c} + (d_z^2) \frac{1}{4ab^2} + \right. \\
& \quad (d_x^3) \frac{-1}{4b^2c} + (d_z^3) \frac{1}{4ab^2} + (d_x^4) \frac{-1}{4b^2c} + (d_z^4) \frac{-1}{4ab^2} + \\
& \quad (d_x^5) \frac{1}{4b^2c} + (d_z^5) \frac{-1}{4ab^2} + (d_x^6) \frac{1}{4b^2c} + (d_z^6) \frac{1}{4ab^2} + \\
& \quad (d_x^7) \frac{1}{4b^2c} + (d_z^7) \frac{1}{4ab^2} + (d_x^8) \frac{1}{4b^2c} + (d_z^8) \frac{-1}{4ab^2} + \\
& \quad (d_x^{10}) \frac{1}{2b^2c} + (d_z^{10}) \frac{-1}{2ab^2} + (d_x^{12}) \frac{1}{2b^2c} + (d_z^{12}) \frac{1}{2ab^2} + \\
& \quad \left. (d_x^{14}) \frac{-1}{2b^2c} + (d_z^{14}) \frac{-1}{2ab^2} + (d_x^{16}) \frac{-1}{2b^2c} + (d_z^{16}) \frac{1}{2ab^2} \right] + \\
& \tilde{f}_{2133} \left[ (d_x^1) \frac{-1}{4bc^2} + (d_z^1) \frac{-1}{8abc} + (d_x^2) \frac{-1}{4bc^2} + (d_z^2) \frac{1}{8abc} + \right. \\
& \quad (d_x^3) \frac{1}{4bc^2} + (d_z^3) \frac{-1}{8abc} + (d_x^4) \frac{1}{4bc^2} + (d_z^4) \frac{1}{8abc} + \\
& \quad (d_x^5) \frac{-1}{4bc^2} + (d_z^5) \frac{1}{8abc} + (d_x^6) \frac{-1}{4bc^2} + (d_z^6) \frac{-1}{8abc} + \\
& \quad (d_x^7) \frac{1}{4bc^2} + (d_z^7) \frac{1}{8abc} + (d_x^8) \frac{1}{4bc^2} + (d_z^8) \frac{-1}{8abc} + \\
& \quad \left. (d_x^{17}) \frac{1}{2bc^2} + (d_x^{18}) \frac{1}{2bc^2} + (d_x^{19}) \frac{-1}{2bc^2} + (d_x^{20}) \frac{-1}{2bc^2} \right] + \\
& \tilde{f}_{2231} \left[ (d_y^1) \frac{-1}{8abc} + (d_z^1) \frac{-1}{4ab^2} + (d_y^2) \frac{1}{8abc} + (d_z^2) \frac{1}{4ab^2} + \right. \\
& \quad (d_y^3) \frac{-1}{8abc} + (d_z^3) \frac{1}{4ab^2} + (d_y^4) \frac{1}{8abc} + (d_z^4) \frac{-1}{4ab^2} + \\
& \quad (d_y^5) \frac{1}{8abc} + (d_z^5) \frac{-1}{4ab^2} + (d_y^6) \frac{-1}{8abc} + (d_z^6) \frac{1}{4ab^2} + \\
& \quad (d_y^7) \frac{1}{8abc} + (d_z^7) \frac{1}{4ab^2} + (d_y^8) \frac{-1}{8abc} + (d_z^8) \frac{-1}{4ab^2} + \\
& \quad \left. (d_z^{10}) \frac{-1}{2ab^2} + (d_z^{12}) \frac{1}{2ab^2} + (d_z^{14}) \frac{-1}{2ab^2} + (d_z^{16}) \frac{1}{2ab^2} \right] + \\
& \tilde{f}_{2232} \left[ (d_y^1) \frac{-1}{4b^2c} + (d_y^2) \frac{-1}{4b^2c} + (d_y^3) \frac{-1}{4b^2c} + (d_y^4) \frac{-1}{4b^2c} + \right. \\
& \quad (d_y^5) \frac{1}{4b^2c} + (d_y^6) \frac{1}{4b^2c} + (d_y^7) \frac{1}{4b^2c} + (d_y^8) \frac{1}{4b^2c} + \\
& \quad \left. (d_y^{10}) \frac{1}{2b^2c} + (d_y^{12}) \frac{1}{2b^2c} + (d_y^{14}) \frac{-1}{2b^2c} + (d_y^{16}) \frac{-1}{2b^2c} \right] + \\
& \tilde{f}_{2233} \left[ (d_y^1) \frac{-1}{4bc^2} + (d_z^1) \frac{-1}{4b^2c} + (d_y^2) \frac{-1}{4bc^2} + (d_z^2) \frac{-1}{4b^2c} + \right. \\
& \quad (d_y^3) \frac{1}{4bc^2} + (d_z^3) \frac{-1}{4b^2c} + (d_y^4) \frac{1}{4bc^2} + (d_z^4) \frac{-1}{4b^2c} + \\
& \quad (d_y^5) \frac{-1}{4bc^2} + (d_z^5) \frac{1}{4b^2c} + (d_y^6) \frac{-1}{4bc^2} + (d_z^6) \frac{1}{4b^2c} + \\
& \quad (d_y^7) \frac{1}{4bc^2} + (d_z^7) \frac{1}{4b^2c} + (d_y^8) \frac{1}{4bc^2} + (d_z^8) \frac{1}{4b^2c} + \\
& \quad \left. (d_z^{10}) \frac{1}{2b^2c} + (d_z^{12}) \frac{1}{2b^2c} + (d_z^{14}) \frac{-1}{2b^2c} + (d_z^{16}) \frac{-1}{2b^2c} \right] +
\end{aligned}$$

$$\begin{aligned}
& \tilde{f}_{3111} \left[ (d_x^1) \frac{-1}{4a^2c} + (d_x^2) \frac{-1}{4a^2c} + (d_x^3) \frac{-1}{4a^2c} + (d_x^4) \frac{-1}{4a^2c} + \right. \\
& \quad (d_x^5) \frac{1}{4a^2c} + (d_x^6) \frac{1}{4a^2c} + (d_x^7) \frac{1}{4a^2c} + (d_x^8) \frac{1}{4a^2c} + \\
& \quad \left. (d_x^9) \frac{1}{2a^2c} + (d_x^{11}) \frac{1}{2a^2c} + (d_x^{13}) \frac{-1}{2a^2c} + (d_x^{15}) \frac{-1}{2a^2c} \right] + \\
& \tilde{f}_{3112} \left[ (d_x^1) \frac{-1}{8abc} + (d_x^2) \frac{1}{8abc} + (d_x^3) \frac{-1}{8abc} + (d_x^4) \frac{1}{8abc} + \right. \\
& \quad \left. (d_x^5) \frac{1}{8abc} + (d_x^6) \frac{-1}{8abc} + (d_x^7) \frac{1}{8abc} + (d_x^8) \frac{-1}{8abc} \right] + \\
& \tilde{f}_{3113} \left[ (d_x^1) \frac{-1}{4ac^2} + (d_x^2) \frac{1}{4ac^2} + (d_x^3) \frac{1}{4ac^2} + (d_x^4) \frac{-1}{4ac^2} + \right. \\
& \quad (d_x^5) \frac{-1}{4ac^2} + (d_x^6) \frac{1}{4ac^2} + (d_x^7) \frac{1}{4ac^2} + (d_x^8) \frac{-1}{4ac^2} + \\
& \quad \left. (d_x^{17}) \frac{1}{2ac^2} + (d_x^{18}) \frac{-1}{2ac^2} + (d_x^{19}) \frac{-1}{2ac^2} + (d_x^{20}) \frac{1}{2ac^2} \right] + \\
& \tilde{f}_{3221} \left[ (d_y^1) \frac{-1}{8abc} + (d_y^2) \frac{1}{8abc} + (d_y^3) \frac{-1}{8abc} + (d_y^4) \frac{1}{8abc} + \right. \\
& \quad \left. (d_y^5) \frac{1}{8abc} + (d_y^6) \frac{-1}{8abc} + (d_y^7) \frac{1}{8abc} + (d_y^8) \frac{-1}{8abc} \right] + \\
& \tilde{f}_{3222} \left[ (d_y^1) \frac{-1}{4b^2c} + (d_y^2) \frac{-1}{4b^2c} + (d_y^3) \frac{-1}{4b^2c} + (d_y^4) \frac{-1}{4b^2c} + \right. \\
& \quad (d_y^5) \frac{1}{4b^2c} + (d_y^6) \frac{1}{4b^2c} + (d_y^7) \frac{1}{4b^2c} + (d_y^8) \frac{1}{4b^2c} + \\
& \quad \left. (d_y^{10}) \frac{1}{2b^2c} + (d_y^{12}) \frac{1}{2b^2c} + (d_y^{14}) \frac{-1}{2b^2c} + (d_y^{16}) \frac{-1}{2b^2c} \right] + \\
& \tilde{f}_{3223} \left[ (d_y^1) \frac{-1}{4bc^2} + (d_y^2) \frac{-1}{4bc^2} + (d_y^3) \frac{1}{4bc^2} + (d_y^4) \frac{1}{4bc^2} + \right. \\
& \quad (d_y^5) \frac{-1}{4bc^2} + (d_y^6) \frac{-1}{4bc^2} + (d_y^7) \frac{1}{4bc^2} + (d_y^8) \frac{1}{4bc^2} + \\
& \quad \left. (d_y^{17}) \frac{1}{2bc^2} + (d_y^{18}) \frac{1}{2bc^2} + (d_y^{19}) \frac{-1}{2bc^2} + (d_y^{20}) \frac{-1}{2bc^2} \right] + \\
& \tilde{f}_{3331} \left[ (d_z^1) \frac{-1}{4ac^2} + (d_z^2) \frac{1}{4ac^2} + (d_z^3) \frac{1}{4ac^2} + (d_z^4) \frac{-1}{4ac^2} + \right. \\
& \quad (d_z^5) \frac{-1}{4ac^2} + (d_z^6) \frac{1}{4ac^2} + (d_z^7) \frac{1}{4ac^2} + (d_z^8) \frac{-1}{4ac^2} + \\
& \quad \left. (d_z^{17}) \frac{1}{2ac^2} + (d_z^{18}) \frac{-1}{2ac^2} + (d_z^{19}) \frac{-1}{2ac^2} + (d_z^{20}) \frac{1}{2ac^2} \right] + \\
& \tilde{f}_{3332} \left[ (d_z^1) \frac{-1}{4bc^2} + (d_z^2) \frac{-1}{4bc^2} + (d_z^3) \frac{1}{4bc^2} + (d_z^4) \frac{1}{4bc^2} + \right. \\
& \quad (d_z^5) \frac{-1}{4bc^2} + (d_z^6) \frac{-1}{4bc^2} + (d_z^7) \frac{1}{4bc^2} + (d_z^8) \frac{1}{4bc^2} + \\
& \quad \left. (d_z^{17}) \frac{1}{4bc^2} + (d_z^{18}) \frac{1}{4bc^2} + (d_z^{19}) \frac{-1}{4bc^2} + (d_z^{20}) \frac{-1}{4bc^2} \right] +
\end{aligned}$$

$$\begin{aligned}
& \tilde{f}_{3121} \left[ (d_x^1) \frac{-1}{8abc} + (d_y^1) \frac{-1}{4a^2c} + (d_x^2) \frac{1}{8abc} + (d_y^2) \frac{-1}{4a^2c} + \right. \\
& \quad (d_x^3) \frac{-1}{8abc} + (d_y^3) \frac{-1}{4a^2c} + (d_x^4) \frac{1}{8abc} + (d_y^4) \frac{-1}{4a^2c} + \\
& \quad (d_x^5) \frac{1}{8abc} + (d_y^5) \frac{1}{4a^2c} + (d_x^6) \frac{-1}{8abc} + (d_y^6) \frac{1}{4a^2c} + \\
& \quad (d_x^7) \frac{1}{8abc} + (d_y^7) \frac{1}{4a^2c} + (d_x^8) \frac{-1}{8abc} + (d_y^8) \frac{1}{4a^2c} + \\
& \quad \left. (d_y^9) \frac{1}{2a^2c} + (d_y^{11}) \frac{1}{2a^2c} + (d_y^{13}) \frac{-1}{2a^2c} + (d_y^{15}) \frac{-1}{2a^2c} \right] + \\
& \tilde{f}_{3122} \left[ (d_x^1) \frac{-1}{4b^2c} + (d_y^1) \frac{-1}{8abc} + (d_x^2) \frac{-1}{4b^2c} + (d_y^2) \frac{1}{8abc} + \right. \\
& \quad (d_x^3) \frac{-1}{4b^2c} + (d_y^3) \frac{-1}{8abc} + (d_x^4) \frac{-1}{4b^2c} + (d_y^4) \frac{1}{8abc} + \\
& \quad (d_x^5) \frac{1}{4b^2c} + (d_y^5) \frac{1}{8abc} + (d_x^6) \frac{1}{4b^2c} + (d_y^6) \frac{-1}{8abc} + \\
& \quad (d_x^7) \frac{1}{4b^2c} + (d_y^7) \frac{1}{8abc} + (d_x^8) \frac{1}{4b^2c} + (d_y^8) \frac{-1}{8abc} + \\
& \quad \left. (d_x^{10}) \frac{1}{2b^2c} + (d_x^{12}) \frac{1}{2b^2c} + (d_x^{14}) \frac{-1}{2b^2c} + (d_x^{16}) \frac{-1}{2b^2c} \right] + \\
& \tilde{f}_{3123} \left[ (d_x^1) \frac{-1}{4bc^2} + (d_y^1) \frac{-1}{4ac^2} + (d_x^2) \frac{-1}{4bc^2} + (d_y^2) \frac{1}{4ac^2} + \right. \\
& \quad (d_x^3) \frac{1}{4bc^2} + (d_y^3) \frac{1}{4ac^2} + (d_x^4) \frac{1}{4bc^2} + (d_y^4) \frac{-1}{4ac^2} + \\
& \quad (d_x^5) \frac{-1}{4bc^2} + (d_y^5) \frac{-1}{4ac^2} + (d_x^6) \frac{-1}{4bc^2} + (d_y^6) \frac{1}{4ac^2} + \\
& \quad (d_x^7) \frac{1}{4bc^2} + (d_y^7) \frac{1}{4ac^2} + (d_x^8) \frac{1}{4bc^2} + (d_y^8) \frac{-1}{4ac^2} + \\
& \quad (d_x^{17}) \frac{1}{2bc^2} + (d_y^{17}) \frac{1}{2ac^2} + (d_x^{18}) \frac{1}{2bc^2} + (d_y^{18}) \frac{-1}{2ac^2} + \\
& \quad \left. (d_x^{19}) \frac{-1}{2bc^2} + (d_y^{19}) \frac{-1}{2ac^2} + (d_x^{20}) \frac{-1}{2bc^2} + (d_y^{20}) \frac{1}{2ac^2} \right] + \\
& \tilde{f}_{3131} \left[ (d_x^1) \frac{-1}{4ac^2} + (d_z^1) \frac{-1}{4a^2c} + (d_x^2) \frac{1}{4ac^2} + (d_z^2) \frac{-1}{4a^2c} + \right. \\
& \quad (d_x^3) \frac{1}{4ac^2} + (d_z^3) \frac{-1}{4a^2c} + (d_x^4) \frac{-1}{4ac^2} + (d_z^4) \frac{-1}{4a^2c} + \\
& \quad (d_x^5) \frac{-1}{4ac^2} + (d_z^5) \frac{1}{4a^2c} + (d_x^6) \frac{1}{4ac^2} + (d_z^6) \frac{1}{4a^2c} + \\
& \quad (d_x^7) \frac{1}{4ac^2} + (d_z^7) \frac{1}{4a^2c} + (d_x^8) \frac{-1}{4ac^2} + (d_z^8) \frac{1}{4a^2c} + \\
& \quad (d_z^9) \frac{1}{2a^2c} + (d_z^{11}) \frac{1}{2a^2c} + (d_z^{13}) \frac{-1}{2a^2c} + (d_z^{15}) \frac{-1}{2a^2c} + \\
& \quad \left. (d_x^{17}) \frac{1}{2ac^2} + (d_x^{18}) \frac{-1}{2ac^2} + (d_x^{19}) \frac{-1}{2ac^2} + (d_x^{20}) \frac{1}{2ac^2} \right] +
\end{aligned}$$

$$\begin{aligned}
& \tilde{f}_{3132} \left[ (d_x^1) \frac{-1}{4bc^2} + (d_z^1) \frac{-1}{8abc} + (d_x^2) \frac{-1}{4bc^2} + (d_z^2) \frac{1}{8abc} + \right. \\
& \quad (d_x^3) \frac{1}{4bc^2} + (d_z^3) \frac{-1}{8abc} + (d_x^4) \frac{1}{4bc^2} + (d_z^4) \frac{1}{8abc} + \\
& \quad (d_x^5) \frac{-1}{4bc^2} + (d_z^5) \frac{1}{8abc} + (d_x^6) \frac{-1}{4bc^2} + (d_z^6) \frac{-1}{8abc} + \\
& \quad (d_x^7) \frac{1}{4bc^2} + (d_z^7) \frac{1}{8abc} + (d_x^8) \frac{1}{4bc^2} + (d_z^8) \frac{-1}{8abc} + \\
& \quad \left. (d_x^{17}) \frac{1}{2bc^2} + (d_x^{18}) \frac{1}{2bc^2} + (d_x^{19}) \frac{-1}{2bc^2} + (d_x^{20}) \frac{-1}{2bc^2} \right] + \\
& \tilde{f}_{3133} \left[ (d_z^1) \frac{-1}{4ac^2} + (d_z^2) \frac{1}{4ac^2} + (d_z^3) \frac{1}{4ac^2} + (d_z^4) \frac{-1}{4ac^2} + \right. \\
& \quad (d_z^5) \frac{-1}{4ac^2} + (d_z^6) \frac{1}{4ac^2} + (d_z^7) \frac{1}{4ac^2} + (d_z^8) \frac{-1}{4ac^2} + \\
& \quad \left. (d_z^{17}) \frac{1}{1ac^2} + (d_z^{18}) \frac{-1}{2ac^2} + (d_z^{19}) \frac{-1}{2ac^2} + (d_z^{20}) \frac{1}{2ac^2} \right] + \\
& \tilde{f}_{3231} \left[ (d_y^1) \frac{-1}{4ac^2} + (d_z^1) \frac{-1}{8abc} + (d_y^2) \frac{1}{4ac^2} + (d_z^2) \frac{1}{8abc} + \right. \\
& \quad (d_y^3) \frac{1}{4ac^2} + (d_z^3) \frac{-1}{8abc} + (d_y^4) \frac{-1}{4ac^2} + (d_z^4) \frac{1}{8abc} + \\
& \quad (d_y^5) \frac{-1}{4ac^2} + (d_z^5) \frac{1}{8abc} + (d_y^6) \frac{1}{4ac^2} + (d_z^6) \frac{-1}{8abc} + \\
& \quad (d_y^7) \frac{1}{4ac^2} + (d_z^7) \frac{1}{8abc} + (d_y^8) \frac{-1}{4ac^2} + (d_z^8) \frac{-1}{8abc} + \\
& \quad \left. (d_y^{17}) \frac{1}{2ac^2} + (d_y^{18}) \frac{-1}{2ac^2} + (d_y^{19}) \frac{-1}{2ac^2} + (d_y^{20}) \frac{1}{2ac^2} \right] + \\
& \tilde{f}_{3232} \left[ (d_y^1) \frac{-1}{4bc^2} + (d_z^1) \frac{-1}{4b^2c} + (d_y^2) \frac{-1}{4bc^2} + (d_z^2) \frac{-1}{4b^2c} + \right. \\
& \quad (d_y^3) \frac{1}{4bc^2} + (d_z^3) \frac{-1}{4b^2c} + (d_y^4) \frac{1}{4bc^2} + (d_z^4) \frac{-1}{4b^2c} + \\
& \quad (d_y^5) \frac{-1}{4bc^2} + (d_z^5) \frac{1}{4b^2c} + (d_y^6) \frac{-1}{4bc^2} + (d_z^6) \frac{1}{4b^2c} + \\
& \quad (d_y^7) \frac{1}{4bc^2} + (d_z^7) \frac{1}{4b^2c} + (d_y^8) \frac{1}{4bc^2} + (d_z^8) \frac{1}{4b^2c} + \\
& \quad (d_z^{10}) \frac{1}{2b^2c} + (d_z^{12}) \frac{1}{2b^2c} + (d_z^{14}) \frac{-1}{2b^2c} + (d_z^{16}) \frac{-1}{2b^2c} + \\
& \quad \left. (d_y^{17}) \frac{1}{2bc^2} + (d_y^{18}) \frac{1}{2bc^2} + (d_y^{19}) \frac{-1}{2bc^2} + (d_y^{20}) \frac{-1}{2bc^2} \right] + \\
& \tilde{f}_{3233} \left[ (d_z^1) \frac{-1}{4bc^2} + (d_z^2) \frac{-1}{4bc^2} + (d_z^3) \frac{1}{4bc^2} + (d_z^4) \frac{1}{4bc^2} + \right. \\
& \quad (d_z^5) \frac{-1}{4bc^2} + (d_z^6) \frac{-1}{4bc^2} + 8^5 (d_z^7) \frac{1}{4bc^2} + (d_z^8) \frac{1}{4bc^2} + \\
& \quad \left. (d_z^{17}) \frac{1}{2bc^2} + (d_z^{18}) \frac{1}{2bc^2} + (d_z^{19}) \frac{-1}{2bc^2} + (d_z^{20}) \frac{-1}{2bc^2} \right] \quad (49)
\end{aligned}$$

The calculation of the induced current  $dI$  is then given by:

$$dI = \frac{\partial \iiint \nabla \cdot \tilde{\mathbf{P}} \, dxdydz}{\partial t} = \frac{\partial \iiint \nabla \cdot (\tilde{\mathbf{f}} \cdot \mathbf{B} \cdot \mathbf{d}^e) \, dxdydz}{\partial t} \quad (50)$$

After time discretisation,  $dI$  is given by:

$$dI = v_e \rho_a \frac{\nabla \cdot (\tilde{\mathbf{f}} \cdot \mathbf{B} \cdot \mathbf{d}^e)_0^{n+1} - \nabla \cdot (\tilde{\mathbf{f}} \cdot \mathbf{B} \cdot \mathbf{d}^e)_0^n}{\Delta t} \quad (51)$$

485 which is similar to the induced current in 2D given by (33), but where the subscript 0 refers to the value at the centre of the element.

## 6.2. 2D Validation

The framework was validated by comparing a micromechanical model of one 250  $\mu m$ -long axon to the homogenised model proposed here. The micromechanical axonal model is a 2D plane-stress linear elastic single axon discretised with  
 490 a finite element mesh of quadratic triangular 1  $\mu m$ -long elements, see Fig. 8-a. The axon was submitted to a sigmoid-shaped<sup>1</sup> displacement load reaching (and maintaining) 0.25  $\mu m$  at 11.2  $\mu s$ , thus leading to a wave propagation along the axon swelling the cytoplasm and bending locally the outer surfaces (lines in  
 495 2D) of the axon as it propagates. The other end of the axon was fixed in the  $x$ - and  $y$ -direction preventing the end of the axon from moving. The middle of the axon (middle horizontal line) was also fixed in the  $y$ -direction to ensure that the outer surfaces deformed symmetrically. While the material properties were chosen arbitrarily to:  $E = 4800 \, MPa$  for the Young's modulus and  
 500  $\nu = 0.1$  for the Poisson's ratio, they do bear resemblance to literature value, e.g., giving  $K = 2 \, GPa$  for the bulk modulus [83]. The simulation was run with ABAQUS Explicit [84]. The  $x$ - and  $y$ -displacements from all the nodes were then extracted and imported into MATLAB [85] where rectangular quadratic elements were created by combining each section of four triangular elements  
 505 into one quadratic rectangular element, see Fig. 8-b. New displacements values

---

<sup>1</sup>to avoid spurious oscillations

were given to the corresponding nodes by obtaining an average value for the displacement on the red nodes in Fig. 8-a with their direct neighbouring nodes (to smooth out the inherent noise in the nodal values). Finally, the current influx arising from the membrane bending was then calculated with two methods.

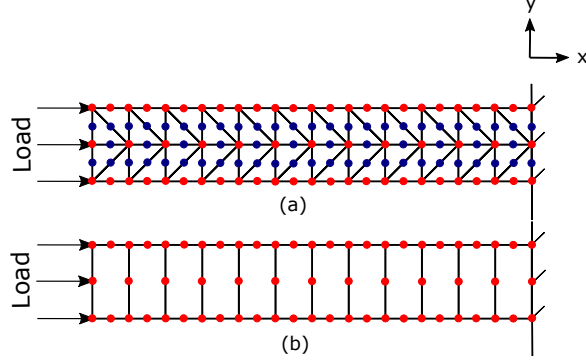


Figure 8: (a) 2D Abaqus model of one axon, and (b) 2D MATLAB homogenised model (250  $\mu\text{m}$  length and number of elements in the  $x$ -direction not to scale).

The first method made use of the membrane nodal displacements, calculated the current induced by the membrane flexoelectric effect, i.e., through curvature-induced membrane polarisation following [86]:

$$P = f c_1 \quad (52)$$

510 where  $c_1$  is the curvature of the membrane of the axon (upper and lower nodes in Fig. 8), and  $f = 2 \times 10^{-9} \text{ C/m}$  is the flexoelectric coefficient [40].

The second method used directly the proposed homgenised formulation.  $\tilde{\mathbf{f}}$  was assumed to be homogeneous throughout the axon ( $\rho_a = 1$ ) with transversely isotropic flexoelectric coefficients  $\tilde{f}_{55} = 0 \text{ C/m}$ ,  $\tilde{f}_{44} = 2 \times 10^{-9} \text{ C/m}$ ,  $\tilde{f}_{22} =$   
515  $0 \text{ C/m}$  and  $\tilde{f}_{11} = 0 \text{ C/m}$  [40]. The induced current per unit length of both methods are shown at 24.5 ns in Fig. 9. While some discrepancies occur (most likely due to the averaging of the nodes in the volumetric method), the results show that the homogeneous model is able to capture the shape and peaks of the current, and scale up the microscale phenomenon with good accuracy without  
520 the need to track the membrane's displacement independently of the rest of the

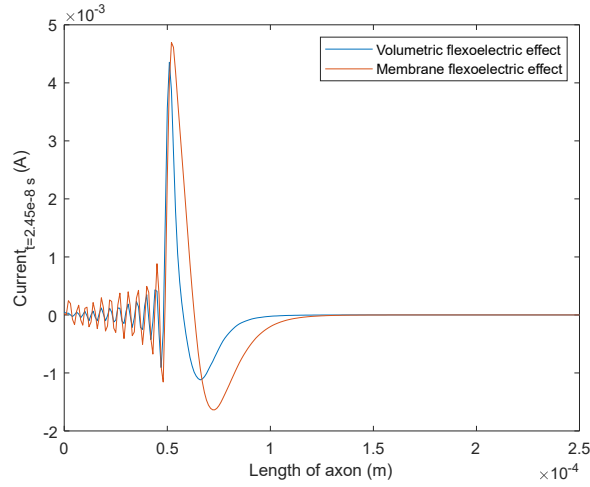


Figure 9: Induced current per unit length calculated by membrane flexoelectric effect and the proposed homogenised volumetric flexoelectric effect at 24.5 ns.

axon.

## References

## References

- [1] World Health Organisation, Global health estimates 2016: Disease burden by cause, age, sex, by country and by region, 2000-2016 (2018).  
 URL [https://www.who.int/healthinfo/global\\_burden\\_disease/estimates/en/index1.html](https://www.who.int/healthinfo/global_burden_disease/estimates/en/index1.html)
- [2] GBD 2016 Neurology Collaborators, Global, regional, and national burden of neurological disorders, 1990-2016: a systematic analysis for the global burden of disease study 2016, *The Lancet Neurology* 18 (5) (2019) 459–480. doi:10.1016/S1474-4422(18)30499-X.
- [3] G. Leinenga, C. Langton, R. Nisbet, J. Götz, Ultrasound treatment of neurological diseases—current and emerging applications, *Nature Reviews Neurology* 12 (3) (2016) 161–174. doi:10.1038/nrneuro1.2016.13.



- 535 [4] P. Dobrakowski, A. Machowska-Majchrzak, B. Labuz-Roszak, K. Majchrzak, E. Kluczevska, K. Pierzchala, Mr-guided focused ultrasound: a new generation treatment of parkinson's disease, essential tremor and neuropathic pain, *Interventional Neuroradiology* 20 (3) (2014) 275–282. doi:<https://doi.org/10.15274/INR-2014-10033>.
- 540 [5] T. Wagner, A. Valero-Cabre, A. Pascual-Leone, Noninvasive human brain stimulation, *Annual Review of Biomedical Engineering* 9 (2007) 527–565. doi:[10.1146/annurev.bioeng.9.061206.133100](https://doi.org/10.1146/annurev.bioeng.9.061206.133100).
- [6] G. Clement, Perspectives in clinical uses of high-intensity focused ultrasound, *Ultrasonics* 42 (10) (2004) 1087–1093. doi:[10.1016/j.ultras.2004.04.003](https://doi.org/10.1016/j.ultras.2004.04.003).
- 545 [7] D. Dalecki, Mechanical bioeffects of ultrasound, *Annual Review of Biomedical Engineering* 6 (2004) 229–248. doi:<https://doi.org/10.1146/annurev.bioeng.6.040803.140126>.
- [8] J. Mueller, W. Legon, A. Opitz, T. F. Sato, W. J. Tyler, Transcranial  
550 focused ultrasound modulates intrinsic and evoked eeg dynamics, *Brain Stimulation* 7 (6) (2014) 900–908. doi:<https://doi.org/10.1016/j.brs.2014.08.008>.
- [9] H. Kim, M. Park, S. Lee, W. Lee, A. Chiu, S. Yoo, Suppression of eeg visual-evoked potentials in rats through neuromodulatory focused ultrasound,  
555 *Neuroreport* 26 (4) (2015) 211–215. doi:[10.1097/WNR.0000000000000330](https://doi.org/10.1097/WNR.0000000000000330).
- [10] S. Yoo, A. Bystritsky, J. Lee, Y. Zhang, K. Fischer, B. Min, N. McDaniel, A. Pascual-Leone, F. Jolesz, Focused ultrasound modulates region-specific brain activity, *NeuroImage* 56 (3) (2011) 1267–1275. doi:[10.1016/j.neuroimage.2011.02.058](https://doi.org/10.1016/j.neuroimage.2011.02.058).
- 560 [11] W. Lee, S. D. Lee, M. Y. Park, L. Foley, E. Purcell-Estabrook, H. Kim, K. Fischer, L.-S. Maeng, S.-S. Yoo, Image-guided focused ultrasound-mediated regional brain stimulation in sheep, *Ultrasound in Medicine*

and Biology 42 (2) (2016) 459–470. doi:<https://doi.org/10.1016/j.ultrasmedbio.2015.10.001>.

- 565 [12] R. F. Dallapiazza, K. F. Timbie, S. Holmberg, J. Gatesman, M. B. Lopes, R. J. Price, G. W. Miller, W. J. Elias, Noninvasive neuromodulation and thalamic mapping with low-intensity focused ultrasound, *Journal of Neurosurgery* 128 (2018) 875–884. doi:<https://doi.org/10.3171/2016.11.JNS16976>.
- 570 [13] D. Folloni, L. Verhagen, R. B. Mars, E. Fouragnan, C. Constans, J.-F. Aubry, M. F. Rushworth, J. Sallet, Manipulation of subcortical and deep cortical activity in the primate brain using transcranial focused ultrasound stimulation, *Neuron* 101 (6) (2019) 1109–1116. doi:<https://doi.org/10.1016/j.neuron.2019.01.019>.
- 575 [14] J. L. Sanguinetti, S. Hameroff, E. E. Smith, T. Sato, C. M. Daft, W. J. Tyler, J. J. Allen, Transcranial focused ultrasound to the right prefrontal cortex improves mood and alters functional connectivity in humans, *frontiers in Human Neuroscience* 14 (52) (2020) 1–13. doi:[10.3389/fnhum.2020.00052](https://doi.org/10.3389/fnhum.2020.00052).
- 580 [15] J. Blackmore, S. Shrivastava, J. Sallet, C. R. Butler, R. O. Cleveland, Ultrasound neuromodulation: A review of results, mechanisms and safety, *Ultrasound in Medicine and Biology* 45 (7) (2019) 1509–1536. doi:[10.1016/j.ultrasmedbio.2018.12.015](https://doi.org/10.1016/j.ultrasmedbio.2018.12.015).
- [16] M. Fini, W. Tyler, Transcranial focused ultrasound: a new tool for non-invasive neuromodulation, *International Review of Psychiatry* 29 (2) (2017) 168–177. doi:[10.1080/09540261.2017.1302924](https://doi.org/10.1080/09540261.2017.1302924).
- 585 [17] E. Sassaroli, N. Vykhodtseva, Acoustic neuromodulation from a basic science prospective, *Journal of Therapeutic Ultrasound* 4 (17) (2016) 1–14. doi:[10.1186/s40349-016-0061-z](https://doi.org/10.1186/s40349-016-0061-z).

- 590 [18] L. Gavrilov, Use of focused ultrasound for stimulation of nerve structures, *Ultrasonics* 22 (3) (1984) 132–138. doi:[https://doi.org/10.1016/0041-624X\(84\)90008-8](https://doi.org/10.1016/0041-624X(84)90008-8).  
URL <https://www.sciencedirect.com/science/article/pii/0041624X84900088>
- 595 [19] H. S. Mayberg, A. M. Lozano, V. Voon, H. E. McNeely, D. Seminowicz, C. Hamani, J. M. Schwalb, S. H. Kennedy, Deep brain stimulation for treatment-resistant depression, *Neuron* 45 (5) (2005) 651–660. doi:[10.1016/j.neuron.2005.02.014](https://doi.org/10.1016/j.neuron.2005.02.014).  
URL <https://doi.org/10.1016/j.neuron.2005.02.014>
- 600 [20] A. M. Lozano, H. S. Mayberg, P. Giacobbe, C. Hamani, R. C. Craddock, S. H. Kennedy, Subcallosal cingulate gyrus deep brain stimulation for treatment-resistant depression, *Biological Psychiatry* 64 (6) (2008) 461–467. doi:[10.1016/j.biopsych.2008.05.034](https://doi.org/10.1016/j.biopsych.2008.05.034).  
URL <https://doi.org/10.1016/j.biopsych.2008.05.034>
- 605 [21] C. Hamani, H. Mayberg, S. Stone, A. Laxton, S. Haber, A. M. Lozano, The subcallosal cingulate gyrus in the context of major depression, *Biological Psychiatry* 69 (4) (2011) 301–308. doi:[10.1016/j.biopsych.2010.09.034](https://doi.org/10.1016/j.biopsych.2010.09.034).  
URL <https://doi.org/10.1016/j.biopsych.2010.09.034>
- 610 [22] H. Duffau, Stimulation mapping of white matter tracts to study brain functional connectivity, *Nature Reviews Neurology* 11 (5) (2015) 255–265. doi:[10.1038/nrneurol.2015.51](https://doi.org/10.1038/nrneurol.2015.51).  
URL <https://doi.org/10.1038/nrneurol.2015.51>
- 615 [23] J. Vion-Bailly, W. A. N’Djin, I. M. Suarez Castellanos, J.-L. Mestas, A. Carpentier, J.-Y. Chapelon, A causal study of the phenomenon of ultrasound neurostimulation applied to an in vivo invertebrate nervous model, *Scientific Reports* 9 (1) (2019) 13738. doi:[10.1038/s41598-019-50147-7](https://doi.org/10.1038/s41598-019-50147-7).  
URL <https://doi.org/10.1038/s41598-019-50147-7>

- [24] P. Zubko, G. Catalan, A. K. Tagantsev, Flexoelectric effect in solids,  
 620 Annual Review of Materials Research 43 (2013) 387–421. doi:<https://doi.org/10.1146/annurev-matsci-071312-121634>.
- [25] J. Narvaez, F. Vasquez-Sancho, G. Catalan, Enhanced flexoelectric-like response in oxide semiconductors, Nature 538 (2016) 219–221. doi:<https://doi.org/10.1038/nature19761>.
- 625 [26] B. Chu, D. R. Salem, Flexoelectricity in several thermoplastic and thermosetting polymers, Applied Physics Letters 101 (10). doi:<https://doi.org/10.1063/1.4750064>.
- [27] F. Vasquez-Sancho, A. Abdollahi, D. Damjanovic, G. Catalan, Flexoelectricity in bones, Advanced Materials 30 (9). doi:<https://doi.org/10.1002/adma.201705316>.  
 630
- [28] A. G. Petrov, Electricity and mechanics of biomembrane systems: Flexoelectricity in living membranes, Analytica Chimica Acta 568 (1-2) (2006) 70–83. doi:<https://doi.org/10.1016/j.aca.2006.01.108>.
- [29] Q. Deng, L. Liu, P. Sharma, Flexoelectricity in soft materials and biological  
 635 membranes, Journal of the Mechanics and Physics of Solids 62 (2014) 209–227. doi:<https://doi.org/10.1016/j.jmps.2013.09.021>.
- [30] L.-T. Gao, X.-Q. Feng, Y. Yin, H. Gao, An electromechanical liquid crystal model of vesicles, Journal of the Mechanics and Physics of Solids 56 (9) (2008) 2844–2862. doi:[10.1016/j.jmps.2008.04.006](https://doi.org/10.1016/j.jmps.2008.04.006).
- 640 [31] W. E. Brownell, F. Qian, B. Anvari, Cell membrane tethers generate mechanical force in response to electrical stimulation, Biophysical Journal 99 (3) (2010) 845–852. doi:<https://doi.org/10.1016/j.bpj.2010.05.025>.
- [32] L. Liu, P. Sharma, Flexoelectricity and thermal fluctuations of lipid bilayer  
 645 membranes: Renormalization of flexoelectric, dielectric, and elastic prop-

erties, *Physical Review E* 87 (2013) 1–8. doi:<https://doi.org/10.1103/PhysRevE.87.032715>.

- [33] A. G. Petrov, B. A. Miller, K. Hristova, P. N. R. Usherwood, Flexoelectric effects in model and native membranes containing ion channels, *European Biophysical Journal* 22 (1993) 289–300. doi:<https://doi.org/10.1007/BF00180263>.  
650
- [34] K. D. Breneman, W. E. Brownell, R. D. Rabbitt, Hair cell bundles: flexoelectric motors of the inner ear, *PLoS One* 4 (4) (2009) 1–9. doi:<https://doi.org/10.1371/journal.pone.0005201>.
- [35] I. Tasaki, K. Kusano, P. Byrne, Rapid mechanical and thermal changes in the garfish olfactory nerve associated with a propagated impulse, *Biophysical Journal* 55 (6) (1989) 1033–1040. doi:[10.1016/S0006-3495\(89\)82902-9](https://doi.org/10.1016/S0006-3495(89)82902-9).  
655
- [36] A. Jérusalem, Z. Al-Rekabi, H. Chen, A. Ercole, M. Malboubi, M. Tamayo-Elizalde, L. Verhagen, S. Contera, Electrophysiological-mechanical coupling in the neuronal membrane and its role in ultrasound neuromodulation and general anaesthesia, *Acta Biomaterialia* 97 (1) (2019) 116–140. doi:<https://doi.org/10.1016/j.actbio.2019.07.041>.  
660
- [37] J. Engelbrecht, T. Peets, K. Tamm, M. Laasmaa, M. Vendelin, On the complexity of signal propagation in nerve fibres, *The Proceedings of the Estonian Academy of Sciences* 67 (1) (2018) 28–38. doi:<https://doi.org/10.3176/proc.2017.4.28>.  
665
- [38] C. S. Drapaca, An electromechanical model of neuronal dynamics using hamilton’s principle, *Frontiers in Cellular Neuroscience* 9 (271) (2015) 1–8. doi:<https://doi.org/10.3389/fncel.2015.00271>.  
670
- [39] A. El Hady, B. Machta, Mechanical surface waves accompany action potential propagation, *Nature Communications* 6 (6697) (2015) 1–7. doi:[10.1038/ncomms7697](https://doi.org/10.1038/ncomms7697).

- [40] H. Chen, D. Garcia-Gonzalez, A. Jerusalem, Computational model of the  
 675 mechanoelectrophysiological coupling in axons with application to neu-  
 romodulation, *Physical Review E* 99 (3) (2019) 1–18. doi:10.1103/  
 PhysRevE.99.032406.
- [41] J. Sallet, R. B. Mars, M. P. Noonan, F.-X. Neubert, S. Jbabdi,  
 J. X. O'Reilly, N. Filippini, A. G. Thomas, M. F. Rushworth, The  
 680 organization of dorsal frontal cortex in humans and macaques, *Jour-  
 nal of Neuroscience* 33 (30) (2013) 12255–12274. arXiv:<https://www.jneurosci.org/content/33/30/12255.full.pdf>, doi:10.1523/  
 JNEUROSCI.5108-12.2013.  
 URL <https://www.jneurosci.org/content/33/30/12255>
- [42] T. Reese, O. Heid, R. Weisskoff, V. Wedeen, Reduction of eddy-current-  
 685 induced distortion in diffusion mri using a twice-refocused spin echo, *Mag-  
 netic Resonance in Medicine* 49 (1) (2003) 177–182. arXiv:<https://onlinelibrary.wiley.com/doi/pdf/10.1002/mrm.10308>, doi:<https://doi.org/10.1002/mrm.10308>.  
 690 URL <https://onlinelibrary.wiley.com/doi/abs/10.1002/mrm.10308>
- [43] T. Behrens, M. Woolrich, M. Jenkinson, H. Johansen-Berg, R. Nunes,  
 S. Clare, P. Matthews, J. Brady, S. Smith, Characterization and  
 propagation of uncertainty in diffusion-weighted mr imaging, *Magnetic  
 Resonance in Medicine* 50 (5) (2003) 1077–1088. arXiv:<https://onlinelibrary.wiley.com/doi/pdf/10.1002/mrm.10609>, doi:<https://doi.org/10.1002/mrm.10609>.  
 695 URL <https://onlinelibrary.wiley.com/doi/abs/10.1002/mrm.10609>
- [44] T. Behrens, H. J. Berg, S. Jbabdi, M. Rushworth, M. Woolrich,  
 Probabilistic diffusion tractography with multiple fibre orienta-  
 700 tions: What can we gain?, *NeuroImage* 34 (1) (2007) 144–155.  
 doi:<https://doi.org/10.1016/j.neuroimage.2006.09.018>.

URL <https://www.sciencedirect.com/science/article/pii/S1053811906009360>

- [45] S. Jbabdi, H. Johansen-Berg, Tractography: Where do we go from here?,  
705 Brain Connectivity 1 (3) (2011) 169–183, pMID: 22433046. arXiv:<https://doi.org/10.1089/brain.2011.0033>, doi:10.1089/brain.2011.0033.  
URL <https://doi.org/10.1089/brain.2011.0033>
- [46] R. B. Mars, S. Foxley, L. Verhagen, S. Jbabdi, J. Sallet, M. P. Noonan,  
F.-X. Neubert, J. L. Andersson, P. L. Croxson, R. I. M. Dunbar, A. A.  
710 Khrapitchev, N. R. Sibson, K. L. Miller, M. F. S. Rushworth, The extreme  
capsule fiber complex in humans and macaque monkeys: a comparative  
diffusion mri tractography study, Brain Structure and Function 221 (8)  
(2016) 4059–4071. doi:10.1007/s00429-015-1146-0.  
URL <https://doi.org/10.1007/s00429-015-1146-0>
- [47] N. Eichert, L. Verhagen, D. Folloni, S. Jbabdi, A. A. Khrapitchev, N. R.  
Sibson, D. Mantini, J. Sallet, R. B. Mars, What is special about the  
human arcuate fasciculus? lateralization, projections, and expansion,  
Cortex 118 (2019) 107–115, the Evolution of the Mind and the Brain.  
doi:<https://doi.org/10.1016/j.cortex.2018.05.005>.  
720 URL <https://www.sciencedirect.com/science/article/pii/S0010945218301515>
- [48] D. Folloni, J. Sallet, A. A. Khrapitchev, N. Sibson, L. Verhagen, R. B.  
Mars, Dichotomous organization of amygdala/temporal-prefrontal bundles  
in both humans and monkeys, eLife 8 (e47175) (2019) 1–23. doi:10.7554/  
725 eLife.47175.
- [49] L. V. Azaroff, J. J. Brophy, Electronic Processes in Materials, McGraw-Hill  
Book Company, 1963.
- [50] H. Le Quang, Q. He, The number and types of all possible rotational sym-  
metries for flexoelectric tensors, Proceedings of the Royal Society A 467  
730 (2011) 2369–2386. doi:10.1098/rspa.2010.0521.

- [51] D. Field, Y. Ammouche, J. M. P  na, A. J  rusalem, Machine learning based multiscale calibration of mesoscopic constitutive models for composite materials: application to brain white matter, *Computational Mechanics* 67 (2021) 1629–1643. doi:<https://doi.org/10.1007/s00466-021-02009-1>.  
735
- [52] L. Minati, W. P. Weglarz, Physical foundations, models, and methods of diffusion magnetic resonance imaging of the brain: A review, *Concepts of Magnetic Resonance Part A* 30 (5) (2007) 278–307. doi:<https://doi.org/10.1002/cmr.a.20094>.
- 740 [53] FEI Amira, Advanced 3d visualisation and volume modeling version 6.0.1 (2020).
- [54] K. Firouzi, N. Saffari, A numerical model for the study of photoacoustic imaging of brain tumours, *arXiv: Medical Physics* arXiv:1512.06792. doi:<https://arxiv.org/ftp/arxiv/papers/1512/1512.06792.pdf>.
- 745 [55] J. K. Mueller, L. Ai, P. Bansal, W. Legon, Computational exploration of wave propagation and heating from transcranial focused ultrasound for neuromodulation, *Journal of Neural Engineering* 13 (5). doi:<https://doi.org/10.1088/1741-2560/13/5/056002>.
- 750 [56] P. A. Hasgall, F. Di Gennaro, C. Baumgartner, E. Neufeld, B. Lloyd, M. C. Gosselin, D. Payne, A. Kingenb ock, N. Kuster, It’s database for thermal and electromagnetic parameters for biological tissues - version 4.0 (2021). doi:[10.13099/VIP21000-04-0](https://doi.org/10.13099/VIP21000-04-0).
- 755 [57] S. A. Goss, R. L. Johnston, F. Dunn, Comprehensive compilation of empirical ultrasonic properties of mammalian tissues, *The Journal of the Acoustical Society of America* 64 (2) (1978) 423–457. doi:<https://doi.org/10.1121/1.382016>.
- [58] A. I. Farrer, H. Od  en, J. de Bever, B. Coats, L. P. D, A. Payne, Characterization and evaluation of tissue-mimicking gelatin phantoms for use



- with mrgfus, *Journal of Therapeutic Ultrasound* 3 (9). doi:10.1186/s40349-015-0030-y.
- [59] M. O. Culjat, D. Goldenberg, P. Tewari, R. S. Singh, A review of tissue substitutes for ultrasound imaging, *Ultrasound in Medicine and Biology* 36 (6) (2010) 861–873. doi:10.1016/j.ultrasmedbio.2010.02.012.
- [60] B. T. Treeby, B. T. Cox, k-wave: Matlab toolbox for the simulation and reconstruction of photoacoustic wave fields, *Journal of Biomedical Optics* 15 (2) (2010) 021314. doi:https://doi.org/10.1117/1.3360308.
- [61] J. Latikka, T. Kuurne, H. Eskola, Conductivity of living intracranial tissues, *Physics in Medicine and Biology* 46 (6) (2001) 1611–1616. doi:https://doi.org/10.1088/0031-9155/46/6/302.
- [62] A. Petrov, Flexoelectric model for active transport. In *Physical and Chemical Basis of Biological Information Transfer*, Plenum Press,, New York, 1975.
- [63] F. Ahmadpoor, Q. Deng, L. P. Liu, P. Sharma, Apparent flexoelectricity in lipid bilayer membranes due to external charge and dipolar distributions, *Physical Review E* 88 (5) (2013) 1–5. doi:https://doi.org/10.1103/PhysRevE.88.050701.
- [64] A. T. Todorov, A. G. Petrov, J. H. Fendler, Flexoelectricity of charged and dipolar bilayer lipid membranes studied by stroboscopic interferometry, *Langmuir* 10 (7) (1994) 2344–2350. doi:https://doi.org/10.1021/1a00019a053.
- [65] J. Mueller, W. Tyler, A quantitative overview of biophysical forces impinging on neural function, *Physical Biology* 11 (5) (2014) 1–15. doi:10.1088/1478-3975/11/5/051001.
- [66] T. Heimburg, A. Jackson, On soliton propagation in biomembranes and nerves, *PNAS* 102 (28) (2005) 9790–9795. doi:https://doi.org/10.1073/pnas.0503823102.

- [67] R. E. Passingham, K. E. Stephan, R. Kotter, The anatomical basis of functional localization in the cortex, *Nature Reviews Neuroscience* 3 (2002) 606–616. doi:<https://doi.org/10.1038/nrn893>.
- 790 [68] R. B. Mars, L. Verhagen, T. E. Gladwin, F. X. Neubert, J. Sallet, M. F. S. Rushworth, Comparing brains by matching connectivity profiles, *Neuroscience and Biobehavioral Reviews* 60 (2016) 90–97. doi:<https://doi.org/10.1016/j.neubiorev.2015.10.008>.
- 795 [69] J. X. O'Reilly, P. L. Croxson, S. Jbabdi, J. Sallet, M. P. Noonan, R. B. Mars, P. G. Browning, C. R. Wilson, A. S. Mitchell, K. L. Miller, M. F. Rushworth, M. G. Baxter, Causal effect of disconnection lesions on inter-hemispheric functional connectivity in rhesus monkeys, *Proceedings of the National Academy of Sciences of the United States of America* 110 (34) (2013) 13982–13987. doi:<https://doi.org/10.1073/pnas.1305062110>.
- 800 [70] Y. Feng, R. J. Okamoto, R. Namani, G. M. Genin, P. V. Bayly, Measurements of mechanical anisotropy in brain tissue and implications for transversely isotropic material models of white matter, *Journal of the Mechanical Behavior of Biomedical Materials* 23 (2013) 117–132. doi:<https://doi.org/10.1016/j.jmbbm.2013.04.007>.
- 805 URL <https://www.sciencedirect.com/science/article/pii/S175161611300129X>
- [71] D. Garcia-Gonzalez, A. Jerusalem, Energy based mechano-electrophysiological model of cns damage at the tissue scale, *Journal of the Mechanics and Physics of Solids* 125 (2019) 22–37. doi:<https://doi.org/10.1016/j.jmps.2018.12.009>.
- 810 URL <https://www.sciencedirect.com/science/article/pii/S0022509618306872>
- [72] S. C. Payne, J. B. Furness, M. J. Stebbing, Bioelectric neuromodulation for gastrointestinal disorders: effectiveness and mechanisms, *Nature Reviews Gastroenterology & Hepatology* 16 (2) (2019) 89–105. doi:

10.1038/s41575-018-0078-6.

URL <https://doi.org/10.1038/s41575-018-0078-6>

- [73] M. G. Jones, E. R. Rogers, J. P. Harris, A. Sullivan, D. M. Ackermann, M. Russo, S. F. Lempka, S. B. McMahon, Neuromodulation using ultra  
820 low frequency current waveform reversibly blocks axonal conduction and chronic pain, *Science Translational Medicine* 13 (608) (2021) 1–12. doi:  
10.1126/scitranslmed.abg9890.  
URL <https://doi.org/10.1126/scitranslmed.abg9890>
- [74] Y. Wu, J. Mo, L. Sui, J. Zhang, W. Hu, C. Zhang, Y. Wang, C. Liu,  
825 B. Zhao, X. Wang, K. Zhang, X. Xie, Deep brain stimulation in treatment-resistant depression: A systematic review and meta-analysis on efficacy and safety, *frontiers in Neuroscience* 15 (655412) (2021) 1–12. doi:  
<https://doi.org/10.3389/fnins.2021.655412>.
- [75] A. M. Lozano, H. S. Mayberg, P. Giacobbe, C. Hamani, R. C. Crad-  
830 dock, S. H. Kennedy, Subcallosal cingulate gyrus deep brain stimulation for treatment-resistant depression, *Biological Psychiatry* 64 (6) (2008) 461–467. doi:  
<https://doi.org/10.1016/j.biopsych.2008.05.034>.
- [76] H. S. Mayberg, A. M. Lozano, V. Voon, H. E. McNeely, D. Seminowicz, C. Hamani, J. M. Schwalb, S. H. Kennedy, Deep brain stimulation for  
835 treatment-resistant depression, *Neuron* 45 (5) (2005) 651–660. doi:  
<https://doi.org/10.1016/j.neuron.2005.02.014>.
- [77] C. Hamani, H. Mayberg, S. Stone, A. Laxton, S. Haber, A. M. Lozano, The subcallosal cingulate gyrus in the context of major depression, *Biological Psychiatry* 69 (4) (2011) 301–308. doi:  
840 <https://doi.org/10.1016/j.biopsych.2010.09.034>.
- [78] J. F. Lehman, B. D. Greenberg, C. C. McIntyre, S. A. Rasmussen, S. N. Haber, Rules ventral prefrontal cortical axons use to reach their targets: Implications for diffusion imaging tractography and deep brain stimulation

- for psychiatric illness, *Journal of Neuroscience* 31 (28) (2011) 10392–10402.  
 845 doi:10.1523/JNEUROSCI.0595-11.2011.
- [79] P. Riva-Posse, K. Seung Choi, P. E. Holtzheimer, C. C. McIntyre, R. E. Gross, A. Chaturvedi, A. L. Crowell, S. J. Garlow, J. K. Rajendra, H. S. Mayberg, Defining critical white matter pathways mediating successful subcallosal cingulate deep brain stimulation for treatment-resistant depression, *Biological Psychiatry* 76 (12) (2014) 963–969. doi:https://doi.org/10.1016/j.biopsych.2014.03.029.  
 850
- [80] K. H. Huebner, *The Finite Element Method for Engineers*, J. Wiley, New York; Chichester, 2001.
- [81] L. Shu, X. Wei, T. Pang, X. Yao, C. Wang, Symmetry of flexoelectric coefficients in crystalline medium, *Journal of Applied Physics* 110 (104106) (2011) 8. doi:https://doi.org/10.1063/1.3662196.  
 855
- [82] E. A. Eliseev, A. N. Morozovska, Hidden symmetry of flexoelectric coupling, *Physical Review B* 98 (2018) 12. doi:10.1103/PhysRevB.98.094108.
- [83] S. Ganpule, N. P. Daphalapurkar, M. Pirtini Cetingul, K. T. Ramesh, Effect of bulk modulus on deformation of the brain under rotational accelerations, *Shock Waves* 28 (1) (2018) 127–139. doi:https://doi.org/10.1007/s00193-017-0791-z.  
 860
- [84] Dassault Systèmes Simulia Corp, *Abaqus/CAE 2018* (2018).
- [85] MathWorks, *Matlab and statistical toolbox release 2017b* (2017).
- 865 [86] A. G. Petrov, Flexoelectricity of model and living membranes, *Biochimica et Biophysica Acta* 1561 (1) (2002) 1–25. doi:https://doi.org/10.1016/S0304-4157(01)00007-7.